UCRL-ID- 127715

SECO
Containment Data Report

T. Stubbs

R. Heinle

June, 1997

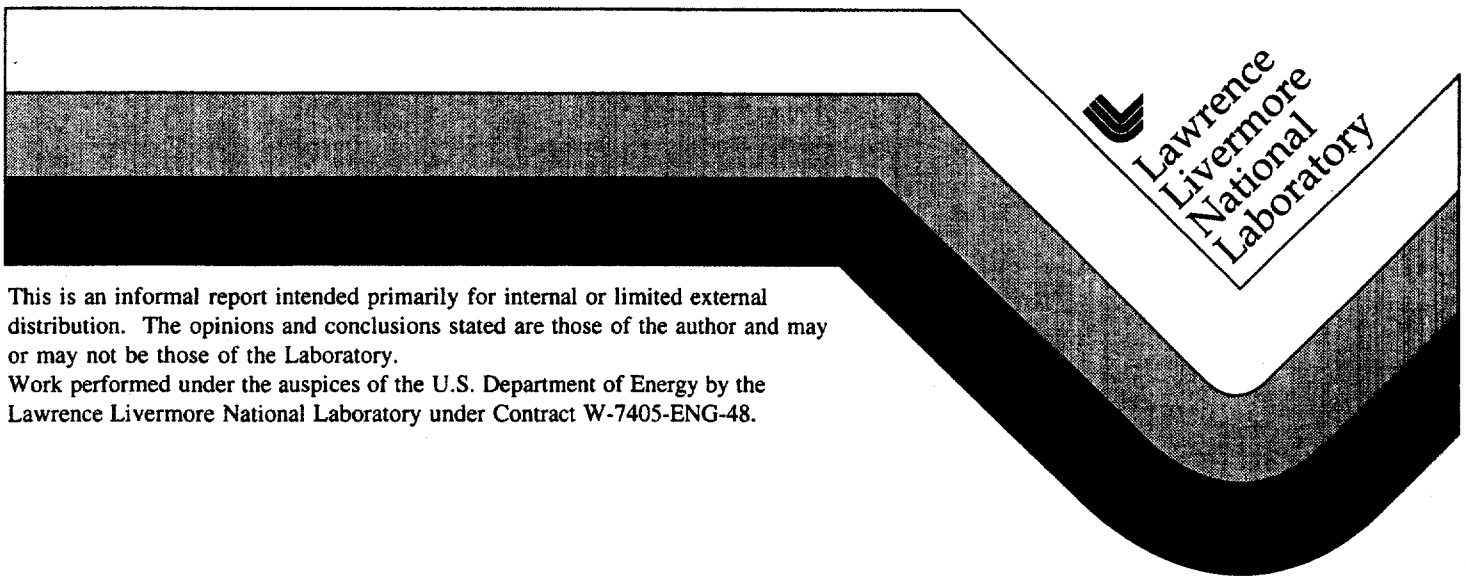

Work performed under the auspices of the U.S. Department of Energy by the Lawrence Livermore National Laboratory under Contract W-7405-ENG-48.

SECO Instrumentation Summary

Instrumentation	Fielded on this Event	Data Return	Present in this Report
Plug Emplacement	yes	yes	no[a]
Radiation	yes	yes	yes
Pressure			
Stemming	yes	yes	yes
Challenge	no	-	-
Cavity	no	-	-
Atmospheric	no	-	-
Motion			
Free Field	no	-	-
Surface	yes	yes	yes
Plug	yes	yes	yes
Stemming	no	-	-
Surface Casing	no	-	-
Emplacement Pipe	no	-	-
Hydroyield [b]	no	-	-
Collapse [c]	yes	yes	yes
Stress	no	-	-
Strain[d]	yes	no	-
Other Measurements	no	-	-

(a) Description only
(b) CORTEX or SLIFER in emplacement hole.
(c) CLIPER in emplacement hole. Pressure and radiation histories are only indication.
(d) Emplacement pipe load.

Event Personnel

Containment Physics	
B. Hudson	LLNL
V. Wheeler	LLNL
J. Kalinowski	EG&G/AVO
T. Stubbs	EG&G/AVO

Instrumentation	
L. Starrh	LLNL
F. Sierra	EG&G/AVO
L. E. Davies	EG&G/NVO
P. Tanner	EG&G/NVO

Contents

1. Event Description

1.1 Site

The SECO event was detonated in hole U8I of the Nevada Test Site as indicated in figure 1.1. The device had a depth-of-burial (DOB) of 200 m in the Tunnel Beds tuffs of area 8, about 200 m above the Paleozoic and 350 m above the standing water level, as shown in figures 1.2 and 1.3[1]. Stemming of the 1.63 m diameter emplacement hole followed the plan shown in figure 1.4. A log of the stemming operations was maintained by Holmes & Narver[2].

Detonation time was 07:00 PST on February 25, 1981 and about 33 minutes later a subsurface collapse, or stemming fall, progressed to beneath the deepest rigid stemming plug at a depth of greater than 120 m.

No radiation arrivals were detected in the emplacement hole above the bottom stemming plug and the SECO containment was considered successful.

1.2 Instrumentation

Figure 1.5 is a schematic layout of the instrumentation designed to monitor the emplacement procedures and stemming performance of the SECO event.

The four stemming plugs were composed of coal-tar epoxy (LAE 59, denoted CTE). A soft layer of coal-tar and aggregate (LAE 59MY, denoted CTA) was poured on the top of each of the plugs to act as a gas seal.

Pressure and radiation was monitored in the coarse stemming at seven locations: on either side of a layer of fines material between the device diagnostics canister and the deepest rigid plug, on either side of the deepest rigid plug and about 8 m below each of the top three plugs.

Vertical motion was monitored in each of the four plugs in the emplacement hole and in the ground surface, 15.24 m from SGZ.

An array of fourteen surface motion stations was fielded for the event VIDE [3] in hole U8k and was activated during the event SECO. This array lay on a line 30° north of west from hole U8k with each buried 0.91 m in the ground surface. The closest station to hole U8k was at a horizontal distance of 300 m while each succeeding station was 60 m farther away. Vertical motion was monitored at each of the fourteen stations but, because of a limitation of both available transducers and recording channels, tri-axial motion was monitored at only four stations An additional four stations sensed bi-axial motion (horizontal-radial and vertical components). The purpose of these measurements was to use a nuclear event as the source for a coarse, single-ended seismic survey through the faults exposed by another nuclear event (DISCUS THROWER, U8a). Results of a refraction study by N. Burkhard, based on the SECO and VIDE data, are presented in the appendix.

Data from each of the above instruments were transmitted to the recording trailer by an analog system and recorded on magnetic tape.

D-cable information was used for quality assurance during the stemming operations and was also recorded post-shot.

Two CLIPER sensors were emplaced in the emplacement hole to monitor cavity collapse and chimney formation; one on the emplacement pipe and device canister, a second on the instrumentation pendant.

A history of the fielding operations of the instrumentation, including the emplacement pipe strain measurements, is outlined in reference 4. Details of the instrumentation are given in reference 5.

1.3. Emplacement

A single strain station (85) was fielded near the top of the emplacement pipe to monitor the load during installation and stemming. This station was monitored randomly during these procedures and was recorded by hand during the device installation only.

Emplacement was detailed by Holmes & Narver[2]. The stemming plugs consisted of four "LAE 59" coal-tar epoxy (CTE) plugs. The bottom three were about 3 m thick while the top was about 5.5 m thick. All plugs were capped with about 1.8 m of soft coal-tar-aggregate "LAE 59MY" epoxy (CTA) to act as a gas sealant. Stemming between the plugs consisted of layers of fines and coarse gravel. The top of the hole (above the top plug) was filled with surface-derived backfill. The emplacement pipe was grouted from the device diagnostics canister to the surface. See figure 1.4.

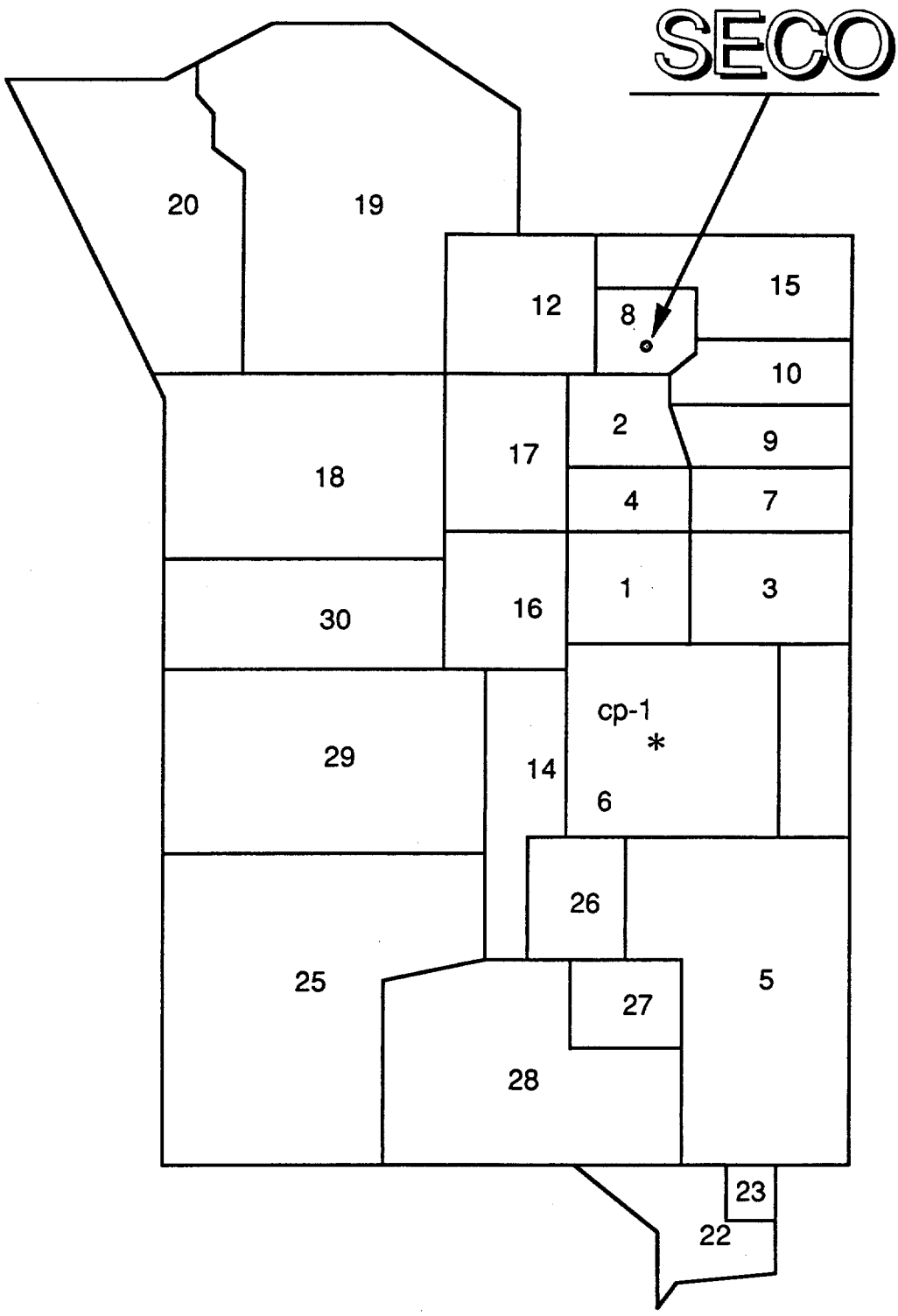

Figure 1.1 Map of the Nevada Test Site indicating the location of hole U8I.

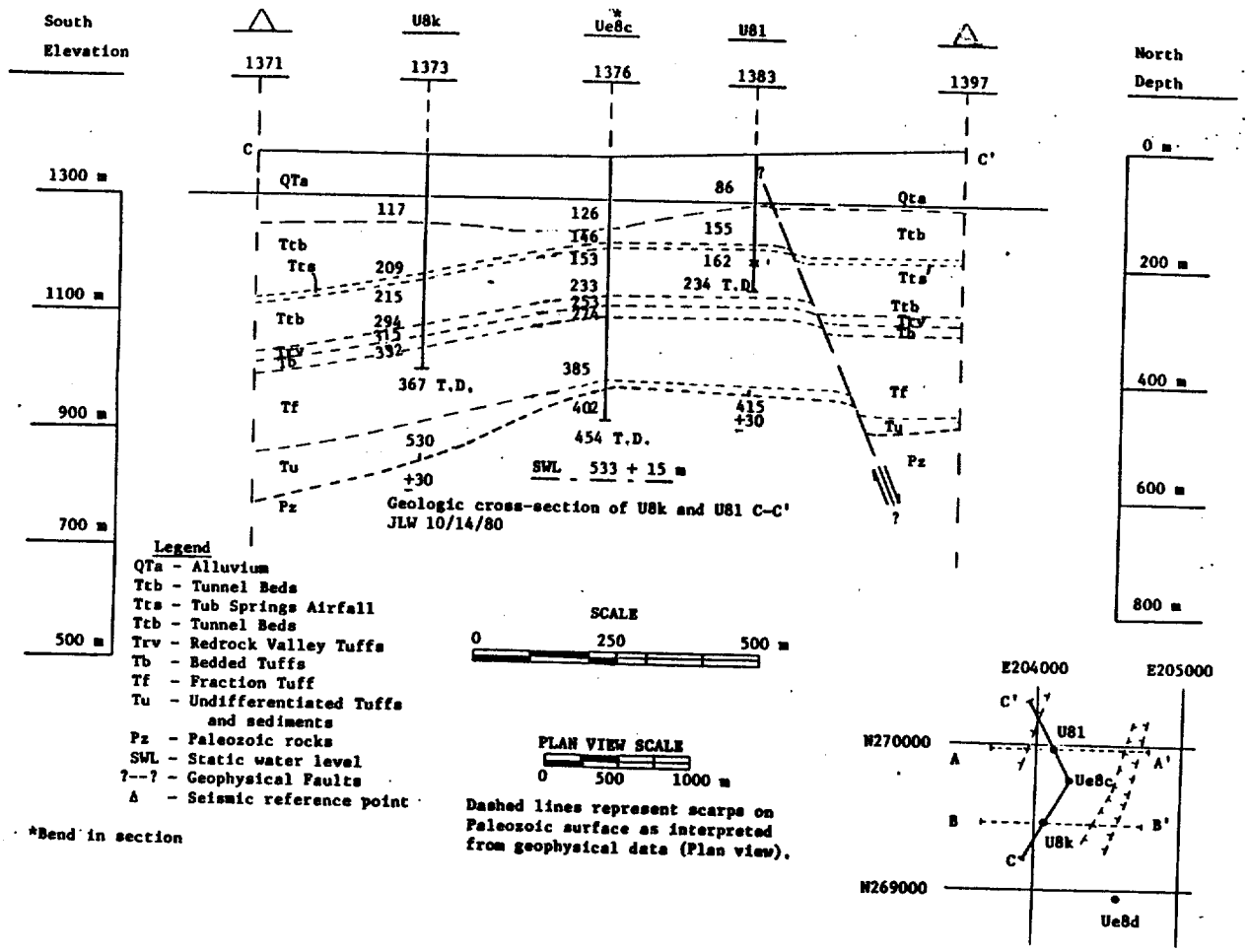

Figure 1.2 North-South geologic cross sections through hole U8l.

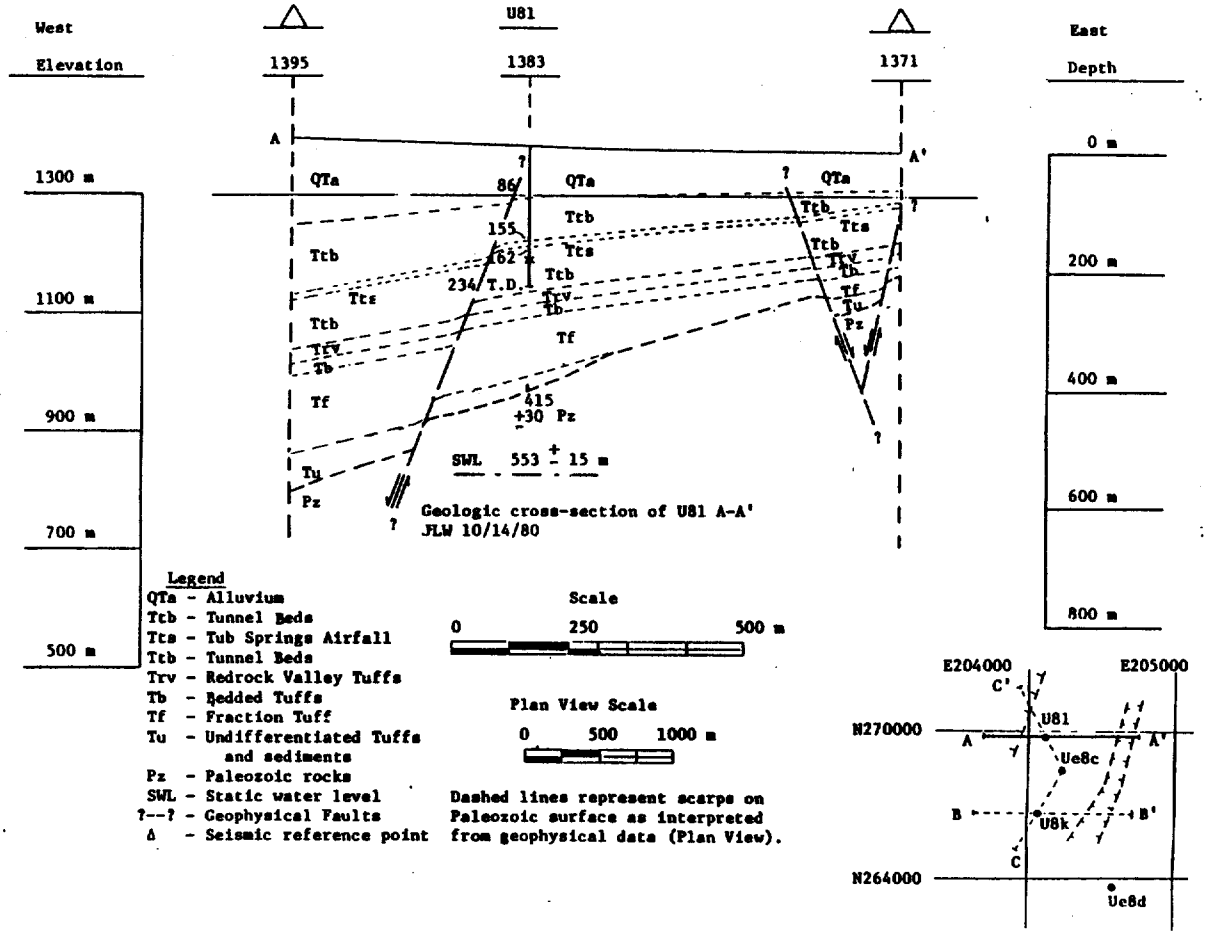

Figure 1.3 East-West geologic cross sections through hole U8l.

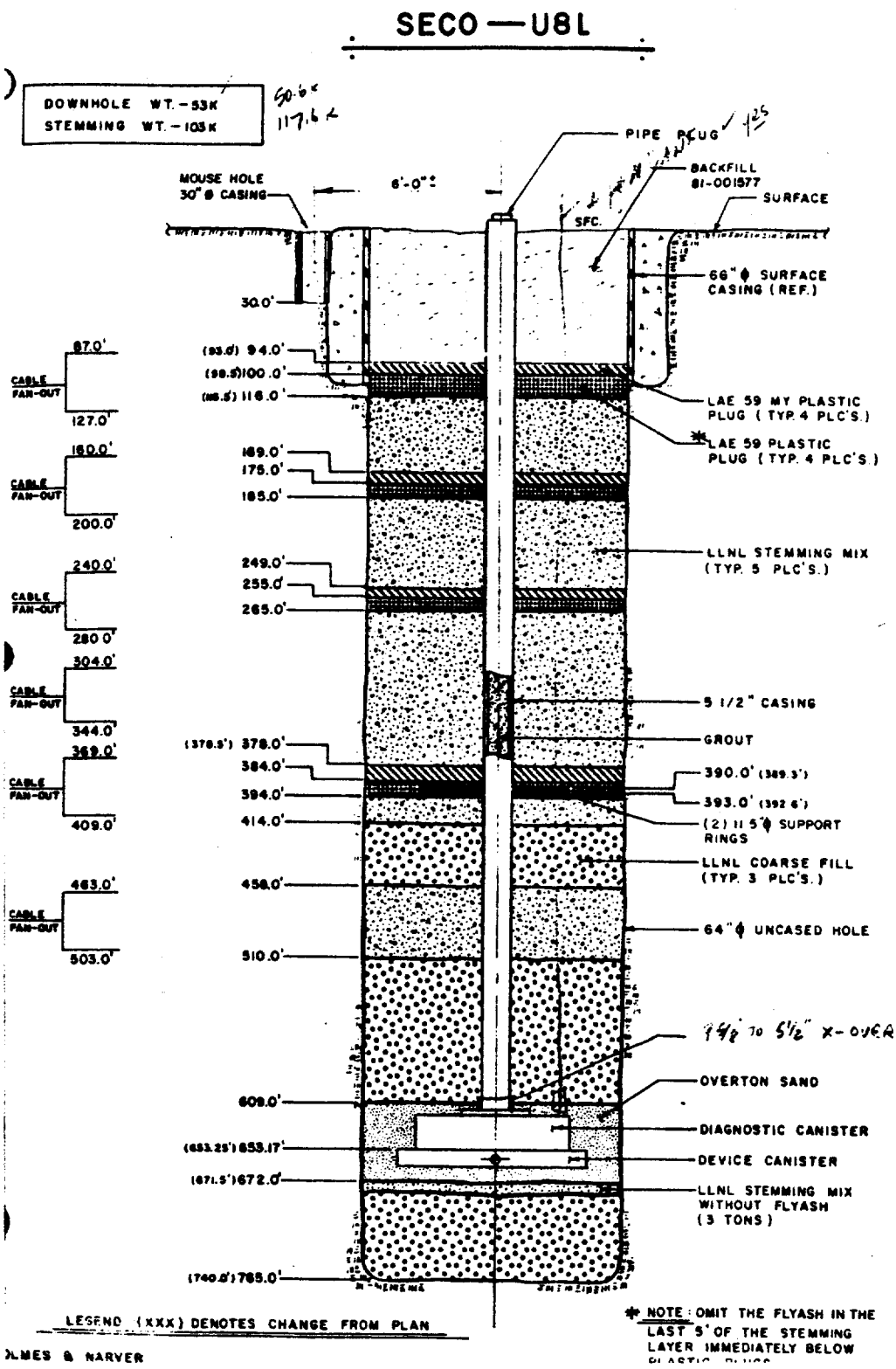

Figure 1.4 As-built stemming plan for the event SECO in Hole U8l.

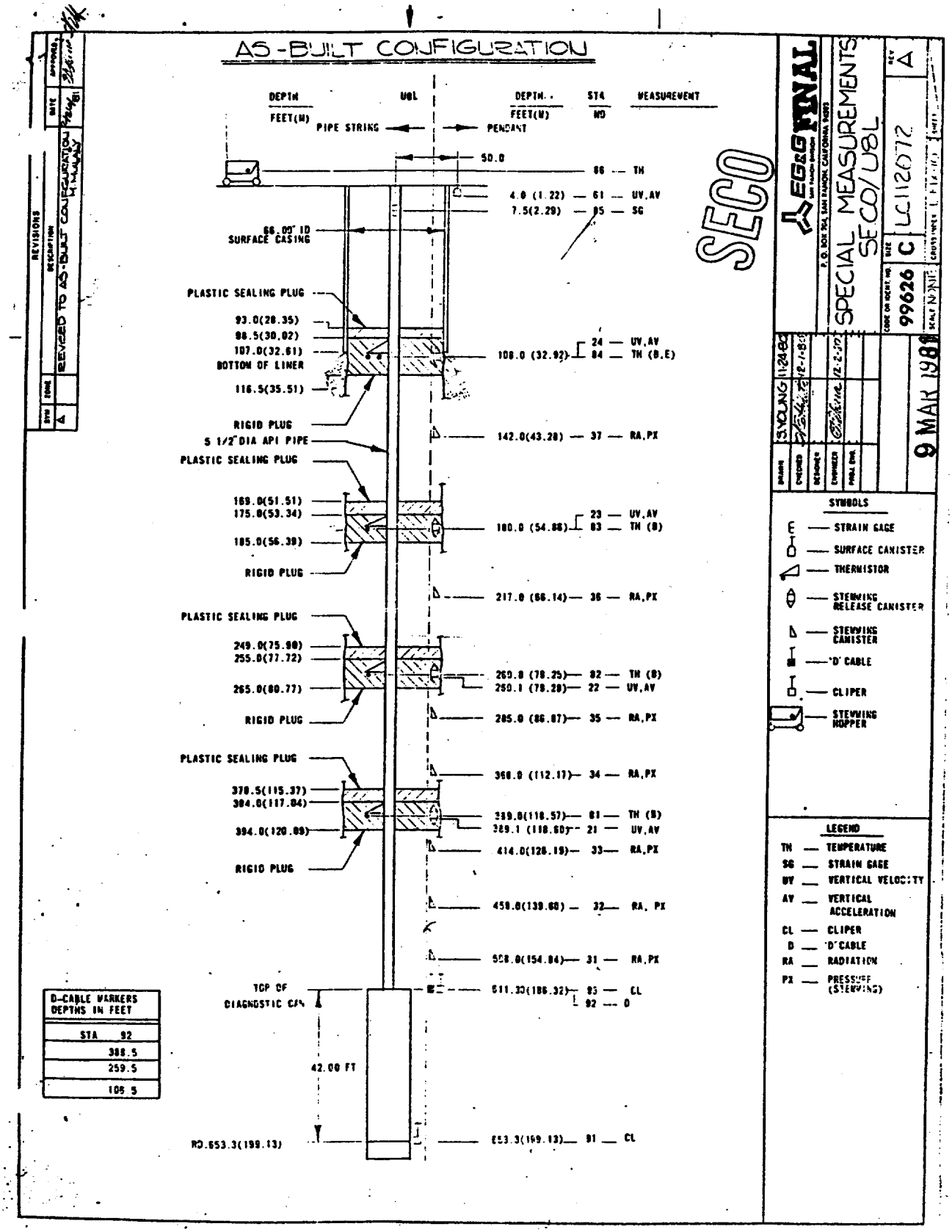

Figure 1.5 As-built containment instrumentation plan for the emplacement hole (U8I) on the SECO event.

2. Stemming Performance

2.1 Radiation and Pressure

As seen in figure 1.5, pressure and radiation was monitored in the coarse stemming at a total of seven stations. Two stations were fielded on either side of a layer of fines material between 31.5 and 47 meters above the diagnostics canister, two were placed on either side of the deepest rigid plug and the remaining three were 6, 10, and 8 meters below rigid plugs 2, 3, and 4, respectively.

All stations transmitted data until recording was terminated at about 33 hours after the detonation. Pressure and radiation data are shown for this full transducer recording time in figures 2.1-2.7. The "continued gaps" seen in several of the traces of figures 2.1-2.7 are occasioned by the requirement to change the analog tape when it ran to the end o f tape. (The length of recording time on a tape was about 3.6 hours). As shown in figure 2.2, station 32 pressure data were lost about 25 ms after detonation time.

To obtain greater definition of the data of stations 31-37, the first 6000 s of all the pressure and radiation wave forms are shown in figures 2.8-2.14. The pressure drops seen at stations 31 and 33 (figures 2.1, 2.3, 2.8, and 2.10) are characteristic of a stemming fall, while locations above the bottom rigid plug (stations 34 through 37) register neither radiation arrivals nor any pressure history that could not be explained by motion of the stemming or ground. Only the bottom station (station 31, figures 2.1 and 2.8) shows a pre-collapse radiation arrival. This occurs at about 500 s.

All pressure and radiation data are consistent with satisfactory containment.

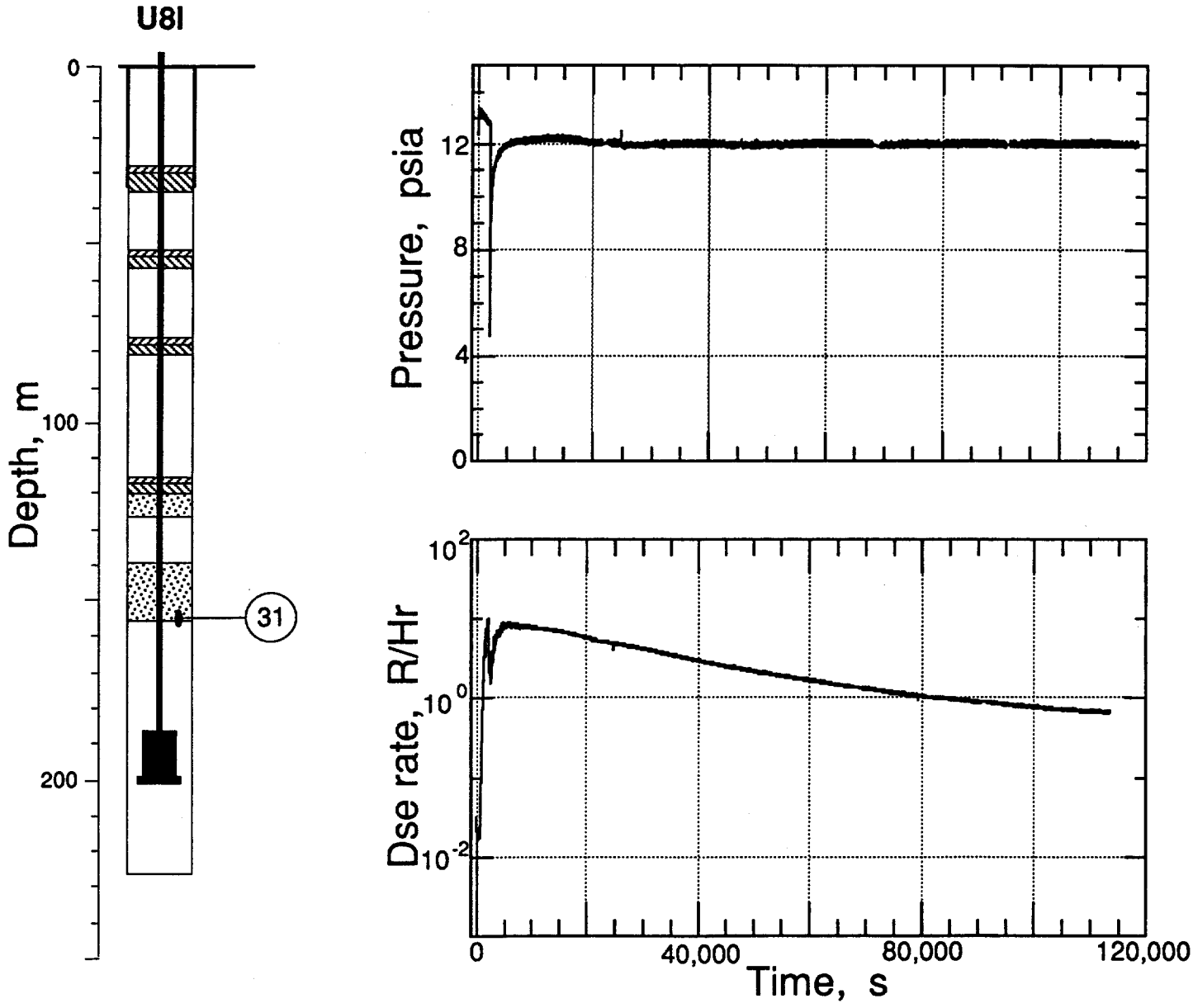

Figure 2.1 Pressure and radiation measured in the coarse stemming at 154.8 mm depth (Station 31, below the deep fines layer). The full recording time of about 33 hours is shown. Gaps in the data are due to the requirement to change the recording tape.

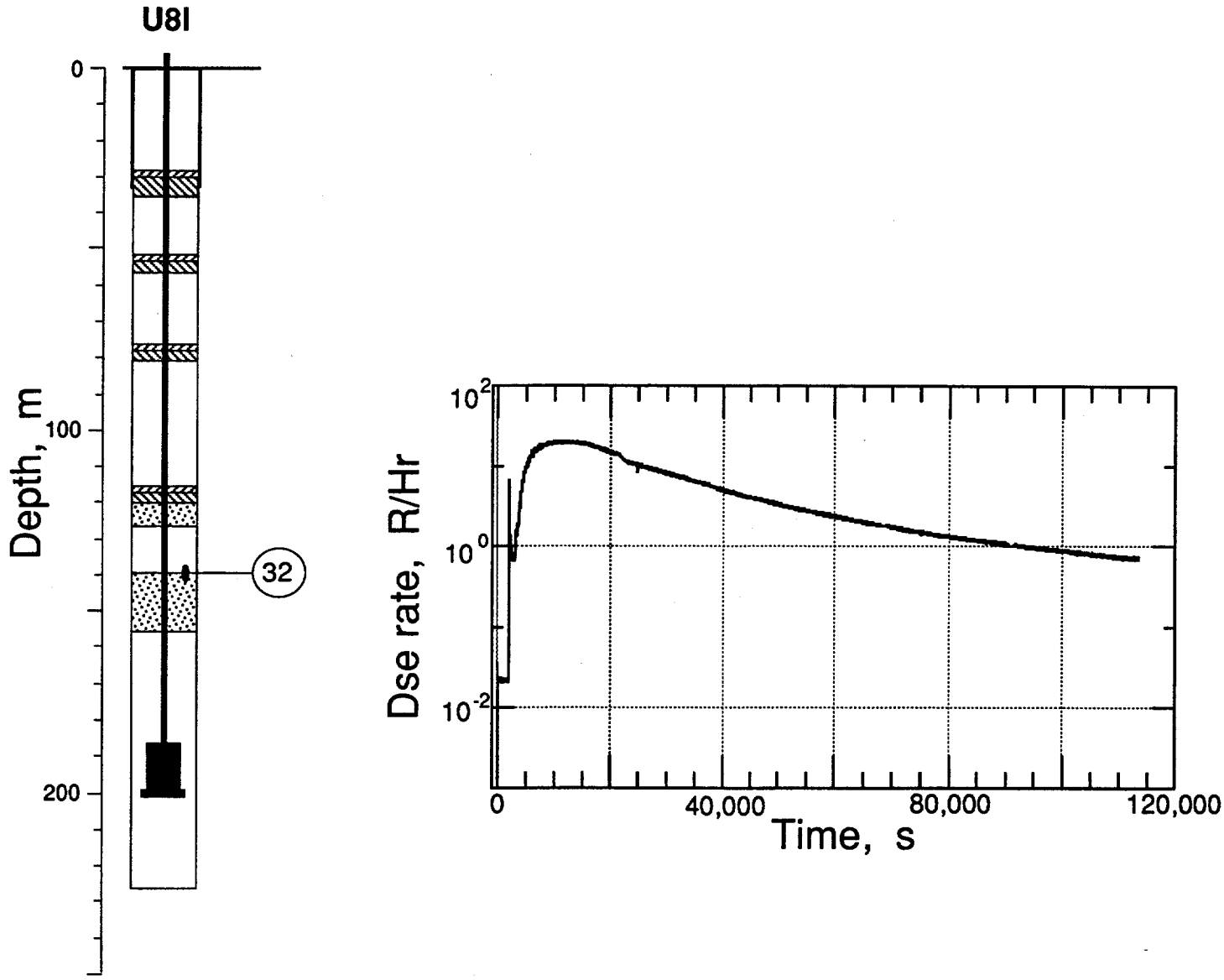

Figure 2.2 Pressure and radiation measured in the coarse stemming at 139.6 m depth (Station 32, above the deep fines layer). The pressure transducer was lost about 25 ms after detonation, the approximate time of shock arrival. The full recording time of about 33 hours is shown. Gaps in the data are due to the requirement to change the recording tape.

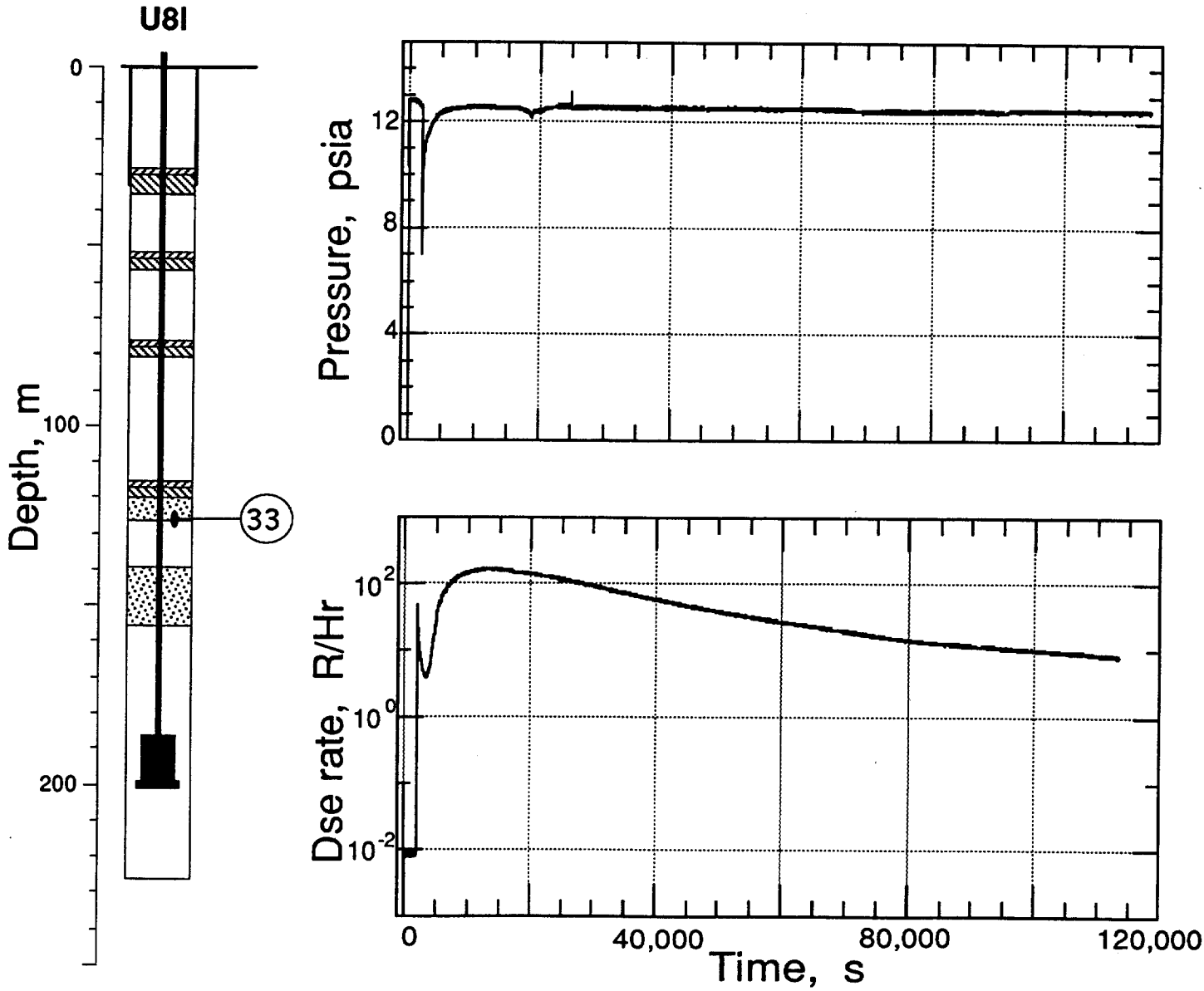

Figure 2.3 Pressure and radiation measured in the coarse stemming at 126.2 m depth (Station 33, below the deepest stemming plug 1). The full recording time of about 33 hours is shown. Gaps in the data are due to the requirement to change the recording tape.

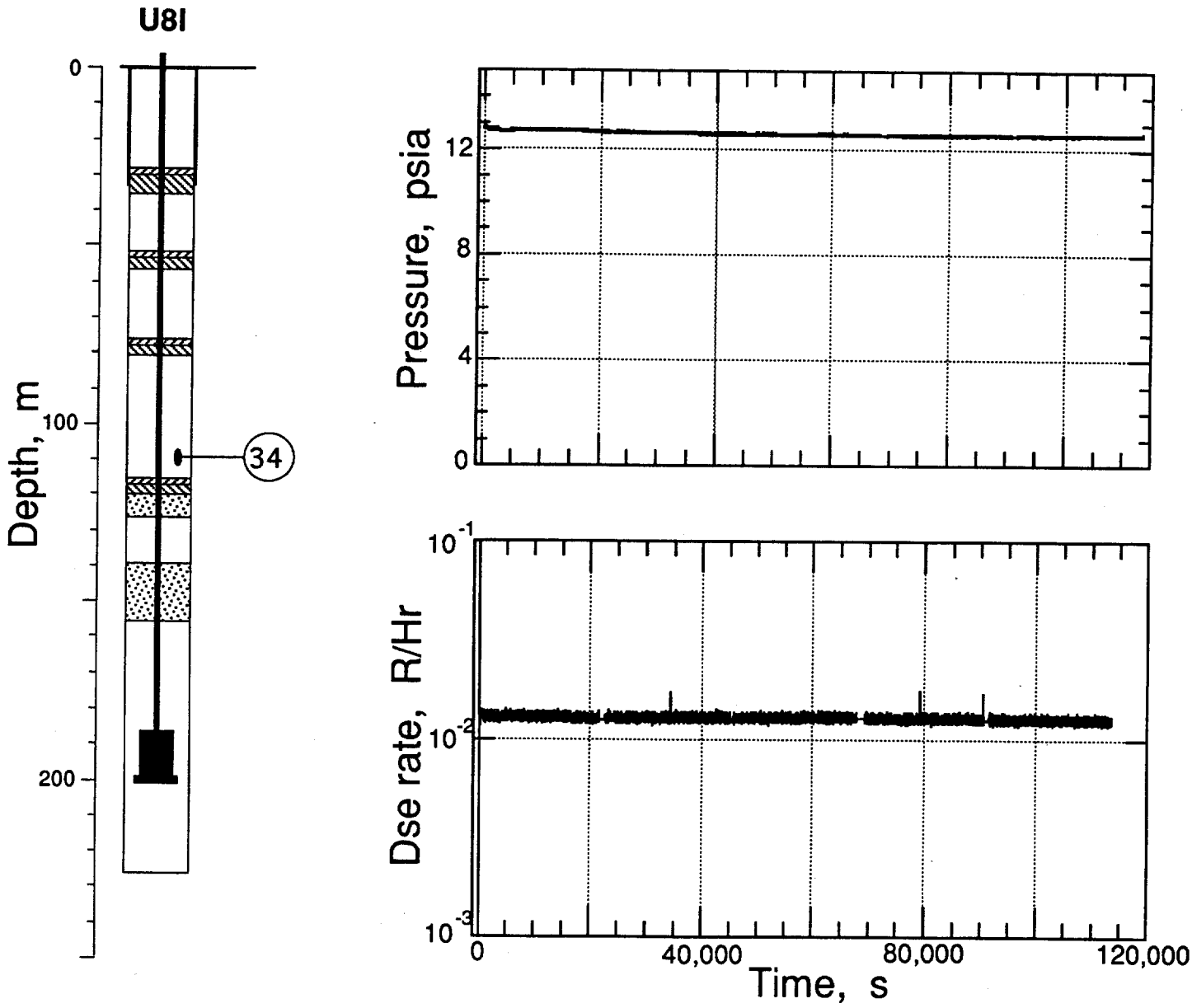

Figure 2.4 Pressure and radiation measured in the coarse stemming at 112.2 m depth (Station 34, above the deepest stemming plug 1). The full recording time of about 33 hours is shown. Gaps in the data are due to the requirement to change the recording tape.

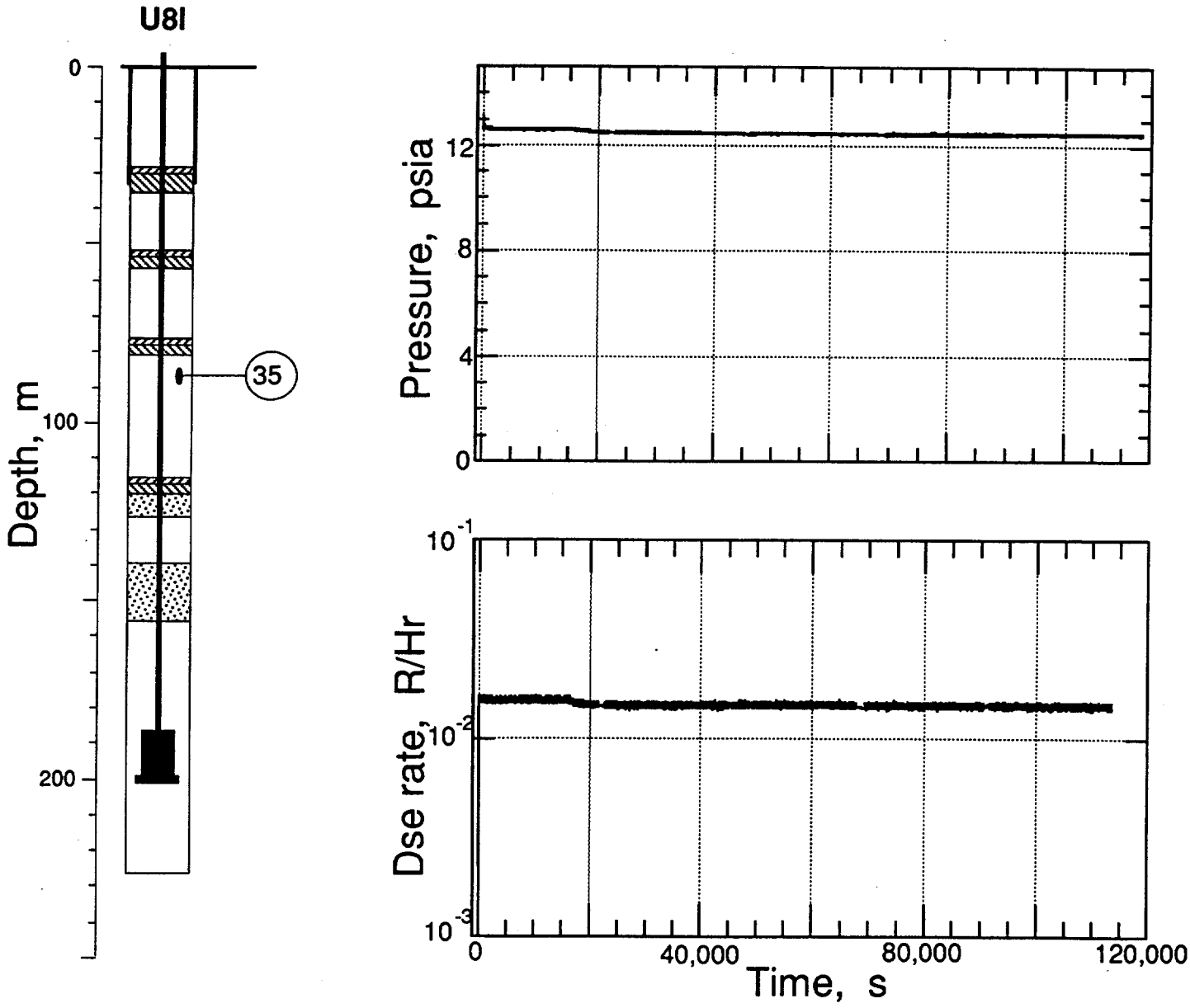

Figure 2.5 Pressure and radiation measured in the coarse stemming at 86.9 m depth (Station 35, below stemming plug 2). The full recording time of about 33 hours is shown. Gaps in the data are due to the requirement to change the recording tape.

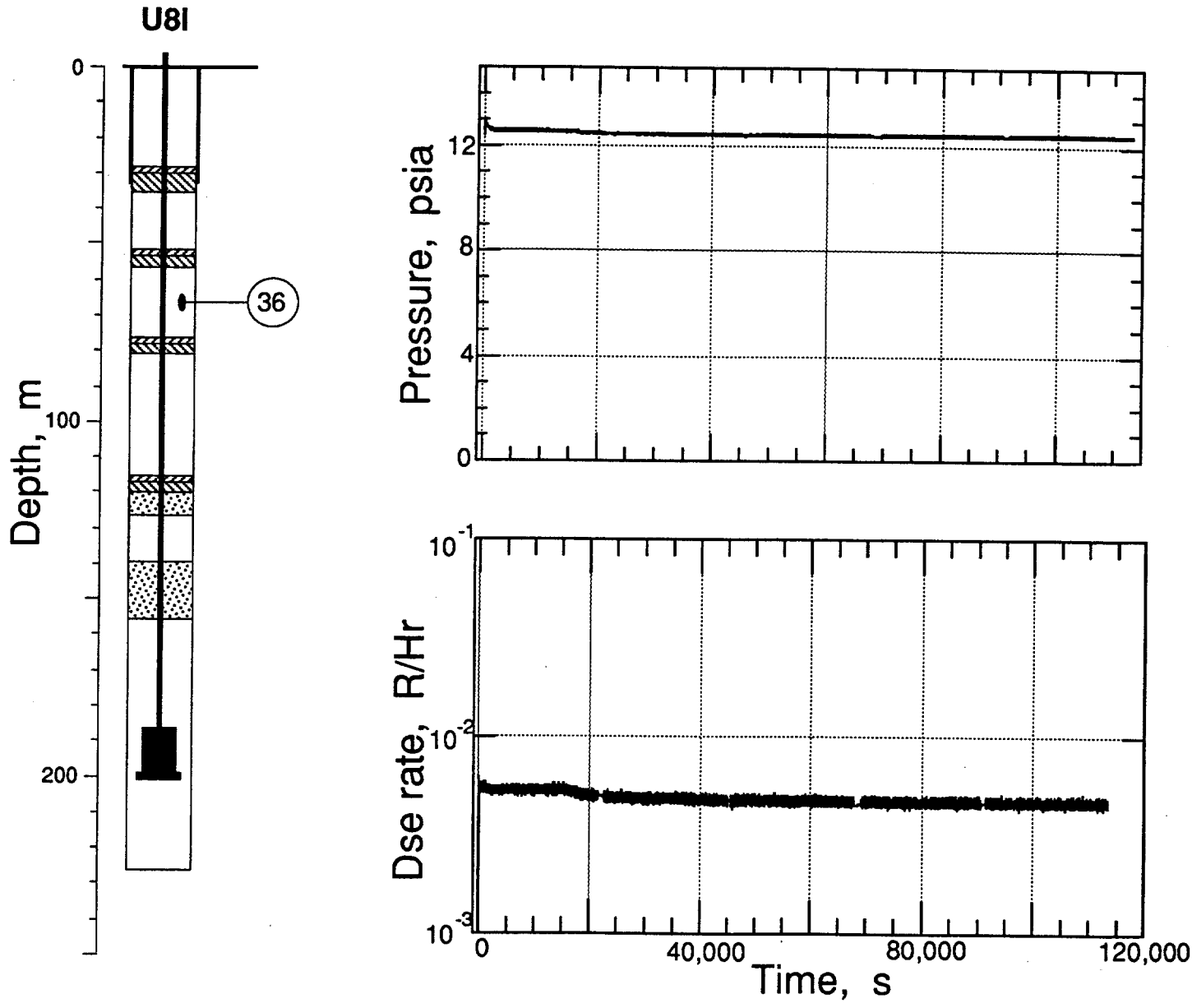

Figure 2.6 Pressure and radiation measured in the coarse stemming at 66.1 m depth (Station 36, between plugs 2 and 3). The full recording time of about 33 hours is shown. Gaps in the data are due to the requirement to change the recording tape.

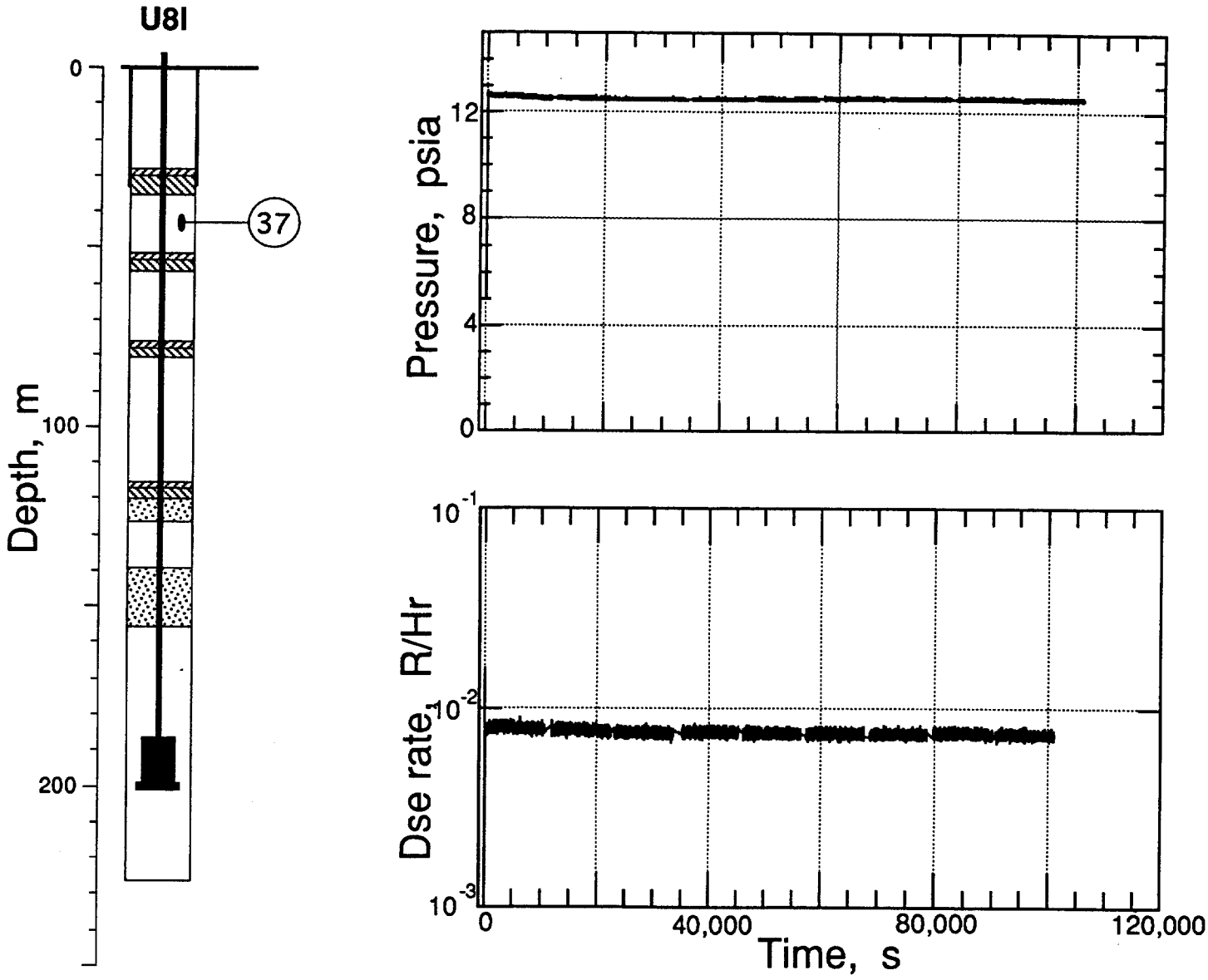

Figure 2.7 Pressure and radiation measured in the coarse stemming at 43.3 m depth (Station 37, about 8 m below the top plug). The full recording time of about 33 hours is shown. Gaps in the data are due to the requirement to change the recording tape.

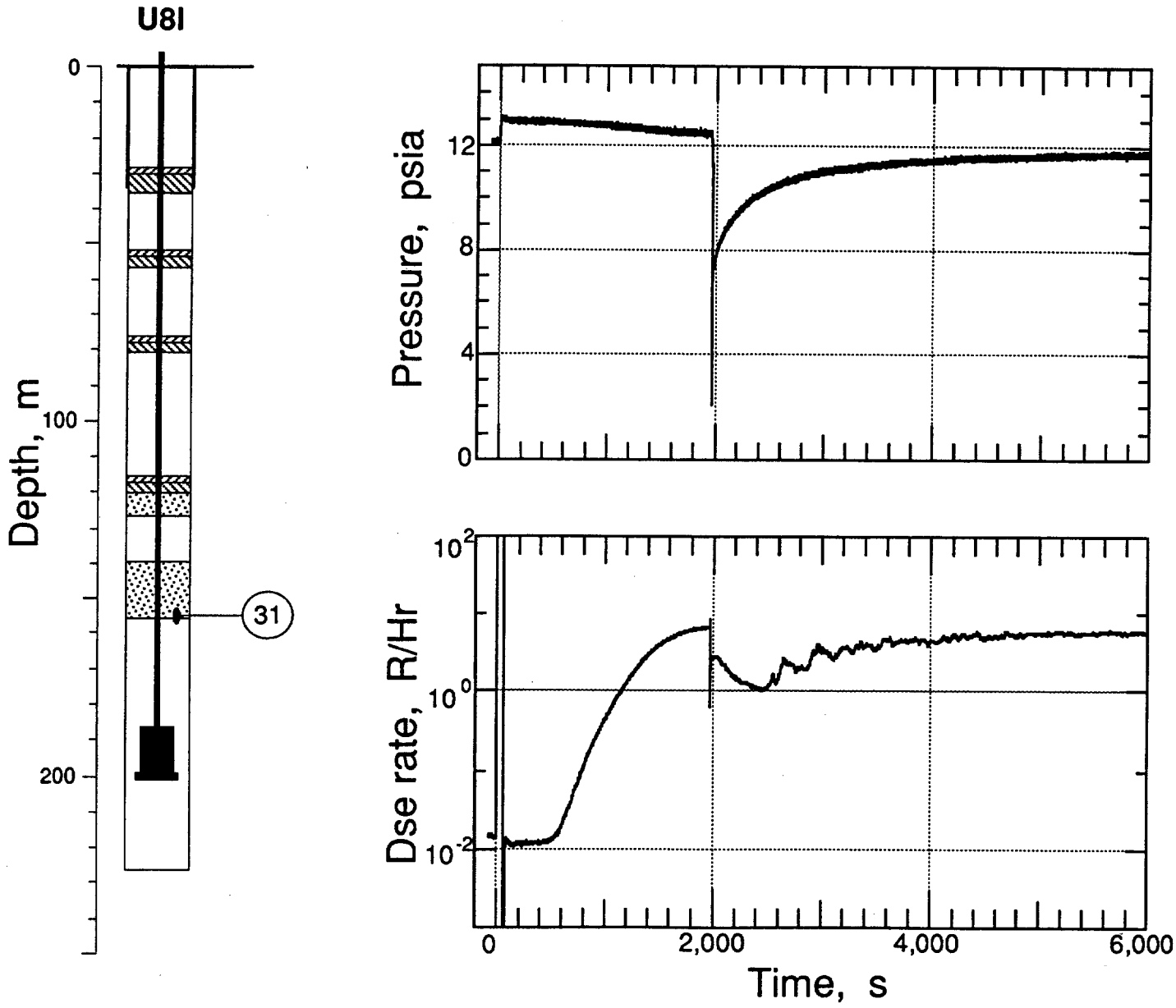

Figure 2.8 Pressure and radiation measured in the coarse stemming at 154.8 mm depth (Station 31, below the deep fines layer).

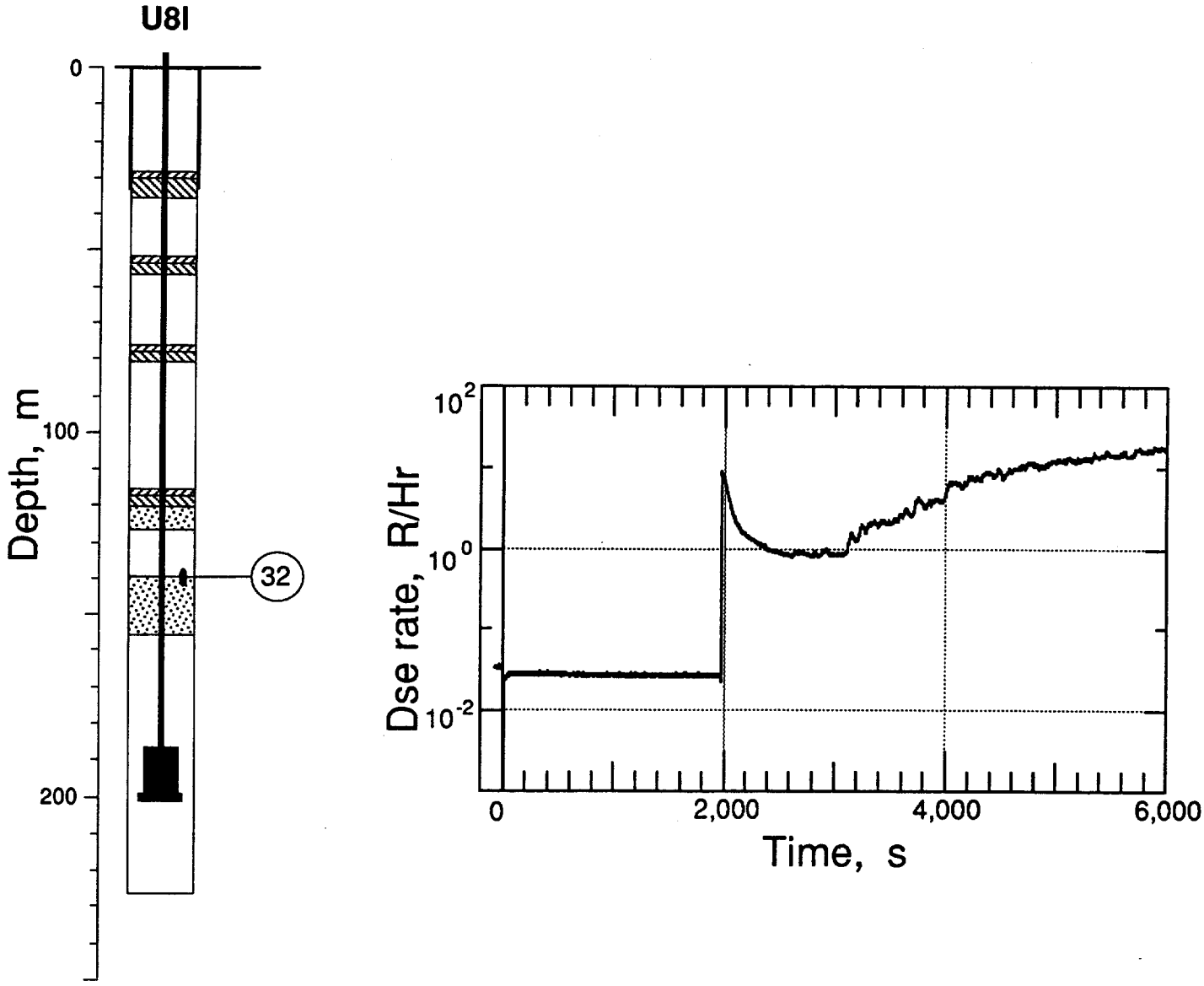

Figure 2.9 Pressure and radiation measured in the coarse stemming at 139.6 m depth (Station 32, above the deep fines layer). The pressure transducer was lost about 25 ms after detonation, the approximate time of shock arrival.

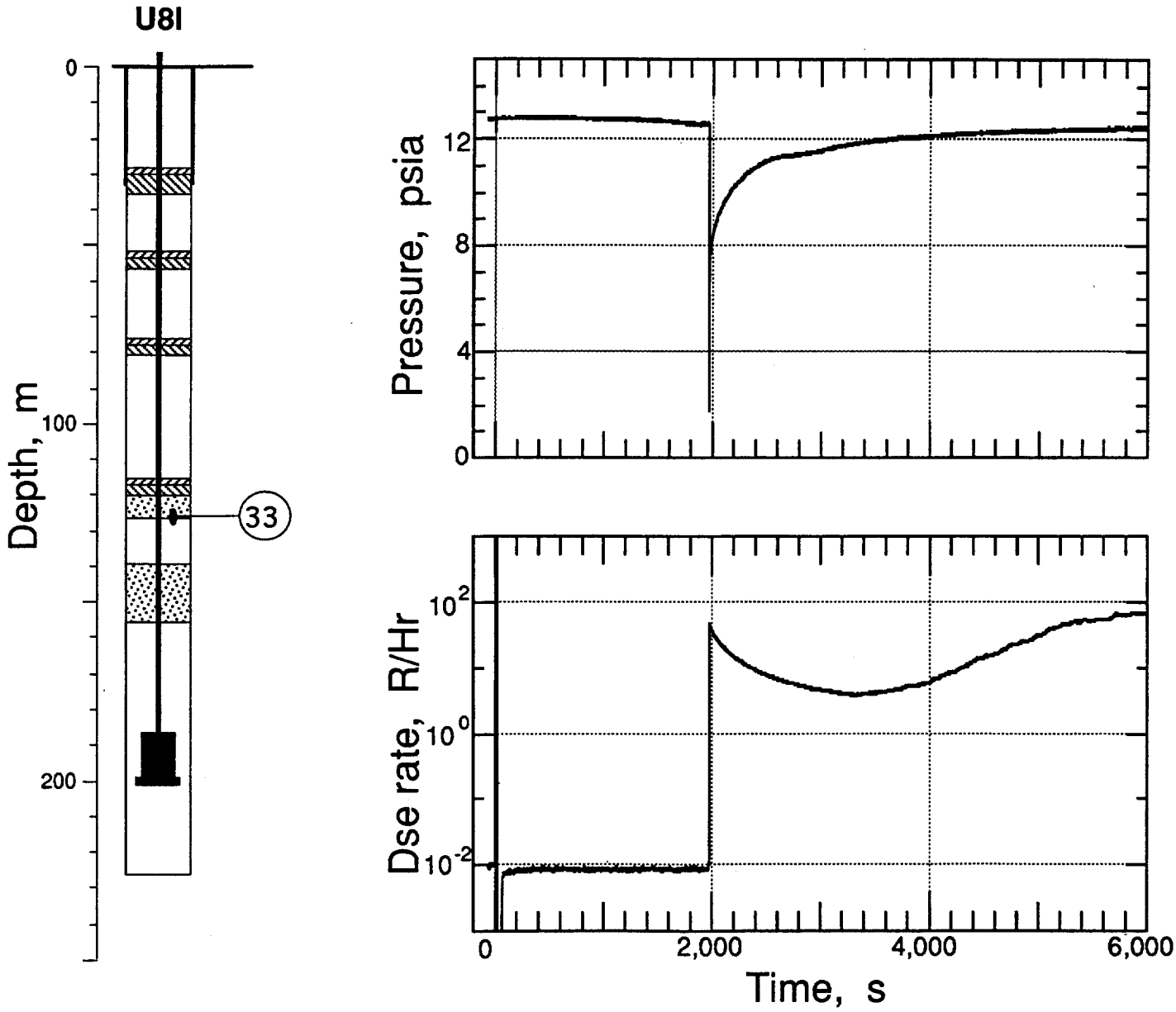

Figure 2.10 Pressure and radiation measured in the coarse stemming at 126.2 m depth (Station 33, below the deepest stemming plug 1).

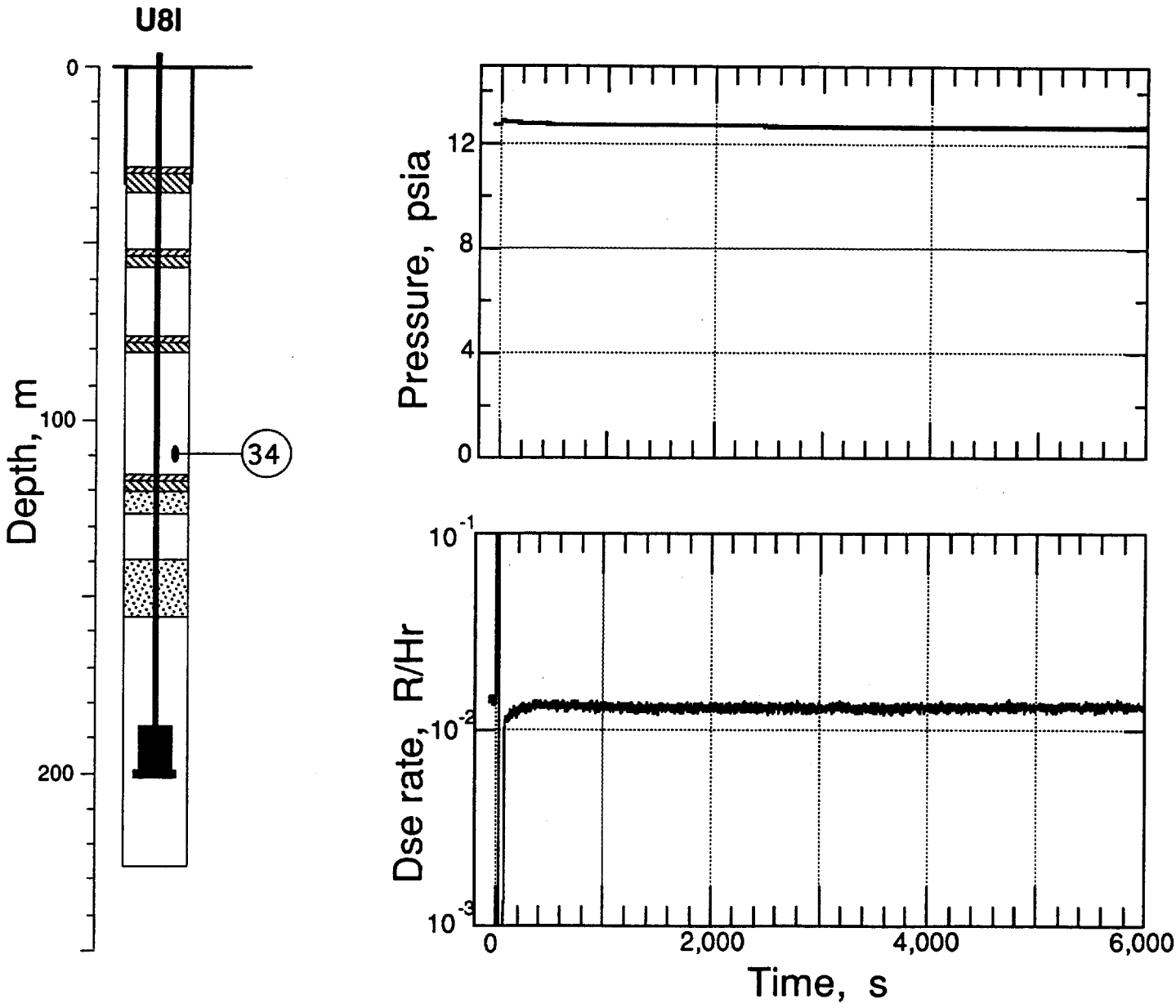

Figure 2.11 Pressure and radiation measured in the coarse stemming at 112.2 m depth (Station 34, above the deepest stemming plug 1).

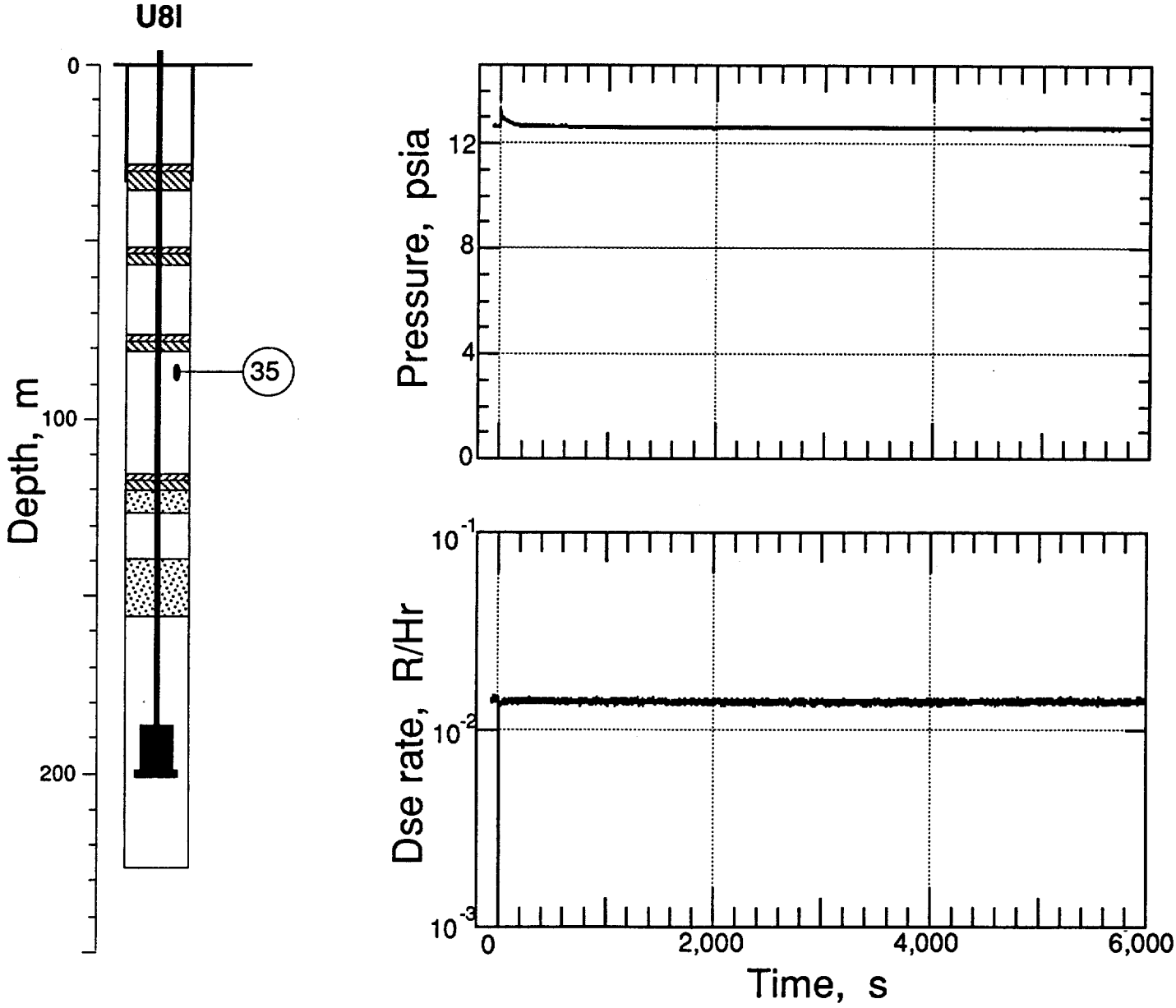

Figure 2.12 Pressure and radiation measured in the coarse stemming at 86.9 m depth (Station 35, below stemming plug 2).

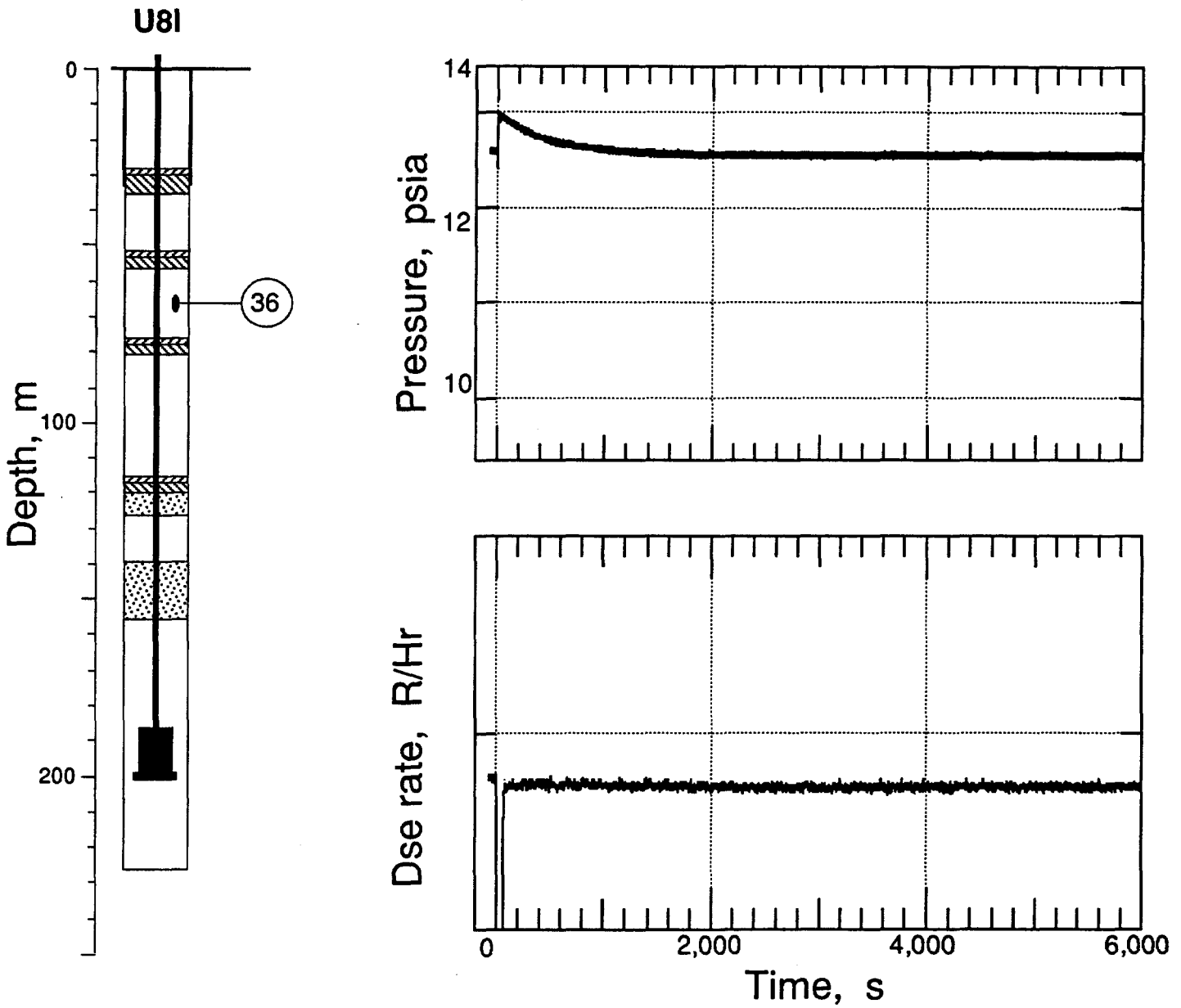

Figure 2.13 Pressure and radiation measured in the coarse stemming at 66.1 m depth (Station 36, between plugs 2 and 3).

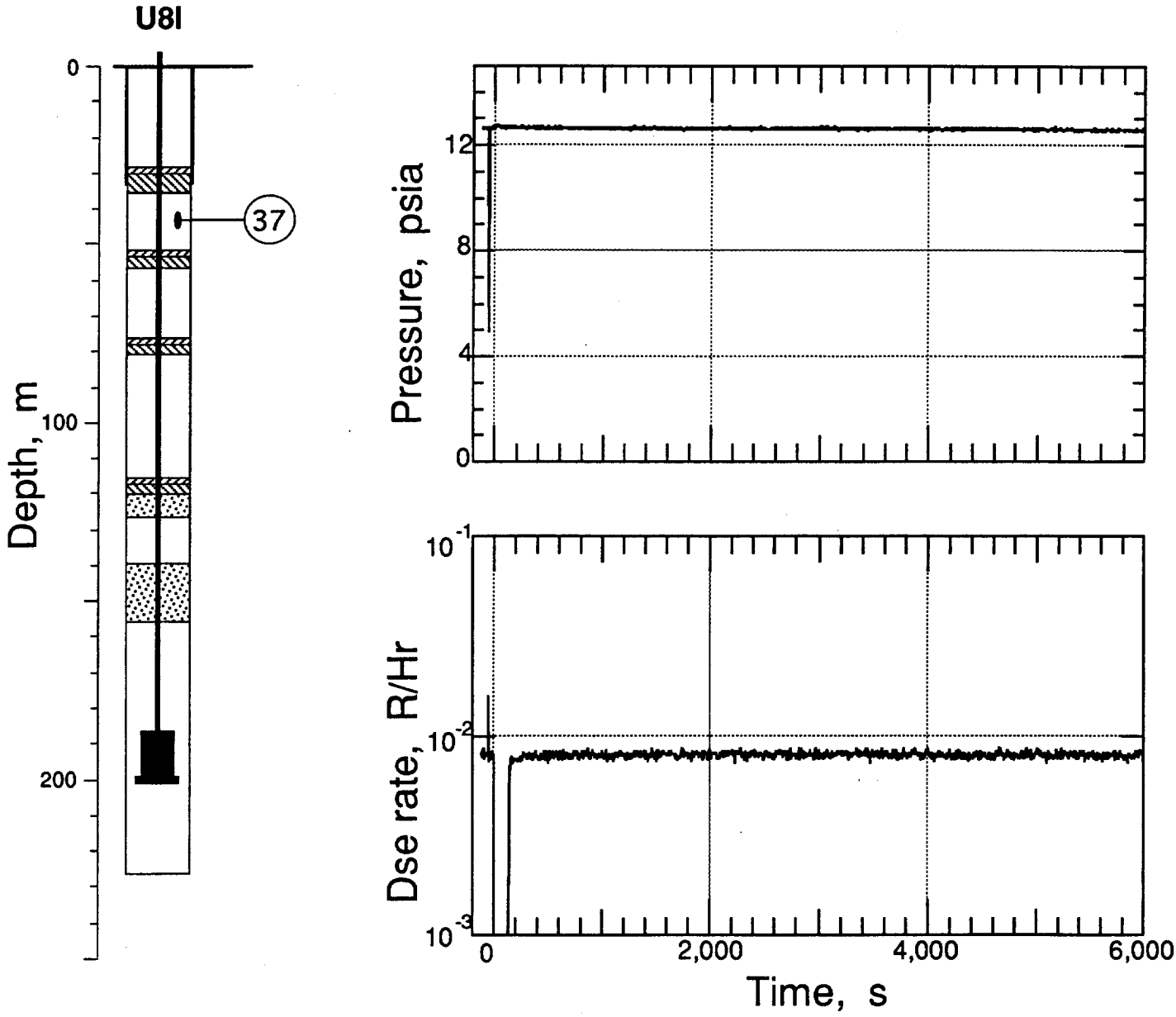

Figure 2.14 Pressure and radiation measured in the coarse stemming at 43.3 m depth (Station 37, about 8 m below the top plug).

2.3 Motion

Explosion-induced histories of the containment related motion measured on the SECO event are shown in figures 2.15-2.19. Characteristics of the associated motion and transducers are given in tables 2.1–2.3.

Two sets of arrivals are noted in table 2.1 for the down-hole motion stations. These are plotted in figure 2.20. The first, traveling at about 3.9 Km/s, is postulated to arise from motion in the emplacement pipe while the second arrival, traveling at about 1.6 Km/s, is close to the sound speed of the medium[1].

2.4 Collapse phenomena

No information is available from the CLIPER sensors and the D-cable data were not processed since it was clear to the experimenters that no containment problems occurred and analysis of the D-cable data would not be necessary. No motion in the bottom rigid plug (station 21) was detected during this time.

Pressure and radiation histories from stations 31 through 34 covering a period of 60 s beginning at 1940 s are shown in figures 2.21 - 2.24. At station 31 (figure 2.21) the pressure history is characteristic of a stemming fall while the radiation shows a slight increase at the beginning of the fall and a decrease and subsequent recovery during the drop. This suggests that the stemming acted as a radiation shield. At station 33 (figure 2.23) the radiation arrival was abrupt, occurring with the termination of the pressure drop. Since the pressure channel at station 32 (figure 2.22) was lost at early time, no comparison with the radiation history can be made for that station, however, the radiation arrival was also abrupt.

The radiation recovery history after collapse at stations 31 and 32 (figures 2.8 and 2.9) was not smooth, suggesting late time discontinuous adjustment of the stemming. At station 33 (figure 2.10) the history after collapse is smooth and reaches a higher level than the stations below it. This suggests that the stemming may have fallen away and left that station exposed to gasses percolating from the stemming column. No activity was seen at any station above the deepest rigid plug and only the station immediately above that plug is displayed (figure 2.24).

Table 2.1 Summary of Containment-Related Motion[a]

Gauge	Slant Range (m)	Arrival Time (ms)	Acceleration Peak (g)	Velocity Peak (m/s)	Displacement Peak (mm)	Displacement Residual (mm)
21av	81.43	20[b]	≥5.4[b], 5.2	0.21	6.9	(c)
21uv		20[b], 46	-	0.24	8.3	3.
22av	120.74	30[b], 70	2.1[b], 2.6	0.12	4.8	1.[d]
22uv		32[b], 74	-	0.17	3.35	1.
23av	145.14	36[b], 85	1.3[b], 1.8	0.11	3.7	1.1
23uv		37[b], 85	-	0.12	3.3	0.9
24av	167.08	42[b], 98	1.05	0.11	3.6	0.15
24uv		100	-	0.09	2.9	1.2
61av	199.36	132	1.2, 5.9[e]	0.21	6.9	-8
61uv[f]		-	-	-	-	-

(a) Peaks are first major peaks.
(b) Pipe-induced motion.
(c) Estimate.
(d) No estimate possible.
(e) Slap-down: Exceeded system limit.
(f) This transducer lost at detonation time.

Table 2.2 Containment-Related Accelerometer Characteristics

Gauge	Natural Frequency (Hz)	Damping Ratio	System Range (g's)
21av	230	0.70	6
22av	230	0.70	4
23av	225	0.75	2.4
24av	200	0.75	2.4
61av	260	0.65	4

Table 2.3 Containment-Related Velocimeter Characteristics

Gauge	Natural Frequency (Hz)	Time to 0.5 Amplitude (s)	Calibration Temperature (°F)	Operate Temperature (°F)	System Range (m/s)
21uv	3.00	31.6	75.20	79.98	3.
22uv	3.08	24.7	75.08	77.08	1.6
23uv	3.13	26.25	74.95	86.54	1.2
24uv	3.01	34.00	74.96	90.03	1.2
61uv	3.75	10.85	74.50	47.59	1.2

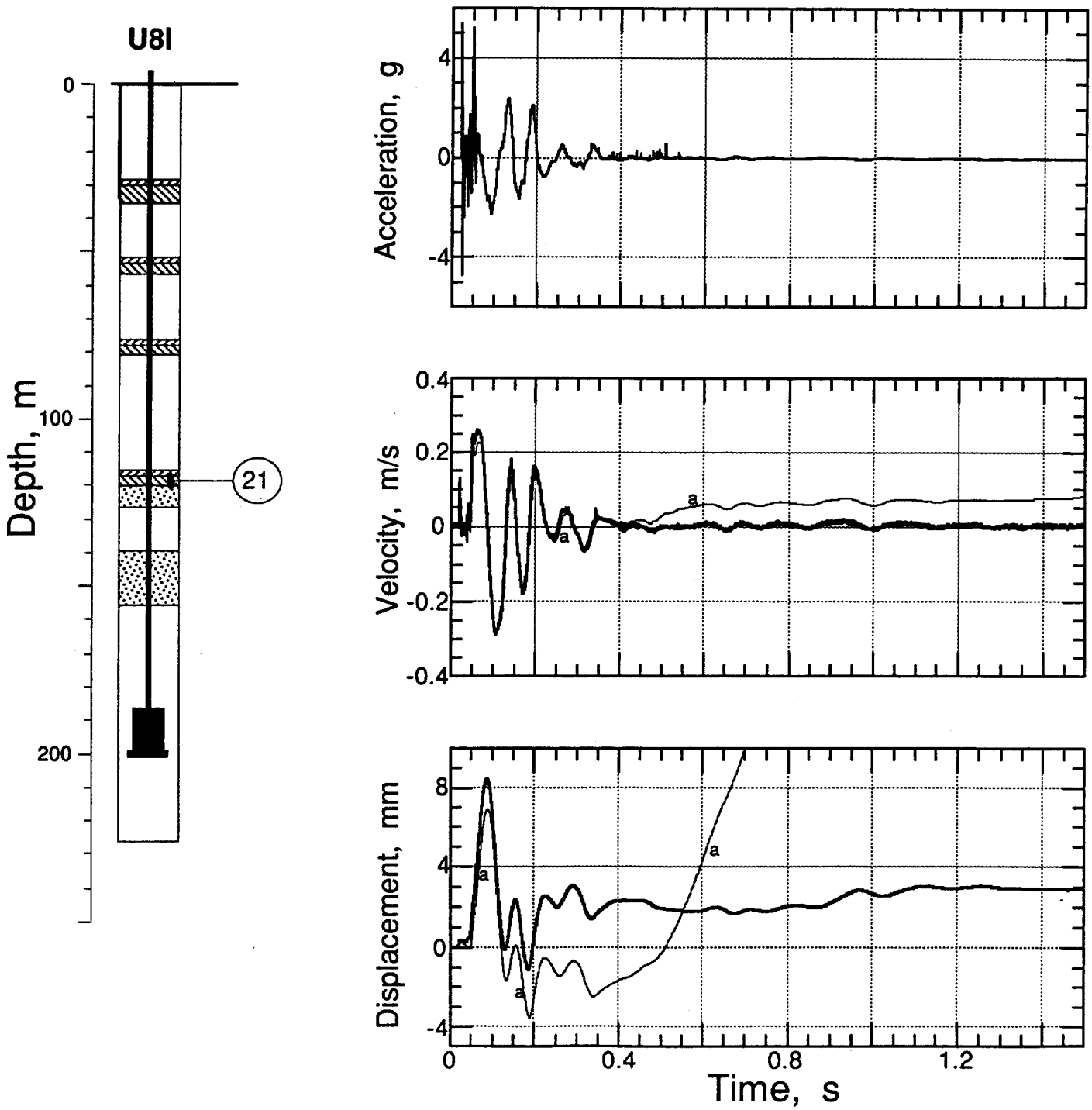

Figure 2.15 Explosion-induced vertical motion of the bottom stemming plug at a depth of 118.6 m (station 21). Traces annotated with "a" are derived from the accelerometer.

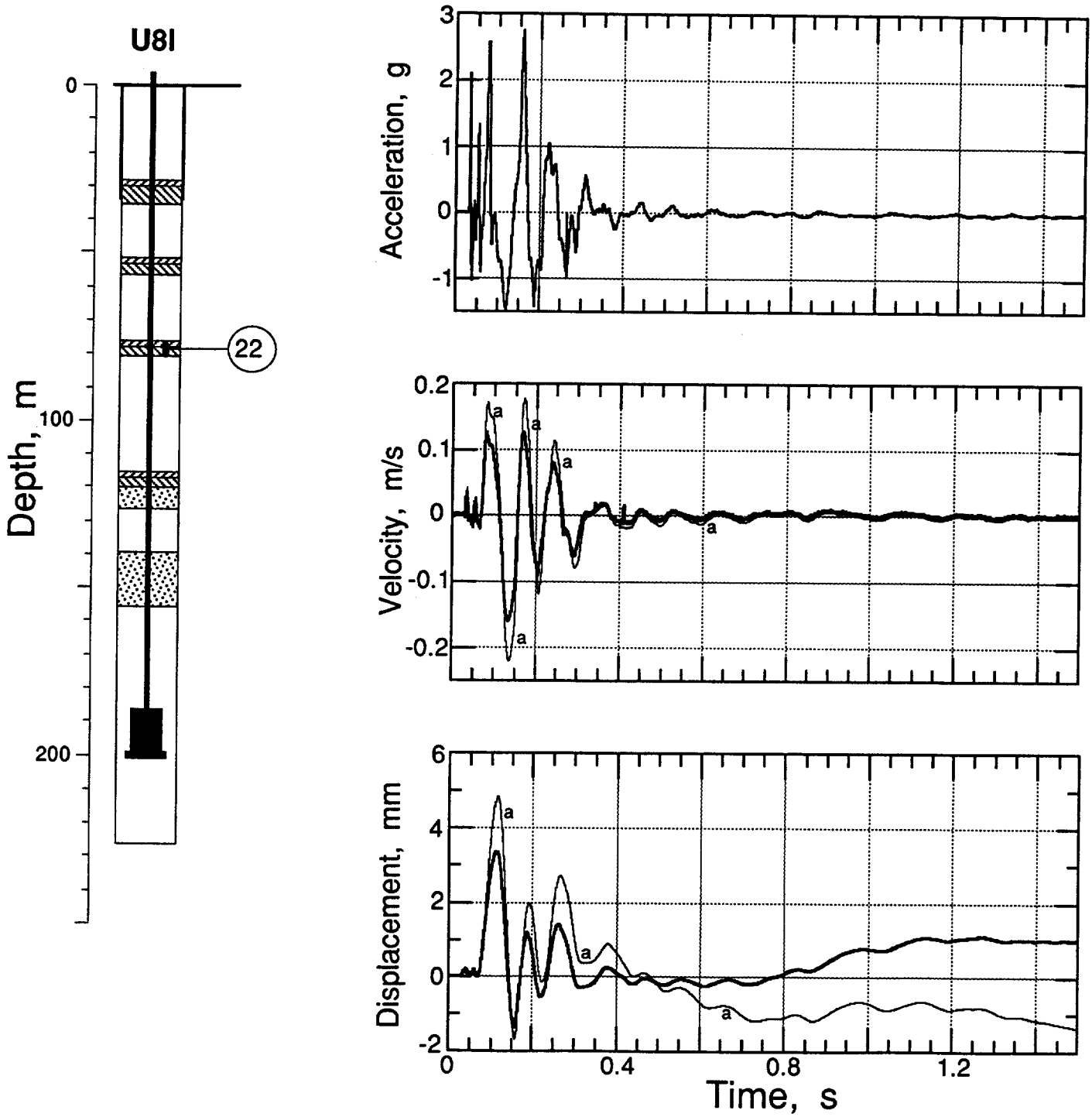

Figure 2.16 Explosion-induced vertical motion of stemming plug 2 at a depth of 79.3 m (station 22). Traces annotated with "a" are derived from the accelerometer.

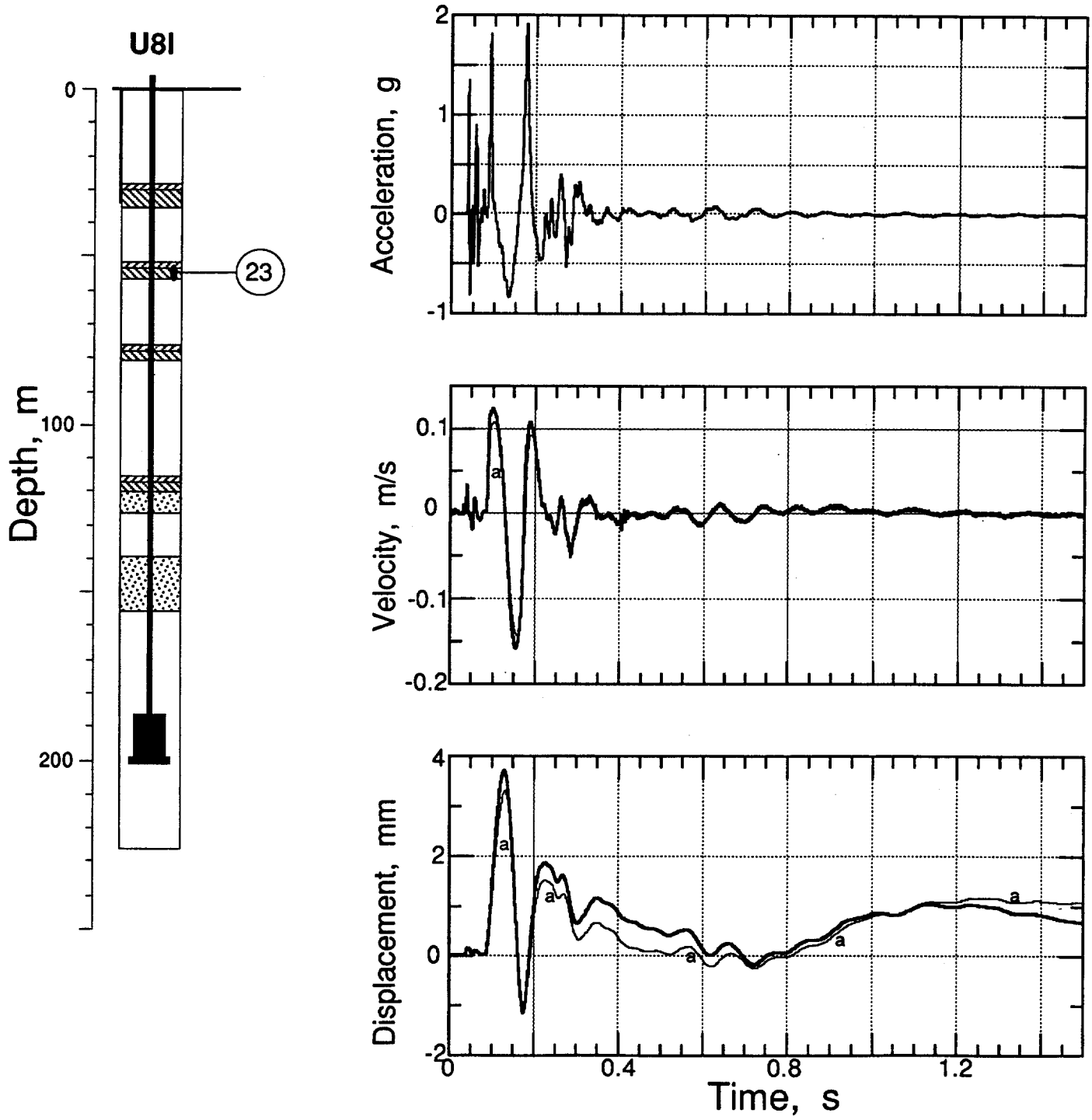

Figure 2.17 Explosion-induced vertical motion of plug 3 at a depth of 54.9 m (station 23). Traces annotated with "a" are derived from the accelerometer.

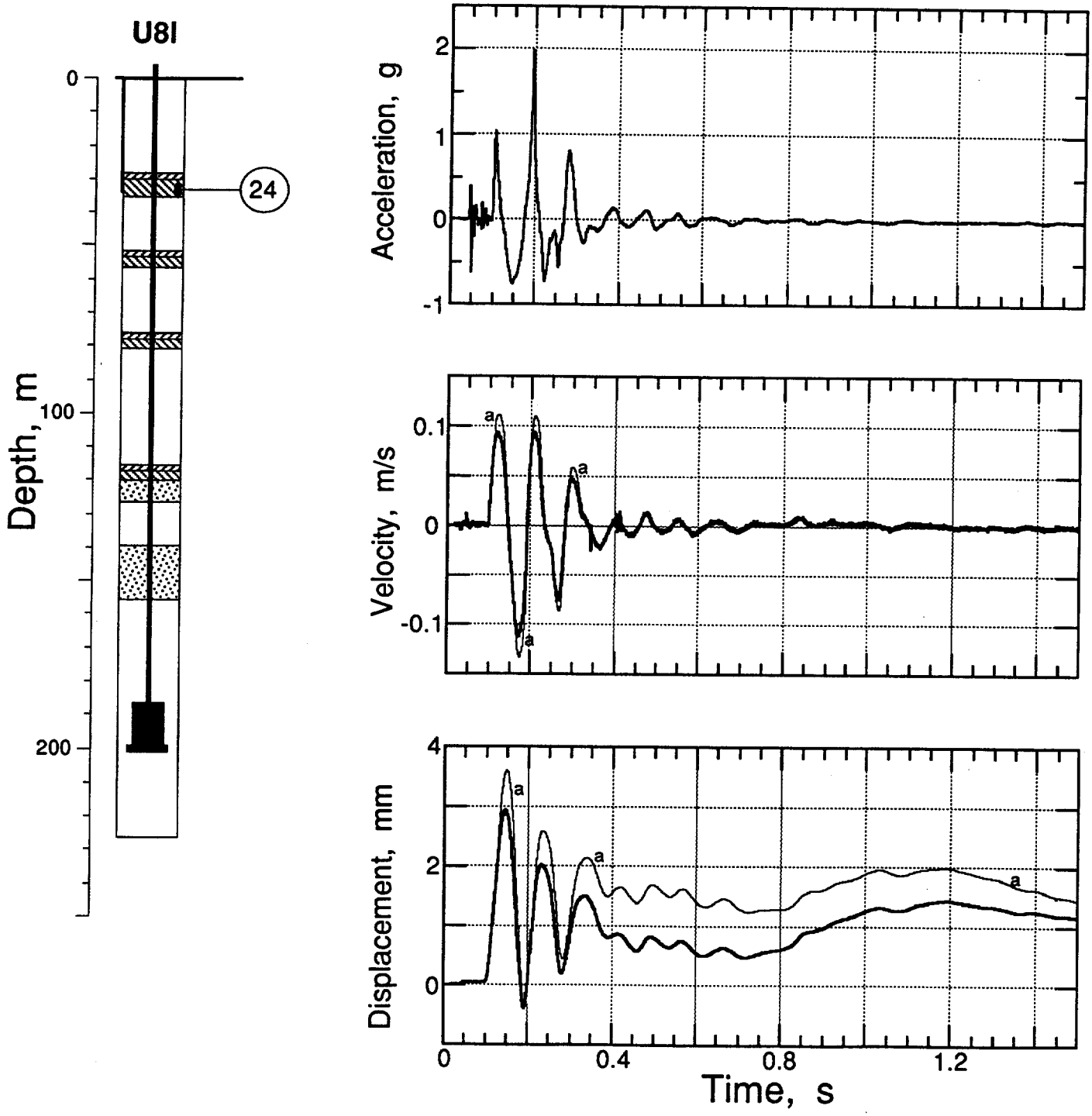

Figure 2.18 Explosion-induced vertical motion of top plug at a depth of 32.9 m (station 24). Traces annotated with "a" are derived from the accelerometer.

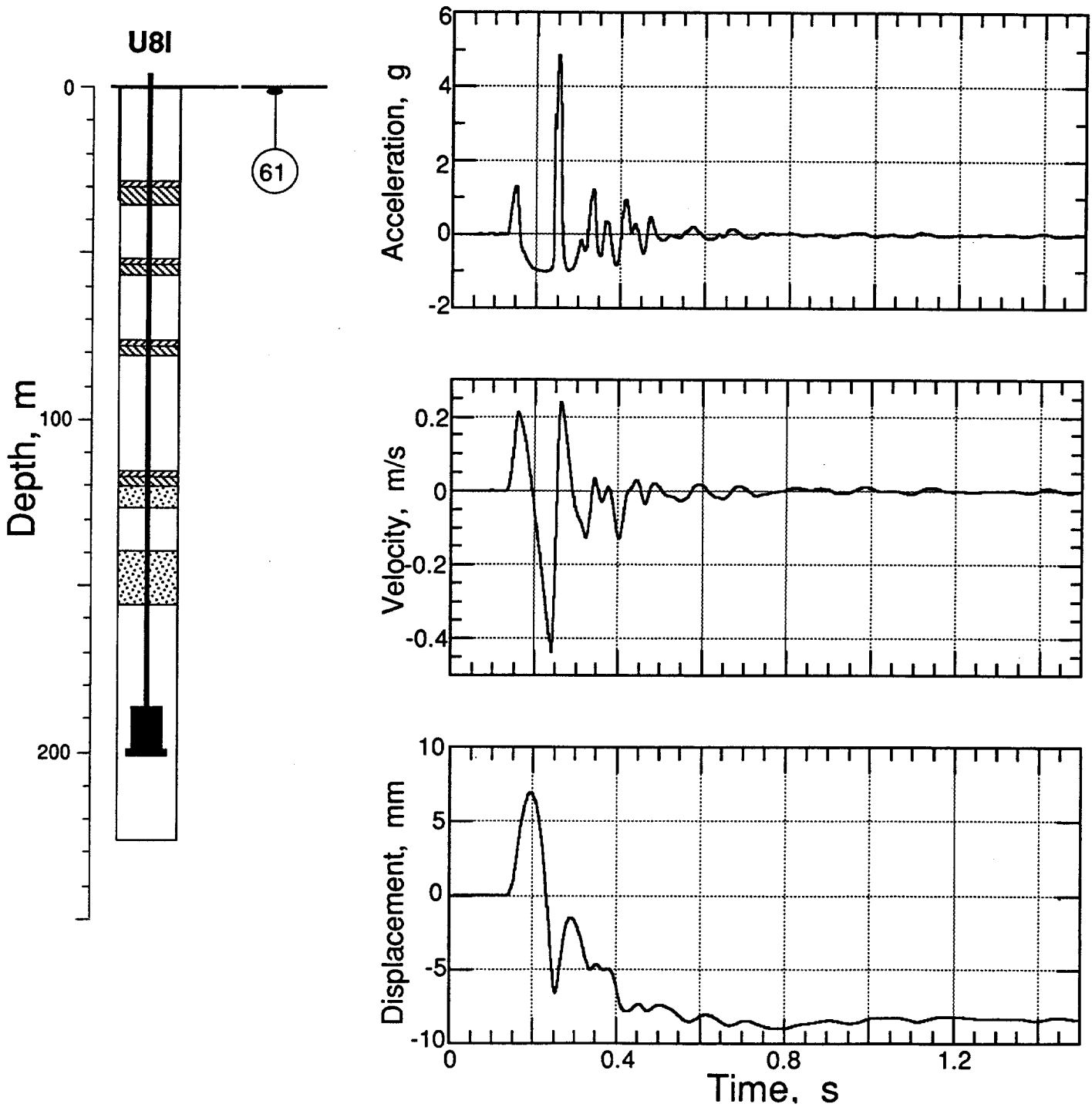

Figure 2.19 Explosion-induced vertical motion of the ground surface at a horizontal range of 15.24 m and a depth of 0.9 m (station 61). Data are derived from the accelerometer only; the velocimeter was inoperative.

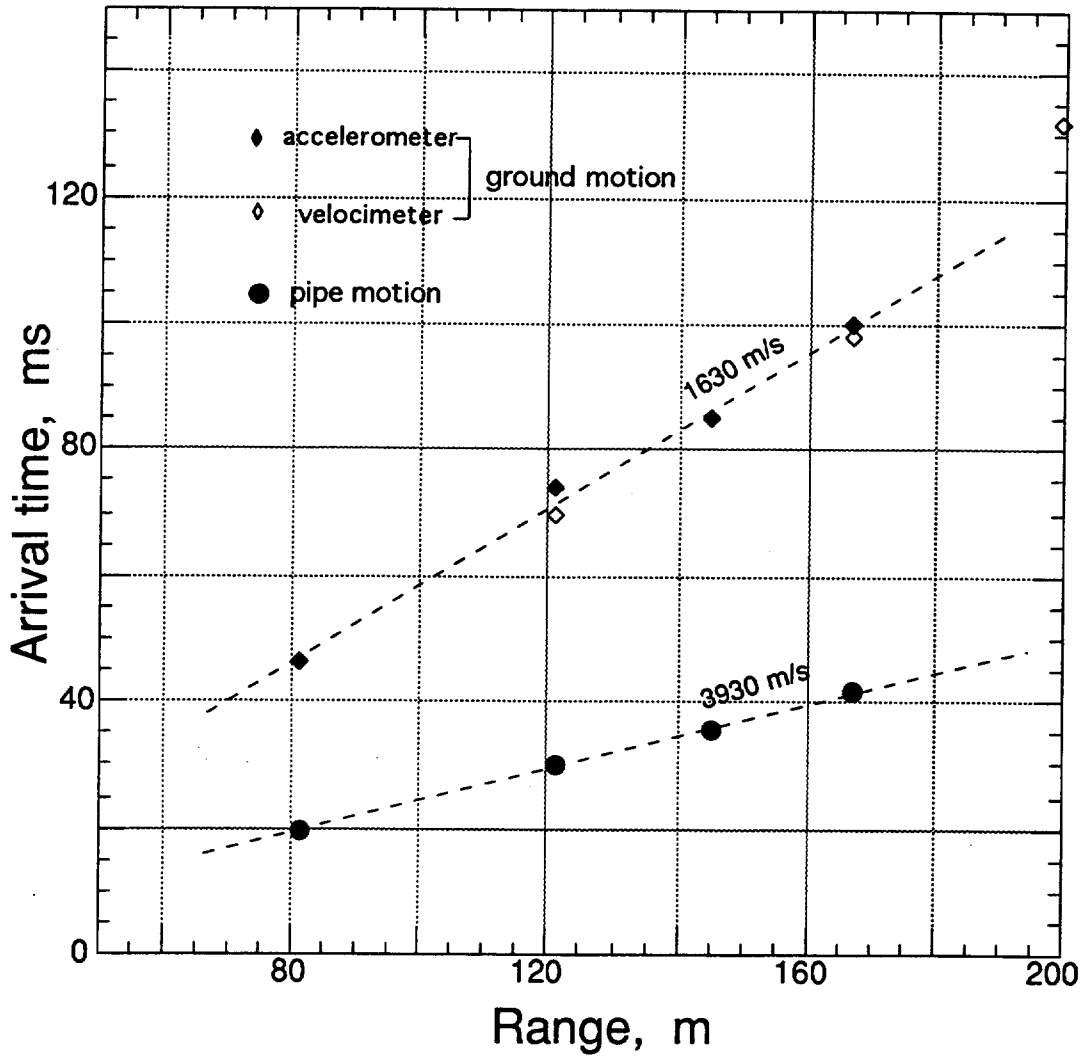

Figure 2.20 First motion arrivals as a function of range for stations in the stemming and at ground zero.

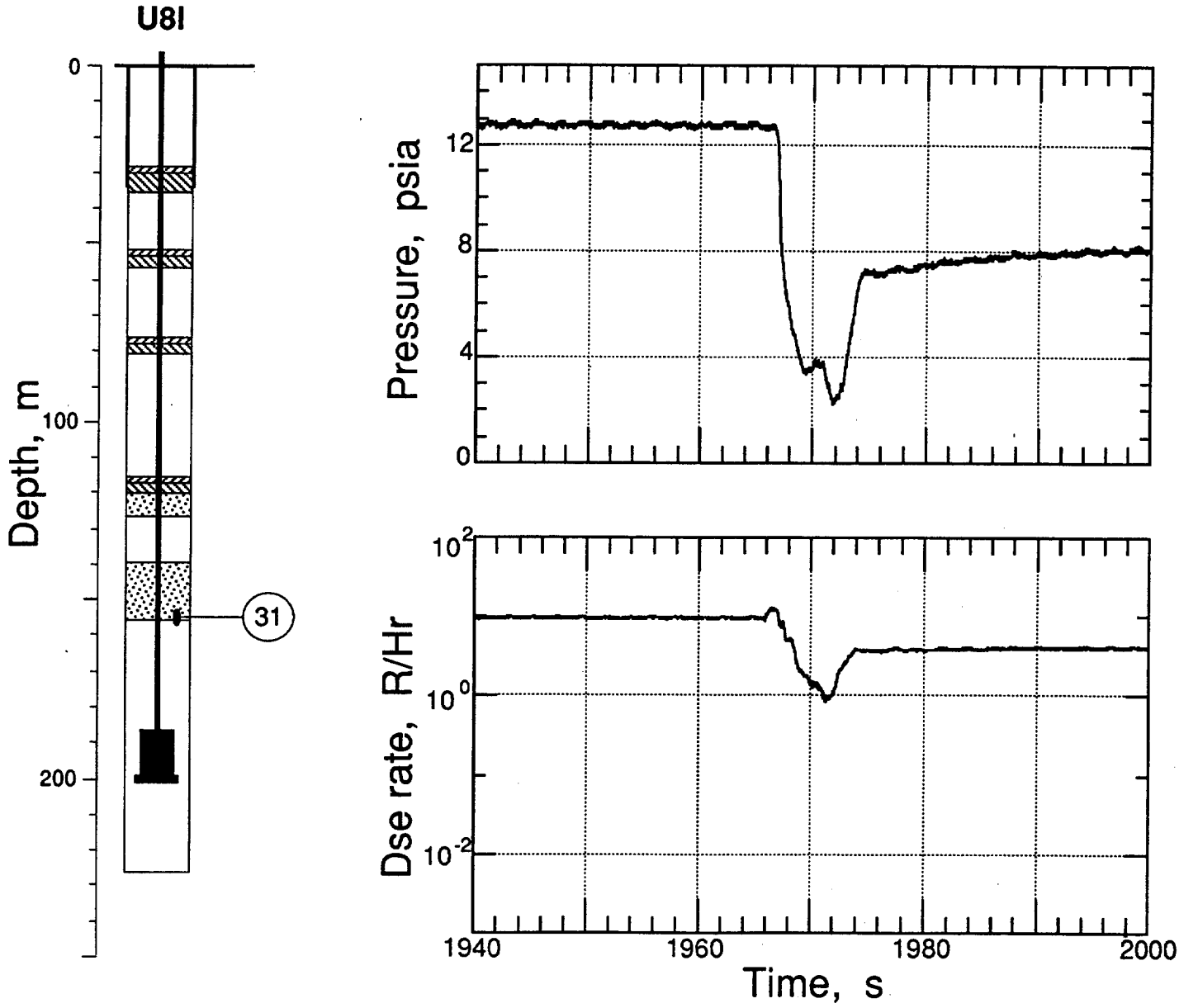

Figure 2.21 Pressure and radiation measured in the coarse stemming at 154.8 mm depth (Station 31, below the deep fines layer). Time interval includes the occurrence of a subsurface stemming fall or collapse.

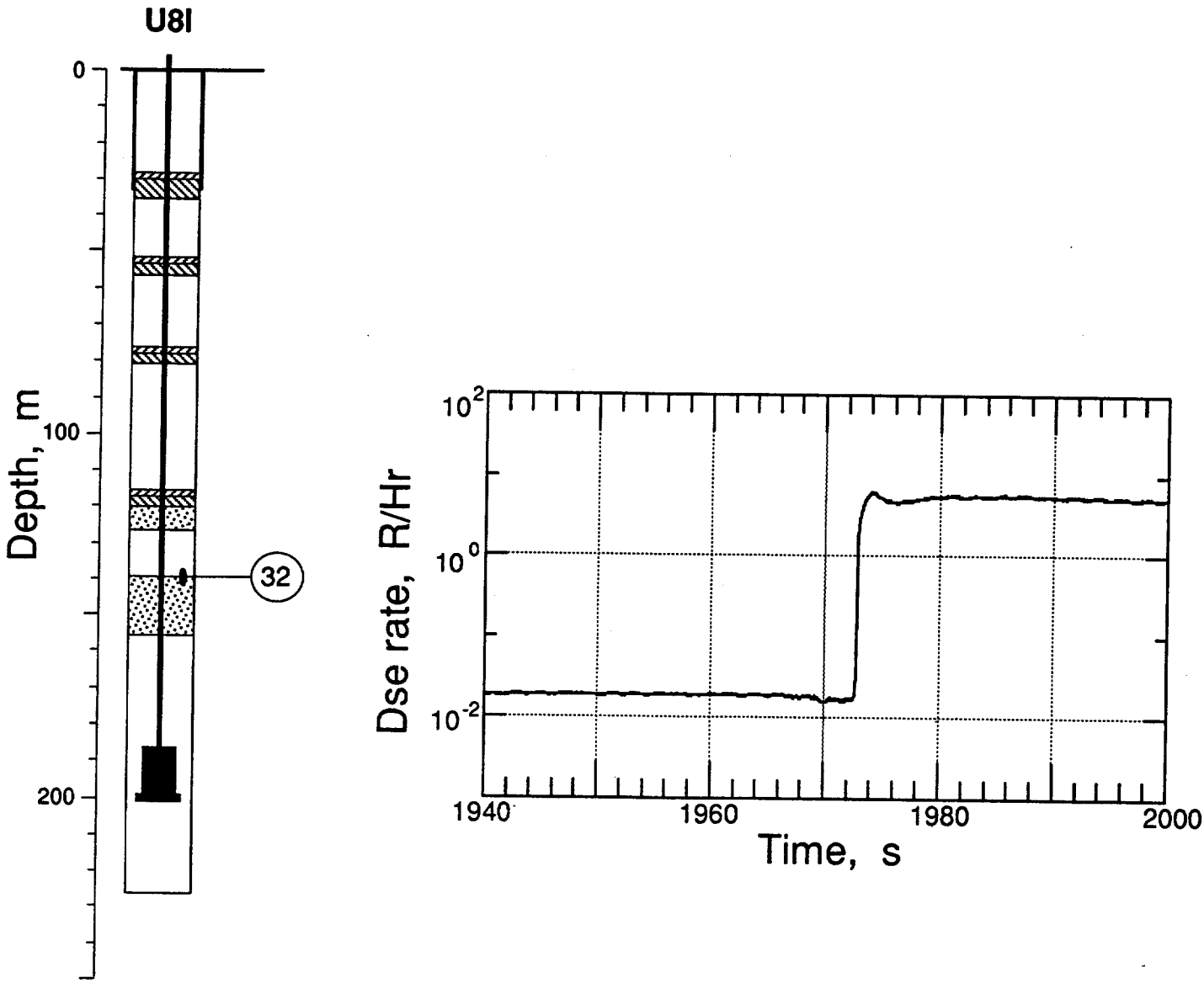

Figure 2.22 Pressure and radiation measured in the coarse stemming at 139.6 m depth (Station 32, above the deep fines layer). The pressure transducer was lost about 25 ms after detonation, the approximate time of shock arrival. Time interval includes the occurrence of a subsurface stemming fall or collapse.

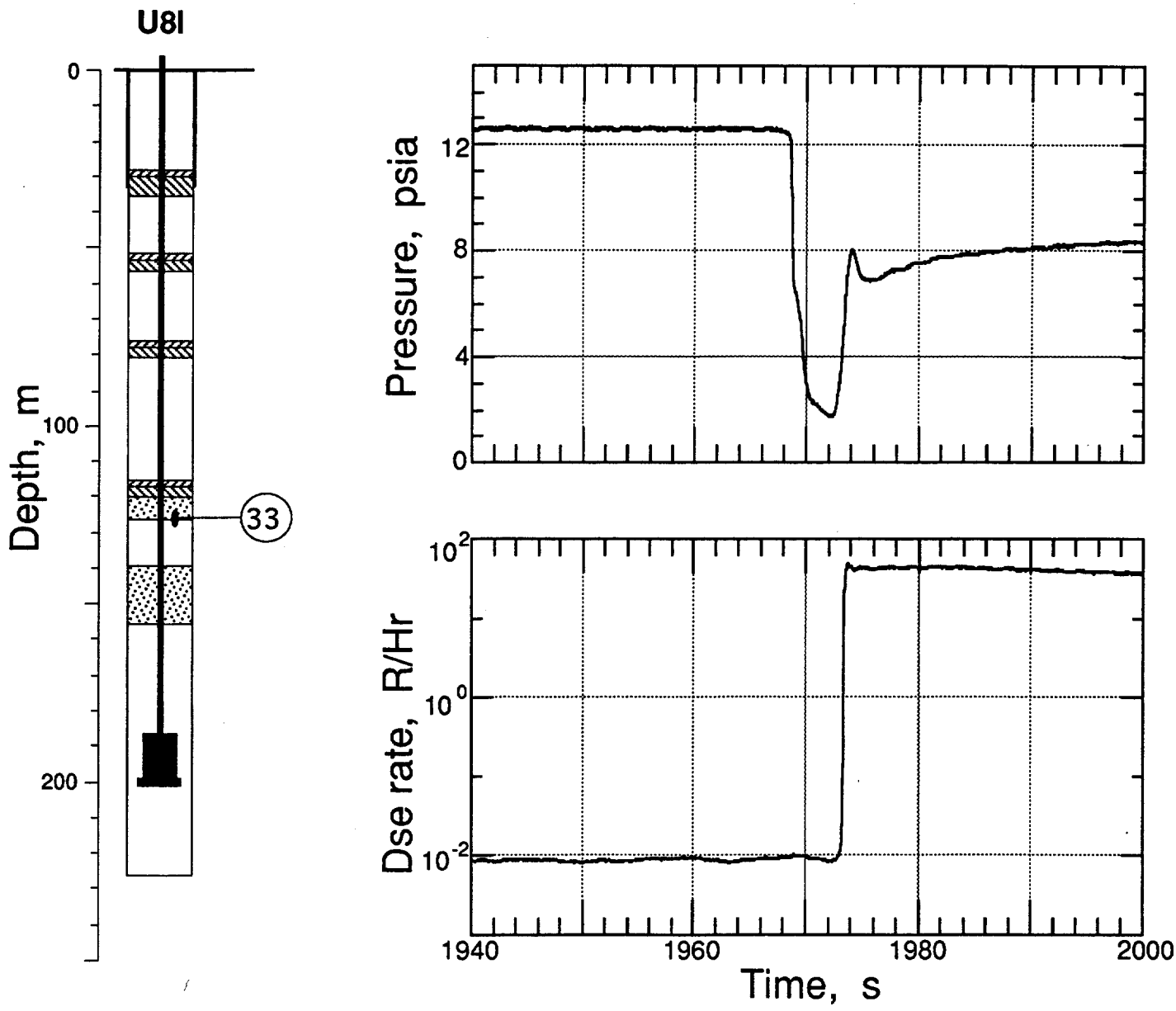

Figure 2.23 Pressure and radiation measured in the coarse stemming at 126.2 m depth (Station 33, below the deepest stemming plug 1). Time interval includes the occurrence of a subsurface stemming fall or collapse.

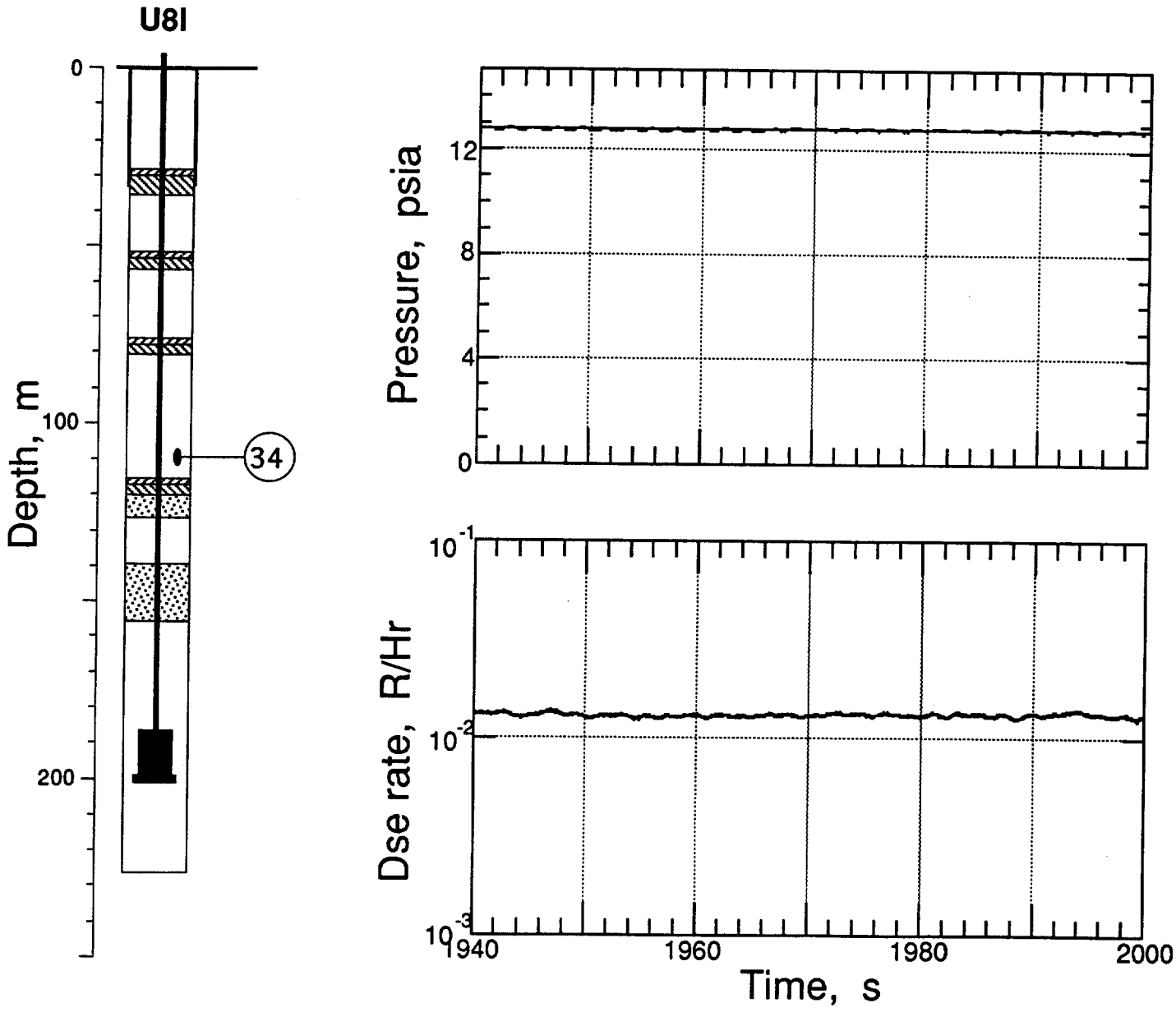

Figure 2.24 Pressure and radiation measured in the coarse stemming at 112.2 m depth (Station 34, above the deepest stemming plug 1). Time interval includes the occurrence of a subsurface stemming fall or collapse.

3. Surface array measurements

As noted earlier, the purpose of these surface array measurements was to use a nuclear event as the source for a coarse, single-ended seismic survey through the faults exposed by the event DISCUS THROWER executed in hole U8a. A surface map showing the location of the surface array, hole U8a and four other subsequent events (including SECO and VIDE) is presented in figure 3.1. Figures 3.2 - 3.27 show the motion obtained from the surface array The first station was at a horizontal range of 300 m from U8k with each succeeding station 60 m farther along. All stations were buried 0.91 m in the ground surface. Four of the fourteen stations included tri-axial motion measurements (vertical, horizontal-radial, and horizontal-transverse) and an additional four included bi-axial measurements (vertical and horizontal-radial). Positive sense motion was vertical, radial outward, and clockwise looking down on the station. Tables 3.1 - 3.3 summarize the motion and the motion transducer properties.

The four stations containing triaxial motions transducers were computationally rotated (about the vertical axis) to obtain the radial and transverse motion with respect to hole U8l resulting in the eight motion histories shown in figures 3.28 - 3.35. Values of the resulting peak motions are given in table 3.2. Displacement trajectories in the horizontal plane are shown in figures 3.36 - 3.39.

First arrivals of the motion are plotted in figure 3.40 while figures 3.41 and 3.42 show the peak acceleration and velocity as a function of range from the detonation point. Both vertical and horizontal- radial motion are represented in figures 3.40 - 3.42.

Table 3.1 Summary of Surface Array Motion[a]

Gauge	Slant Range (m)	Arrival Time (ms)	Acceleration Peak (g)	Velocity Peak (cm/s)	Displacement Peak (mm)
62ar[b]	508.5	329	0.18	3.2	1.15
62at[b]		327	-0.042	0.88	-0.27
62av		326	0.16	3.0	0.80
62uv		330	-	3.1	0.85
63av	522.3	332	0.12	2.2	0.72
63uv		331	-	2.3	0.72
64ar[b]	542.4	338	0.063	1.4	0.42
64av		338	0.096	1.9	0.56
64uv		345	-	2.2	0.58
65av	568.4	351	0.095	1.8	0.53
65uv		352	-	2.0	0.57
66ar[b]	599.1	360	0.11	3.3	0.90
66at[b]		368	-0.01	0.63	-0.05
66av		360	0.057	1.3	0.38
66uv		368	-	1.9	0.61
67ar[a]	634.3	387	0.075	2.0	0.65
67av		383	0.044	1.1	0.37
67uv		390	-	1.3	0.43
68ar[b]	672.7	405	0.060	1.8	0.62
68av		405	0.035	1.2	0.35
68uv		412	-	1.0	0.31
69av	714.6	430	0.048	1.1	0.34
69uv		433	-	1.2	0.034

Table 3.1 Summary of Surface Array Motion (continued)

Gauge	Slant Range (m)	Arrival Time (ms)	Acceleration Peak (g)	Velocity Peak (cm/s)	Displacement Peak (mm)
70ar[b]	758.9	454	0.080	2.2	0.75
70at[b]		453	0.016	0.42	0.14
70av		457	0.048	1.1	0.30
70uv		465	-	0.96	0.39
71av	804.4	485	0.047	1.2	0.35
71uv		495	-	1.4	0.50
72ar[b]	852.7	515	0.047	1.3	0.44
72av		513	0.047	1.2	0.34
72uv		515	-	1.1	0.34
73av	901.8	535	0.031	0.83	0.29
73uv		538	-	0.87	0.31
74ar[b]	952.6	565	0.046	0.017	0.56
74at[b]		565	0.022	0.02	0.20
74av		562	0.047	0.78	0.27
74uv		570	-	0.85	0.31
75av	1004.3	591	0.028	0.75	0.27
75uv		590	-	0.80	0.30

(a) Peaks are first major peaks.

(b) These data were measured in a coordinate system relative to a radius vector 30 degrees North of West extending from hole U8k with transverse being horizontal, normal to this direction in a left-handed system.

Table 3.2 Summary of Surface Motion[a] Horizontal Components Rotated Relative to Hole U8l[b]

Gauge	Slant Range (m)	Arrival Time (ms)	Acceleration Peak (g)	Velocity Peak (cm/s)	Displacement Peak (mm)	Rotation (degrees)
62ar'	508.5	360	0.11	3.6	1.1	79.79
62at'		330	-0.042	-0.85	-0.27	
66ar'	599.1	360	0.11	2.8	0.90	54.94
66at'		365	-.0.008	-0.15	-0.032	
70ar'	758.9	450	0.082	2.2	0.75	39.26
70at'		450	0.016	0.44	0.15	
74ar'	952.6	565	0.047	1.4	0.55	29.82
74at'		560	0.020	0.57	0.18	

(a) Peaks are first major peaks.
(b) Rotation angle is positive in counter-clockwise direction. This is the angle through which the measurement coordinate system must be rotated (about a vertical axis) to yield radial and transverse motions relative to hole U8l.

Table 3.3 Surface Array Accelerometer Characteristics

Gauge	Natural Frequency (Hz)	Damping Ratio	System Range (g's)
62av	150	0.65	3
62ar	280	0.60	3
62at	140	0.75	3
63av	142	0.65	3
64av	251	0.75	3
64ar	239	0.65	3
65av	210	0.75	3
66av	240	0.65	3
66ar	262	0.65	3
66at	269	0.60	3
67av	270	0.85	3
67ar	200	0.65	3
68av	178	0.65	2
68ar	74	0.65	2
69av	170	0.65	2
70av	118	0.65	2
70ar	70	0.65	2
70at	140	0.75	2
71av	141	0.65	2
72av	112	0.70	1
72ar	110	0.65	1
73av	132	0.65	1
74av	74	0.65	1
74ar	108	0.65	1
74at	120	0.65	1
75av	68	0.65	1

Table 3.4 Surface Array Velocimeter Characteristics

Gauge	Natural Frequency (Hz)	Time to 0.5 Amplitude (s)	Calibration Temperature (°F)	Operate Temperature (°F)	System Range (m/s)
62uv	3.55	9.5	74.2	52.24	1
63uv	3.40	9.4	75.4	52.24	1
64uv	3.60	13.9	74.5	52.46	1
65uv	3.49	12.7	74.7	52.01	1
66uv	3.62	12.8	74.5	51.78	1
67uv	3.50	11.9	73.5	51.33	1
68uv	3.31	15.2	73.7	51.33	1
69uv	3.28	19.3	73.8	52.69	1
70uv	3.25	25.0	75.1	52.46	1
71uv	3.43	13.4	73.7	52.24	1
72uv	3.46	13.2	72.8	52.69	1
73uv	3.62	10.9	73.5	53.14	1
74uv	3.51	10.8	73.8	52.19	1
75uv	3.24	22.5	74.3	53.80	1

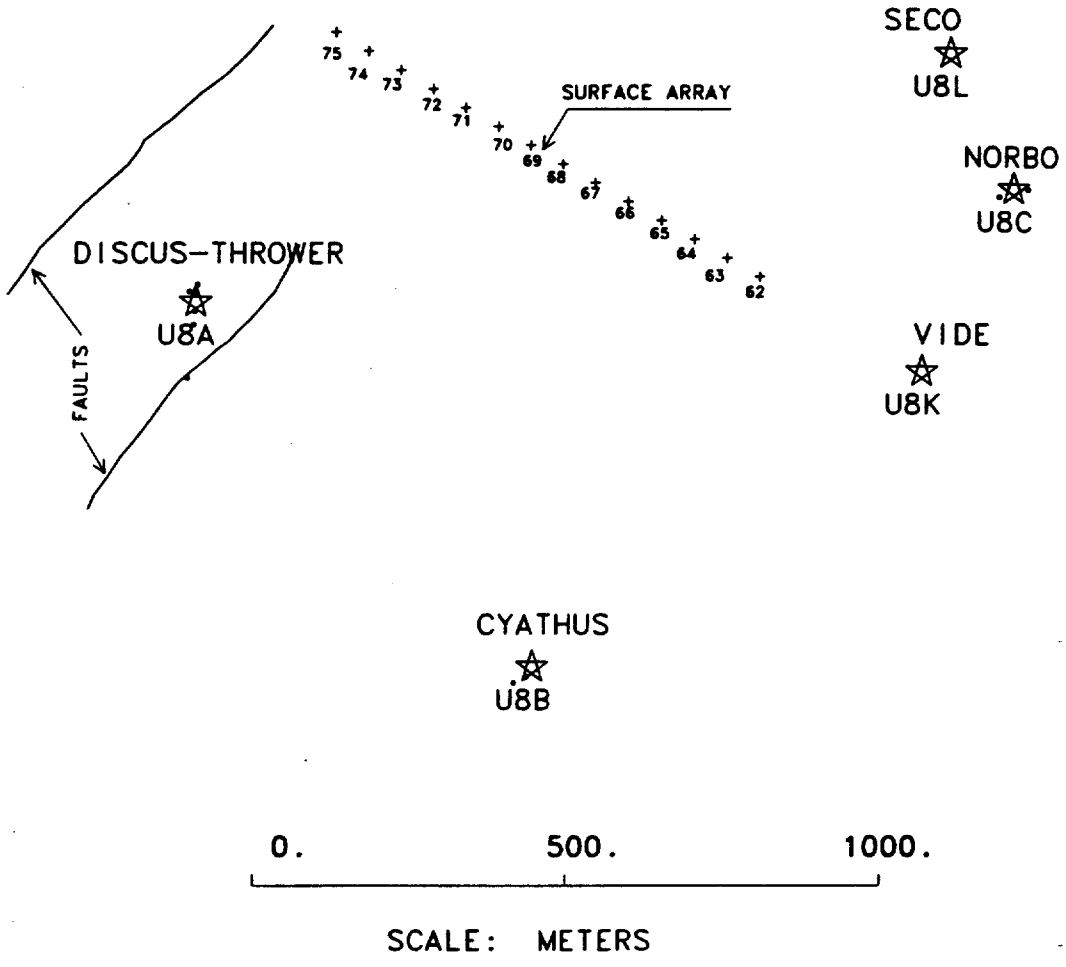

Figure 3.1 Surface map of local area of Hole U8I showing transducer array, fault system and other holes.

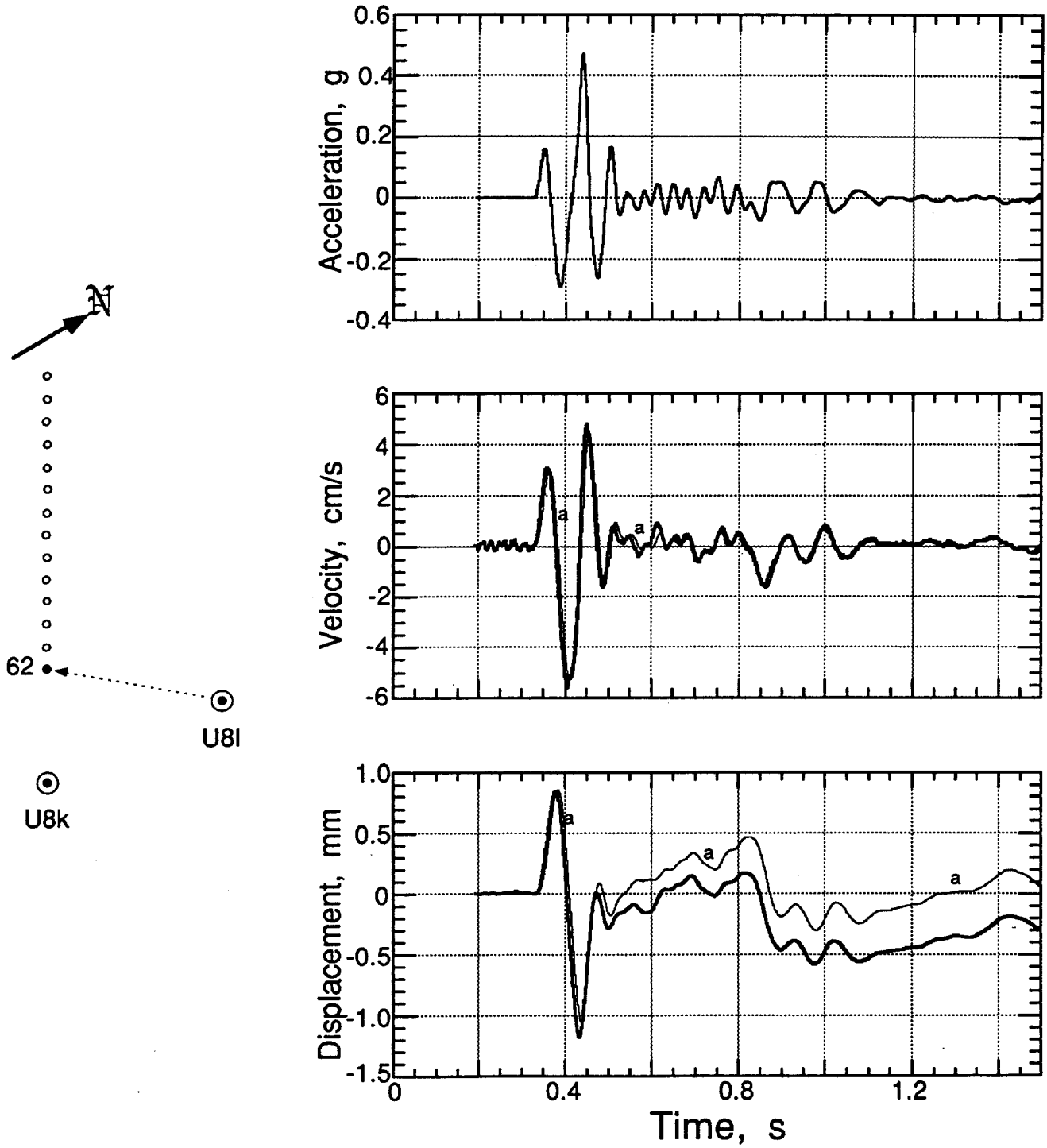

Figure 3.2 Vertical motion of the ground surface at a slant range of 508.5 m and a depth of 0.91 m (station 62). Traces annotated with "a" are derived from the accelerometer.

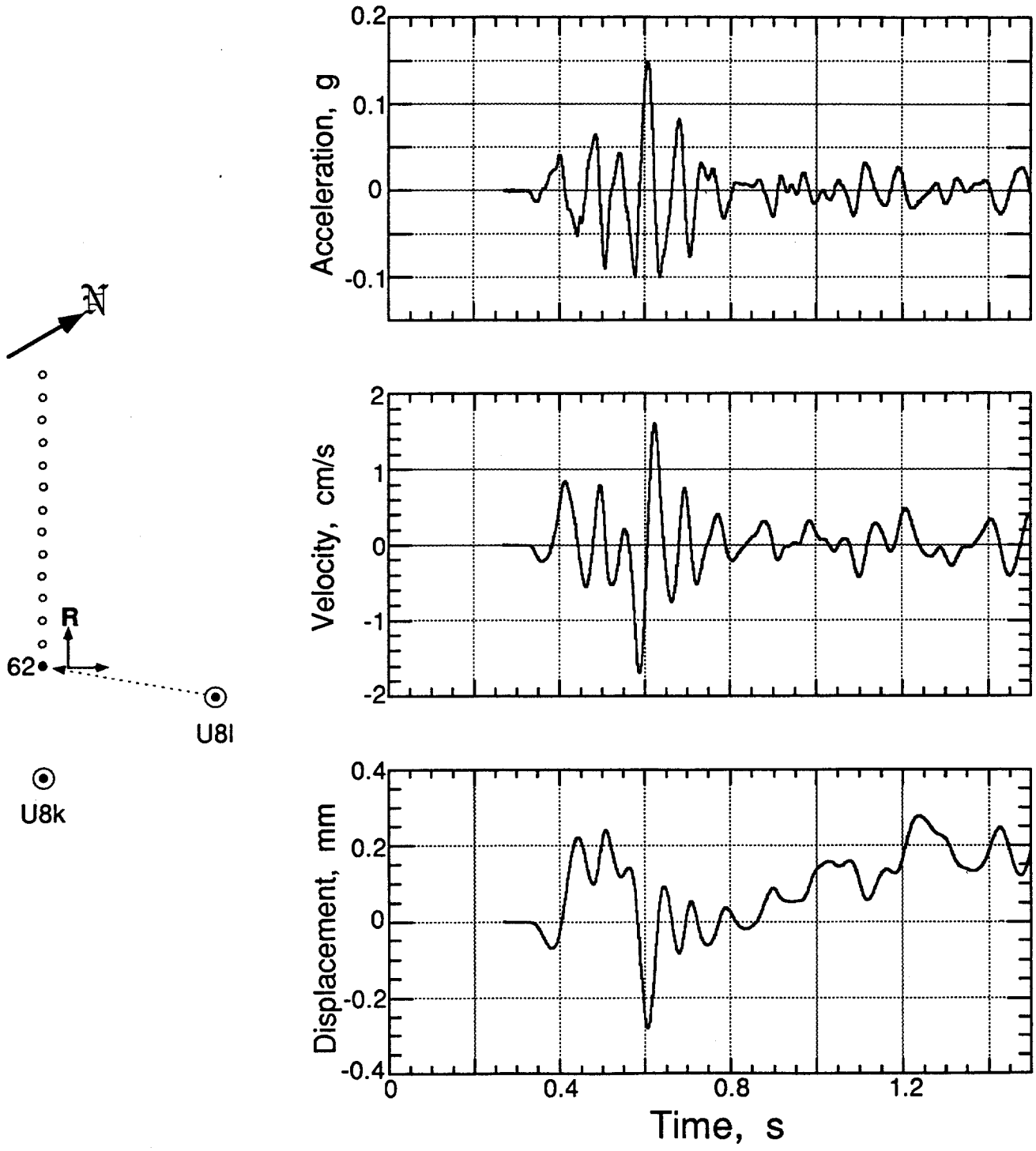

Figure 3.3 Horizontal-radial motion of the ground surface at a slant range of 508.5 m and a depth of 0.91 m (station 62). Motion is positive in a direction [W 30 N].

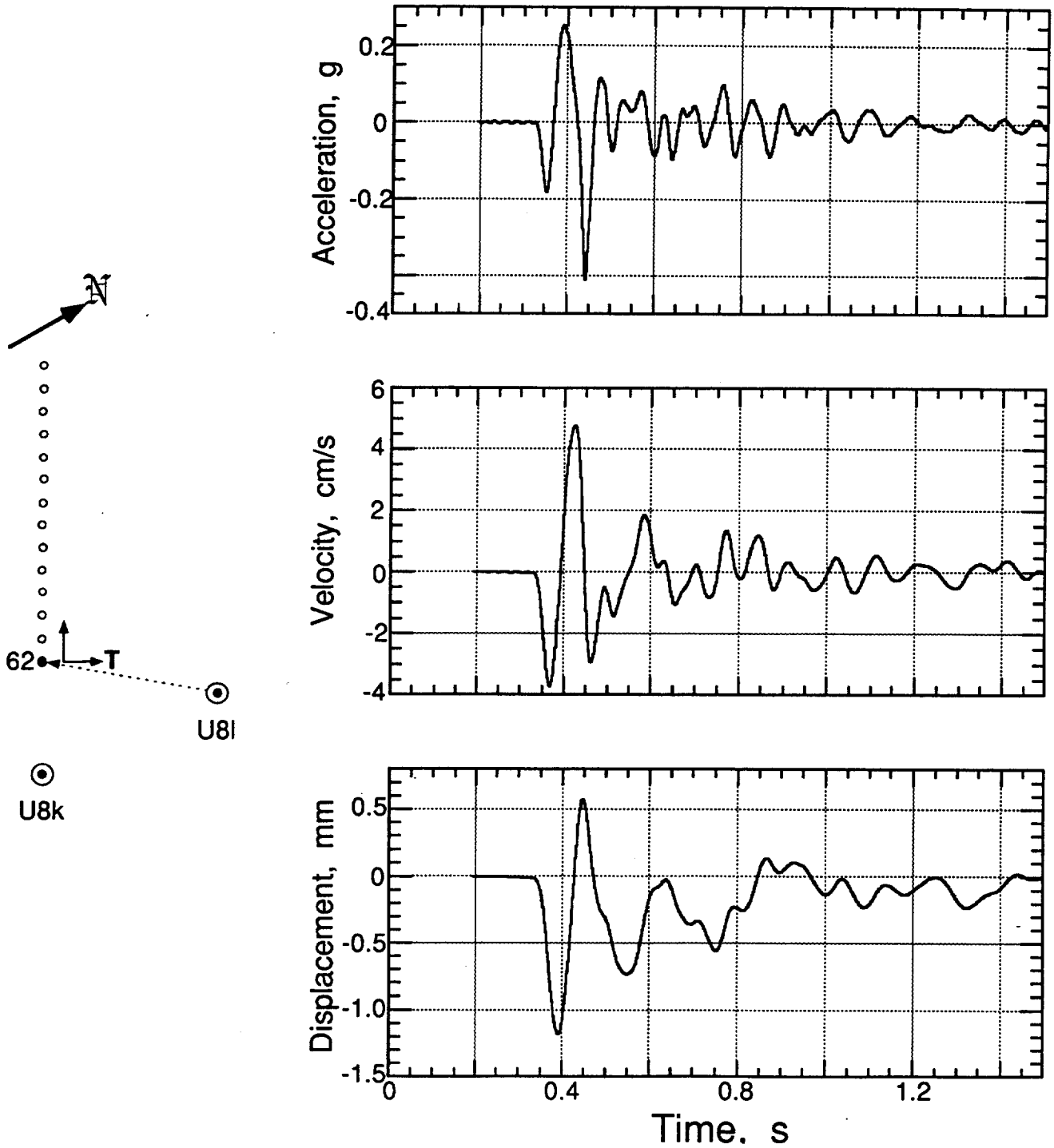

Figure 3.4 Horizontal-transverse motion of the ground surface at a slant range of 508.5 m and a depth of 0.91 m (station 62). Motion is positive in a direction [N 30 E].

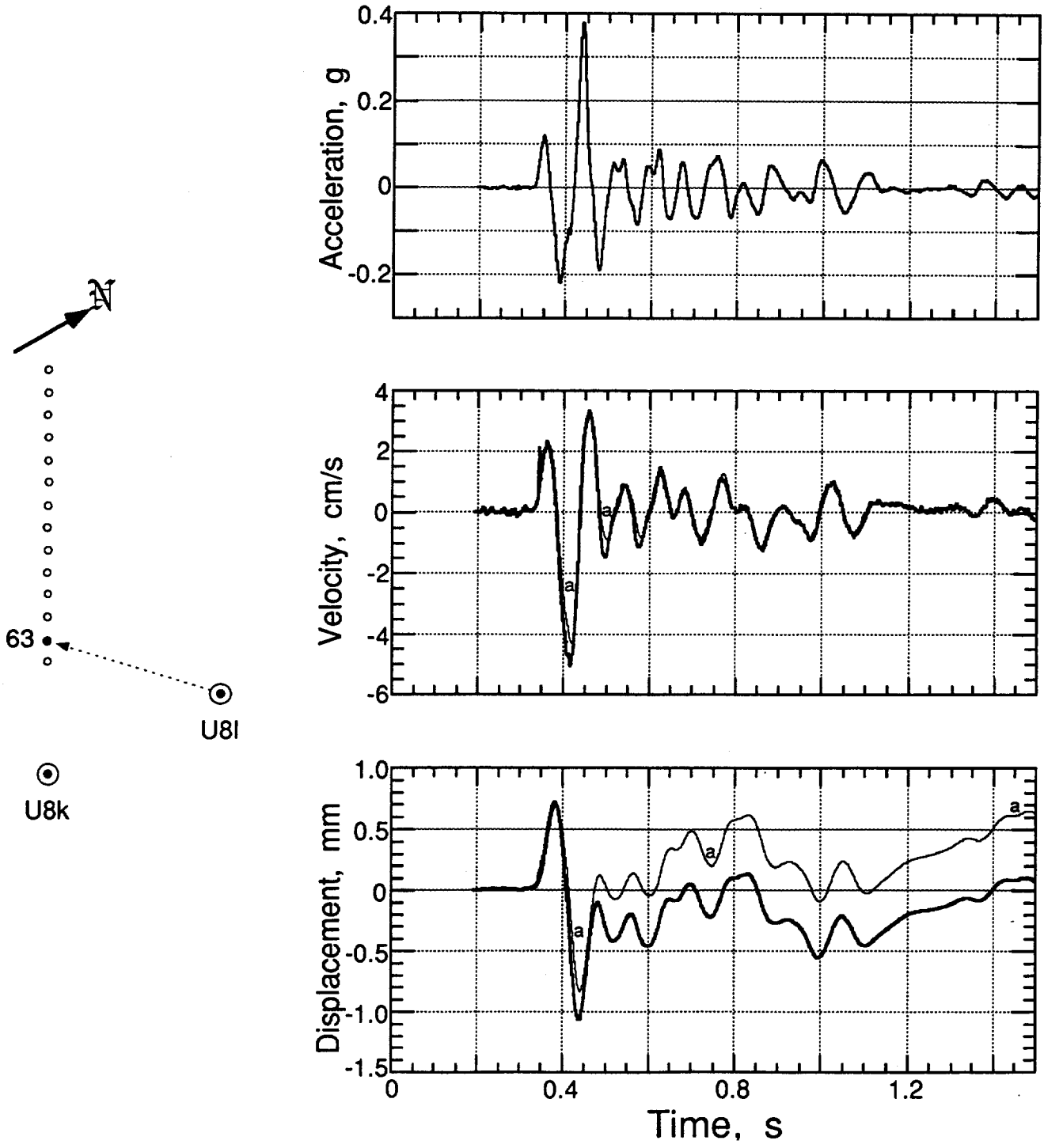

Figure 3.5 Vertical motion of the ground surface at a slant range of 522.3 m and a depth of 0.91 m (station 63). Traces annotated with "a" are derived from the accelerometer.

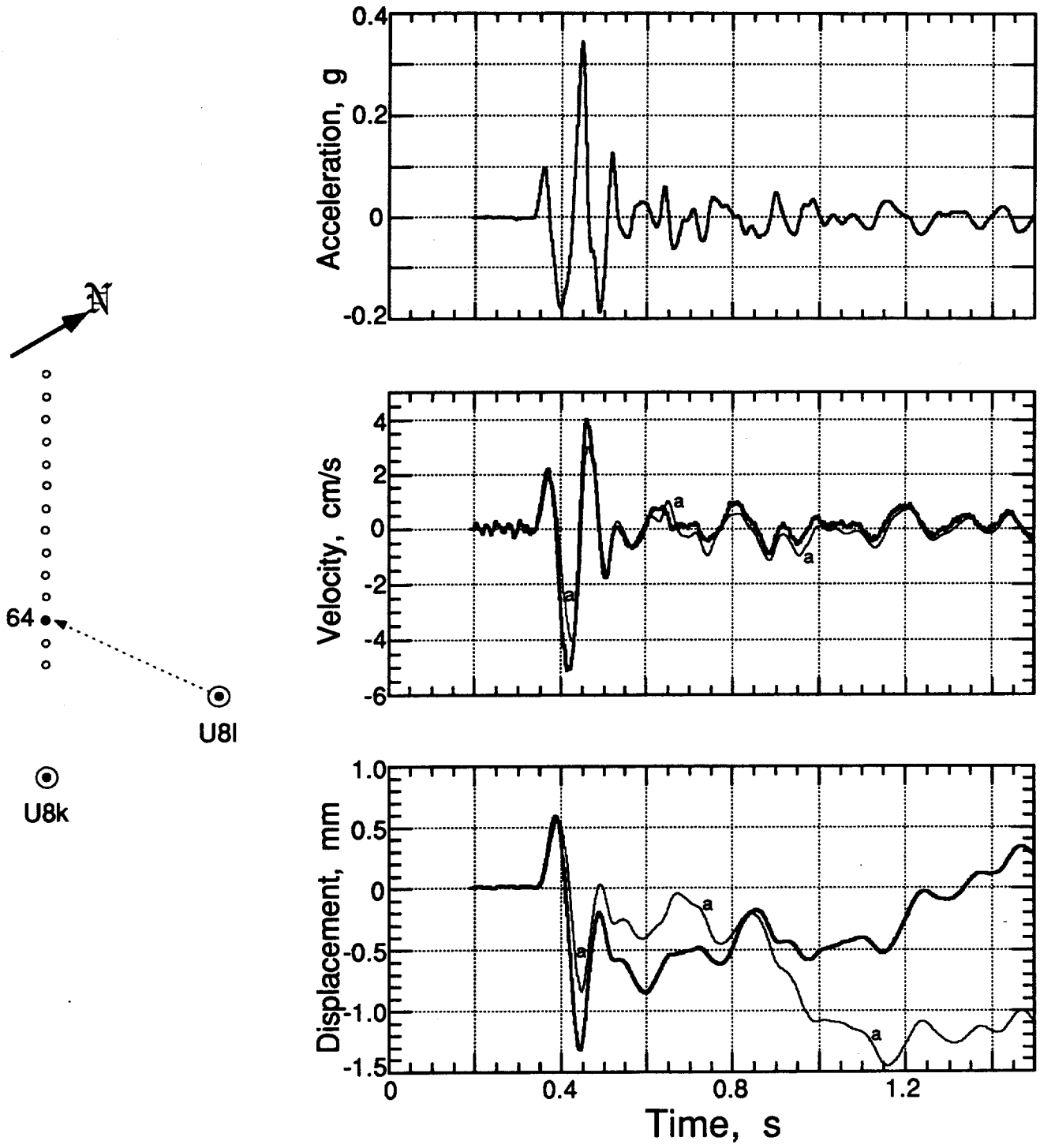

Figure 3.6 Vertical motion of the ground surface at a slant range of 542.4 m and a depth of 0.91 m (station 64). Traces annotated with "a" are derived from the accelerometer.

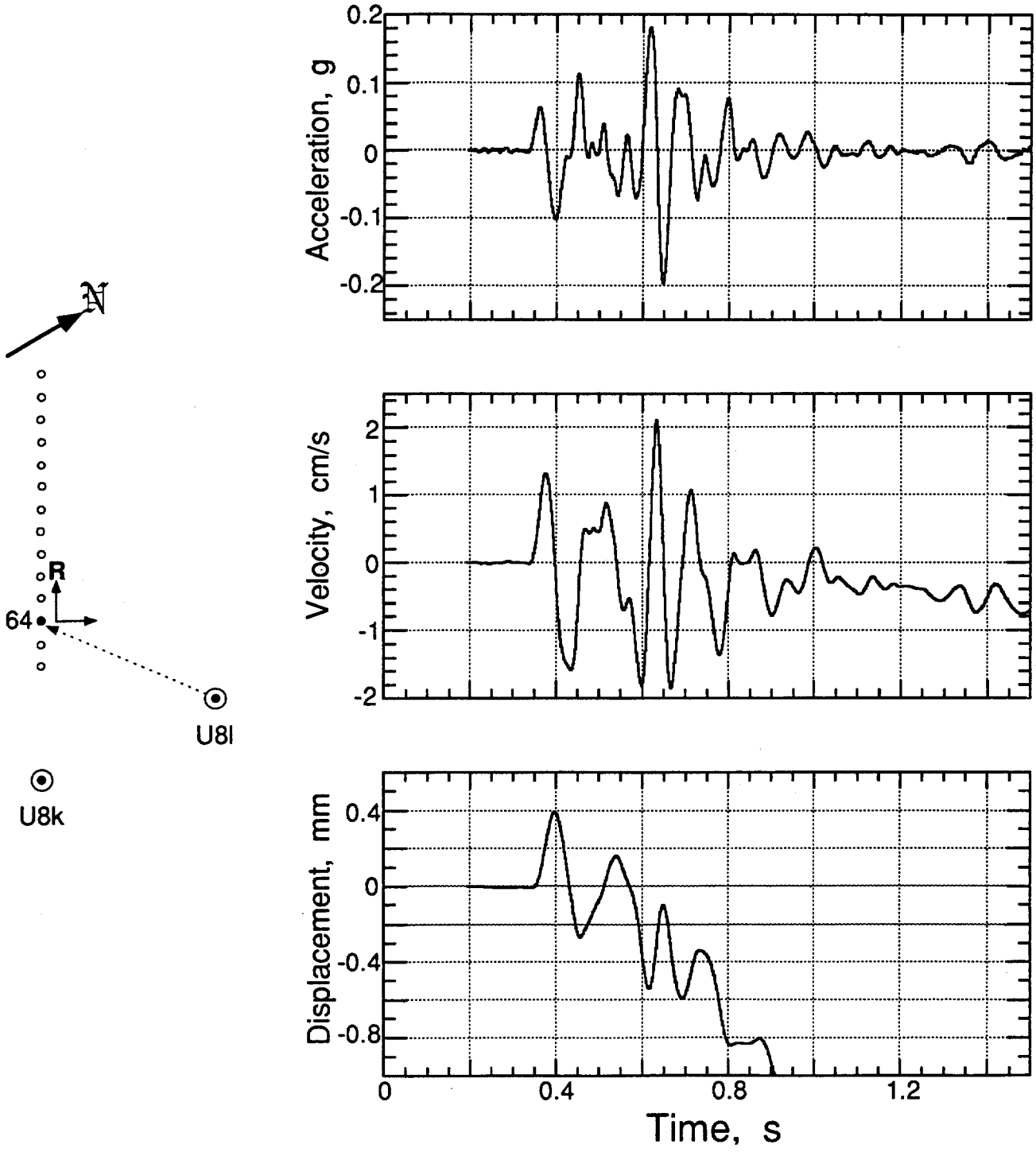

Figure 3.7 Horizontal-radial motion of the ground surface at a slant range of 542.4 m and a depth of 0.91 m (station 64). Motion is positive in a direction W 30 N].

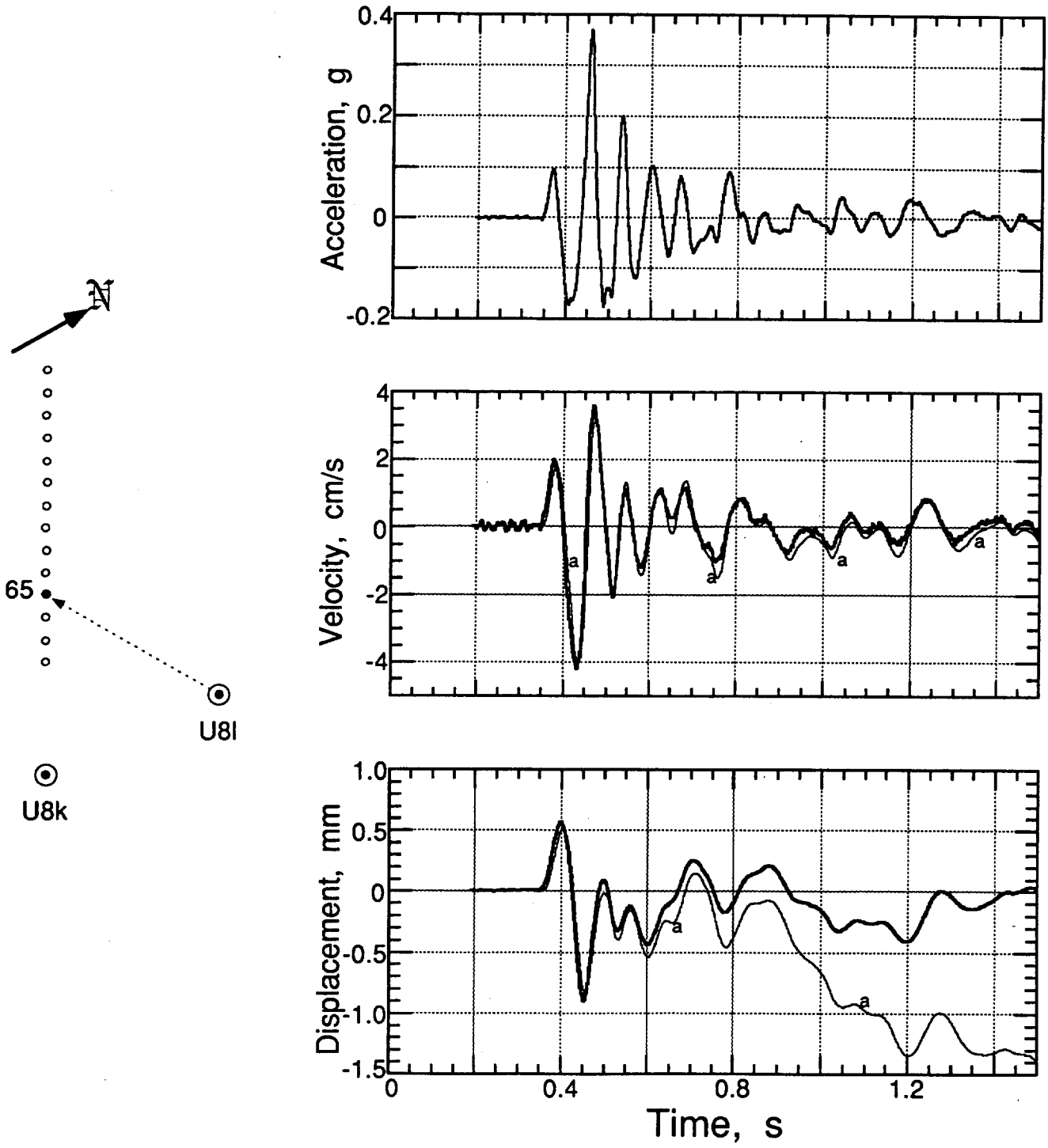

Figure 3.8 Vertical motion of the ground surface at a slant range of 568.4 m and a depth of 0.91 m (station 65). Traces annotated with "a" are derived from the accelerometer.

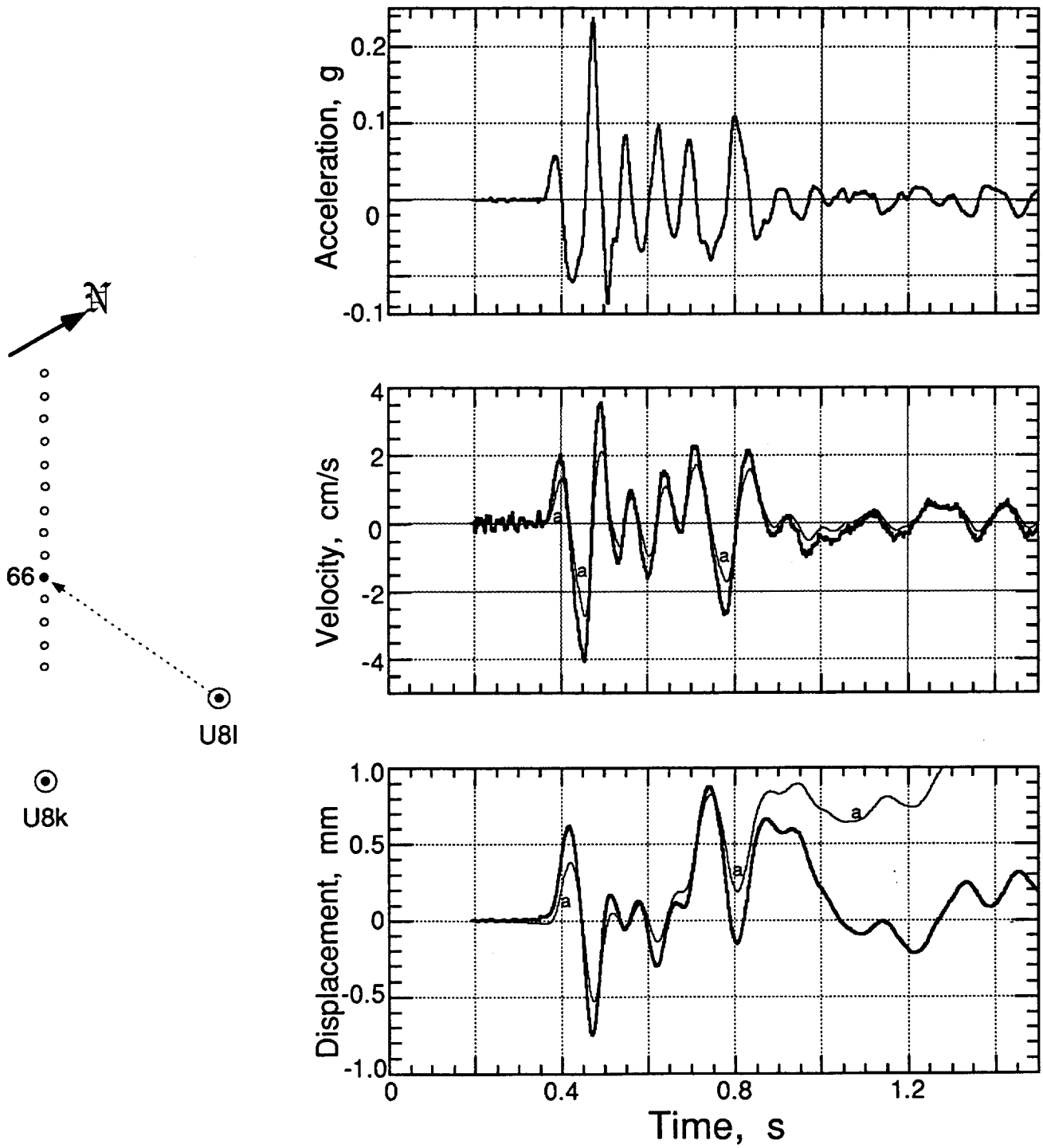

Figure 3.9 Vertical motion of the ground surface at a slant range of 599.1 m and a depth of 0.91 m (station 66). Traces annotated with "a" are derived from the accelerometer.

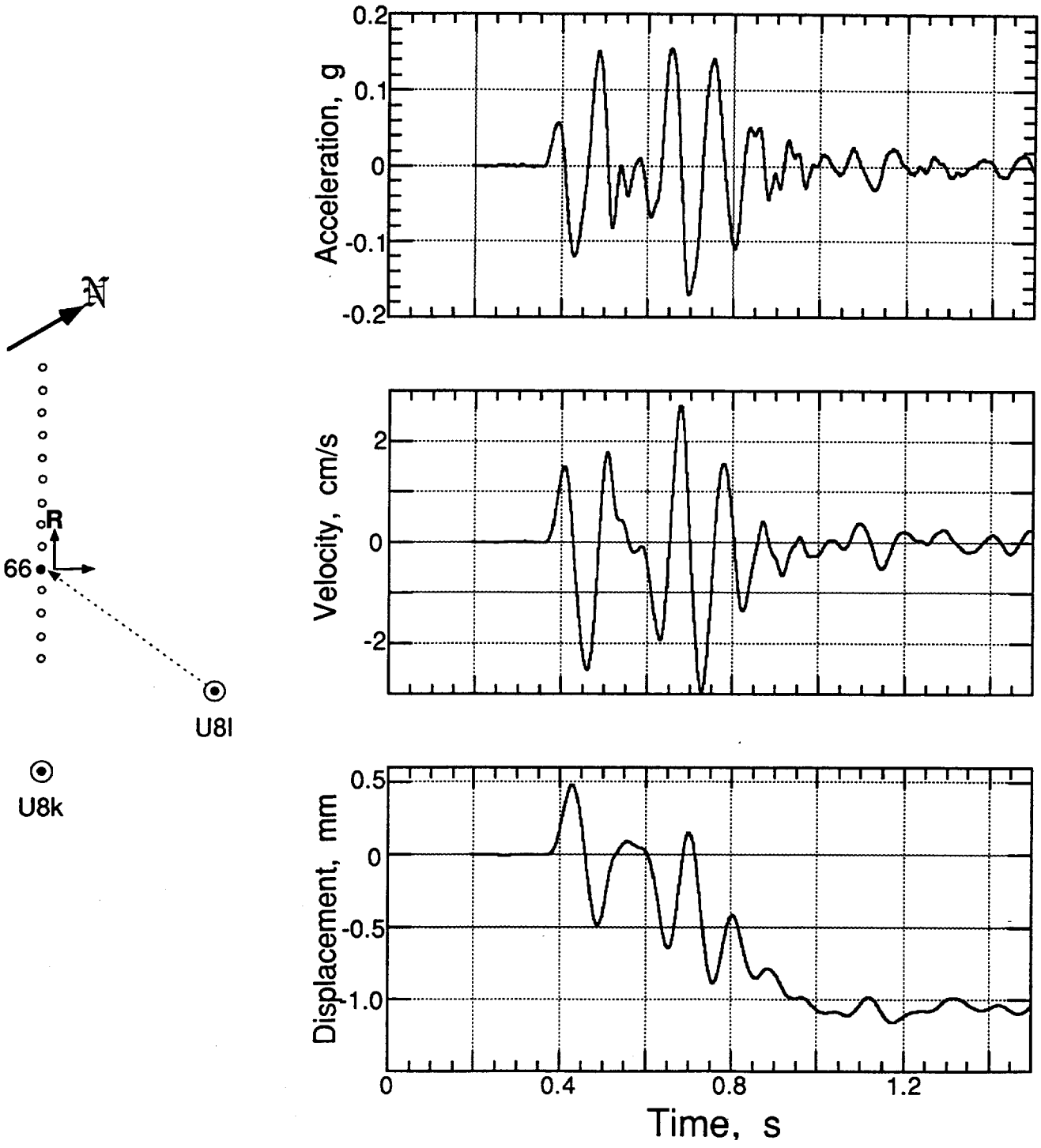

Figure 3.10 Horizontal-radial motion of the ground surface at a slant range of 599.1 m and a depth of 0.91 m (station 66). Motion is positive in a direction [W 30 N].

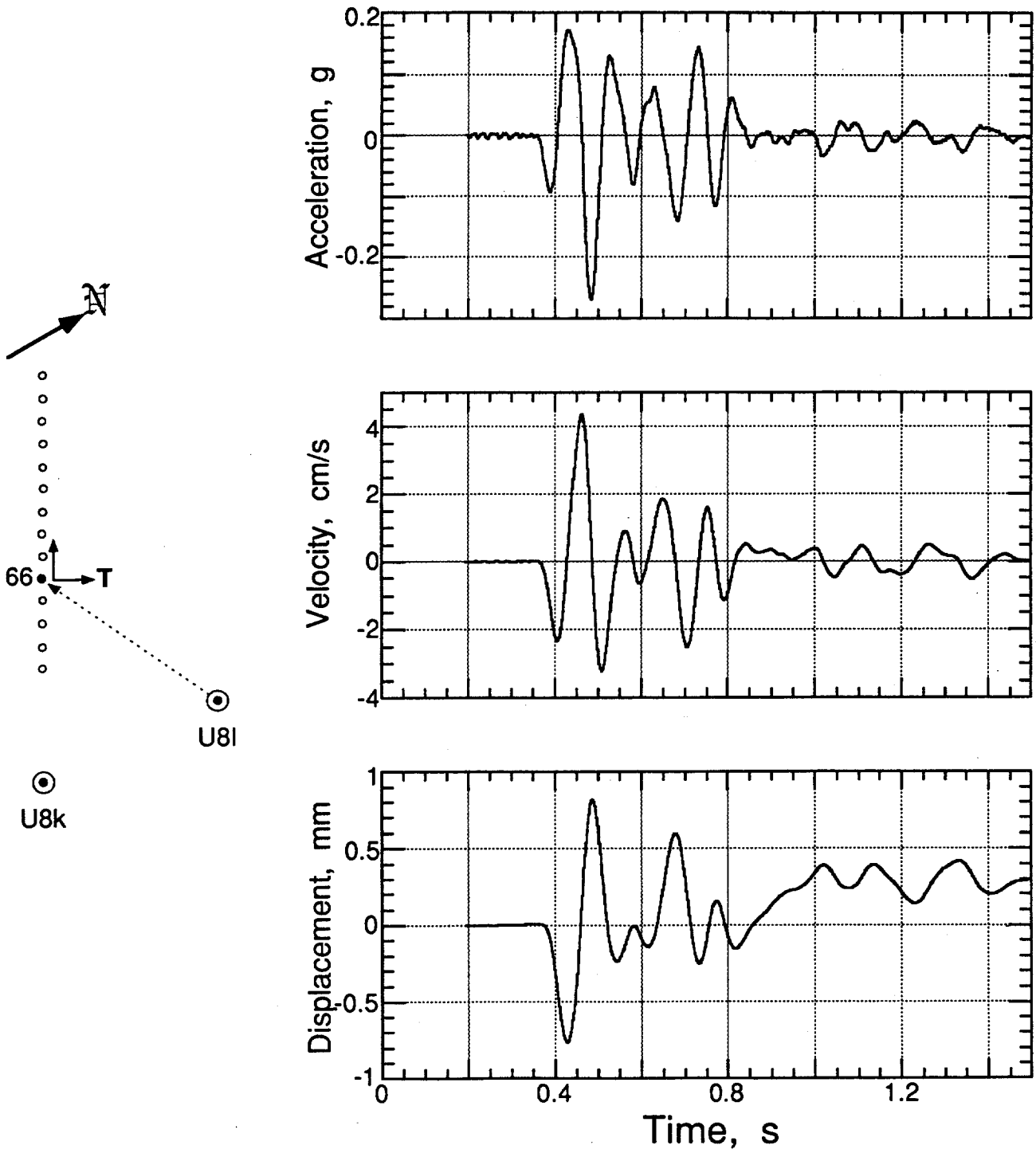

Figure 3.11 Horizontal-transverse motion of the ground surface at a slant range of 599.1 m and a depth of 0.91 m (station 66). Motion is positive in a direction [N 30 E].

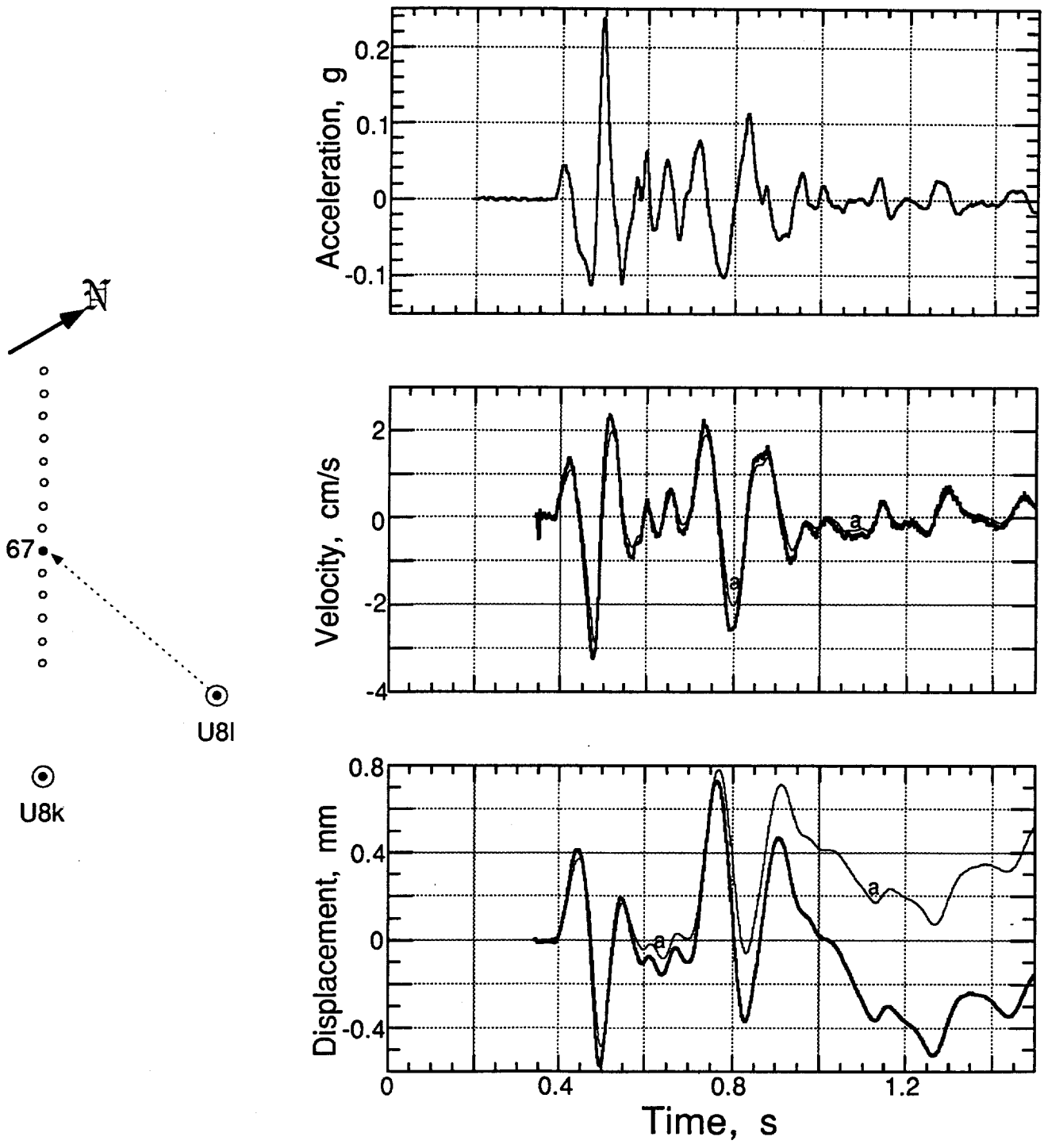

Figure 3.12 Vertical motion of the ground surface at a slant range of 634.3 m and a depth of 0.91 m (station 67). Traces annotated with "a" are derived from the accelerometer.

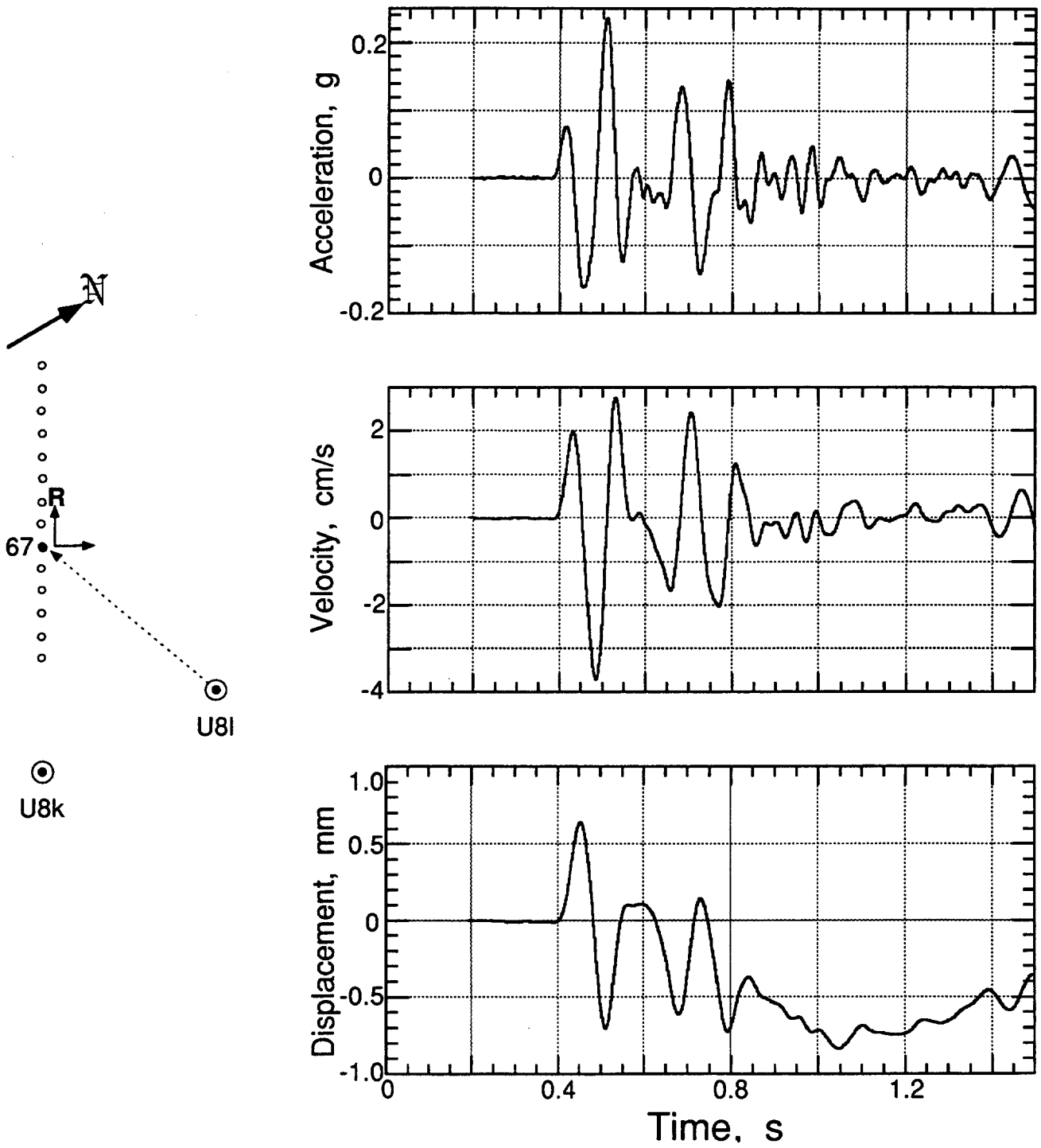

Figure 3.13 Horizontal-radial motion of the ground surface at a slant range of 634.3 m and a depth of 0.91 m (station 67). Motion is positive in a direction [W 30 N].

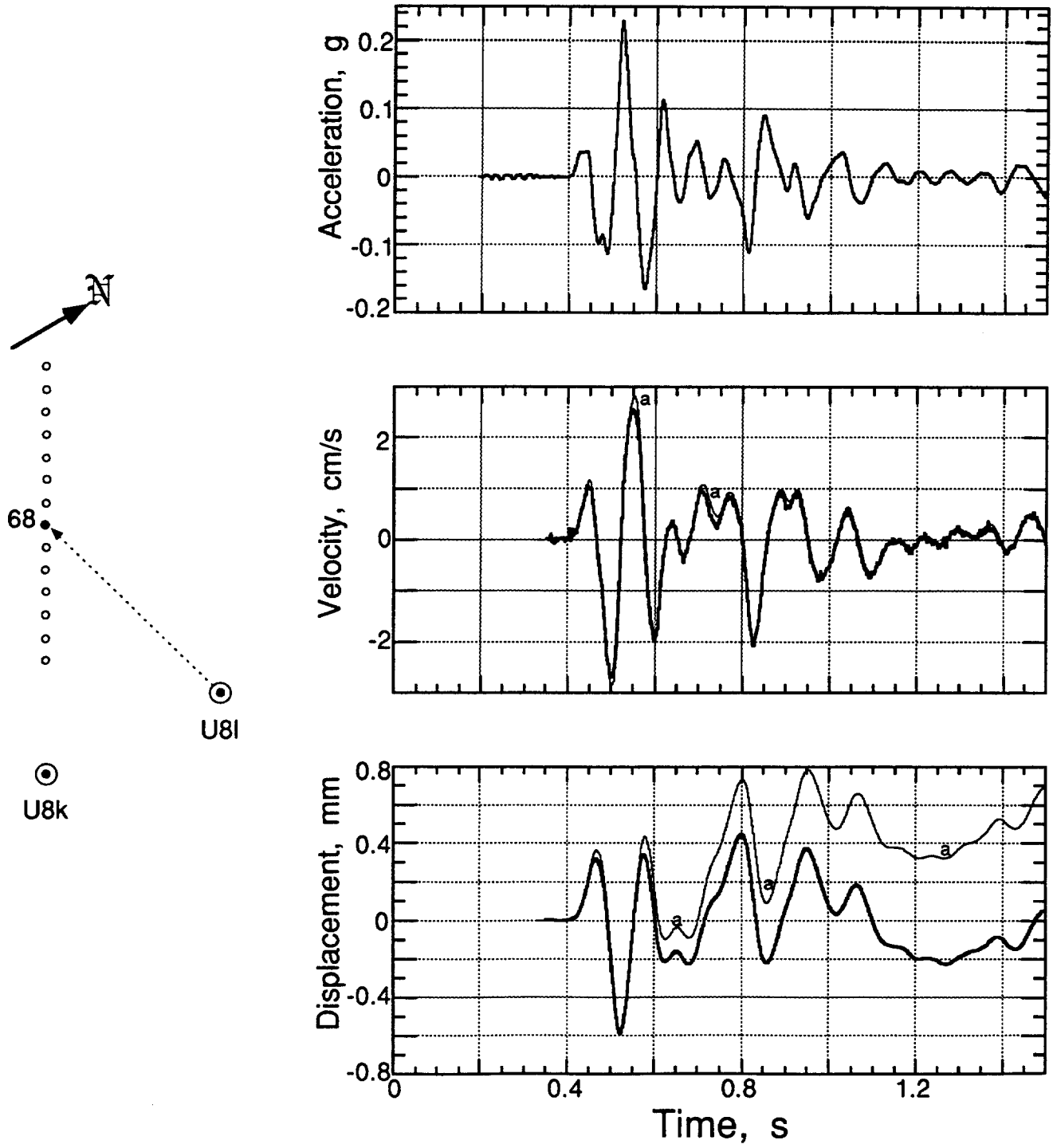

Figure 3.14 Vertical motion of the ground surface at a slant range of 672.7 m and a depth of 0.91 m (station 68). Traces annotated with "a" are derived from the accelerometer.

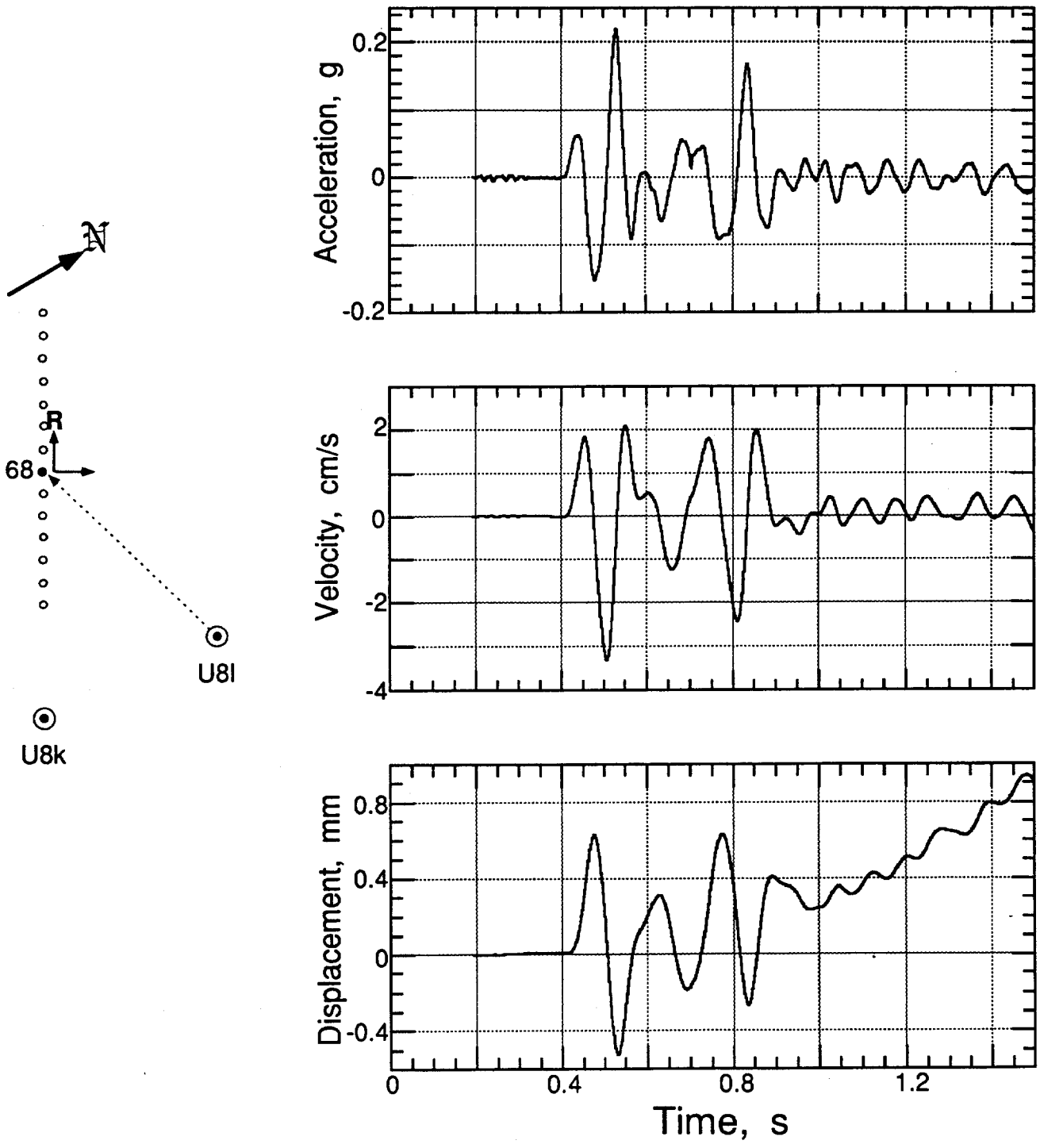

Figure 3.15 Horizontal-radial motion of the ground surface at a slant range of 672.7 m and a depth of 0.91 m (station 68). Motion is positive in a direction [W 30 N].

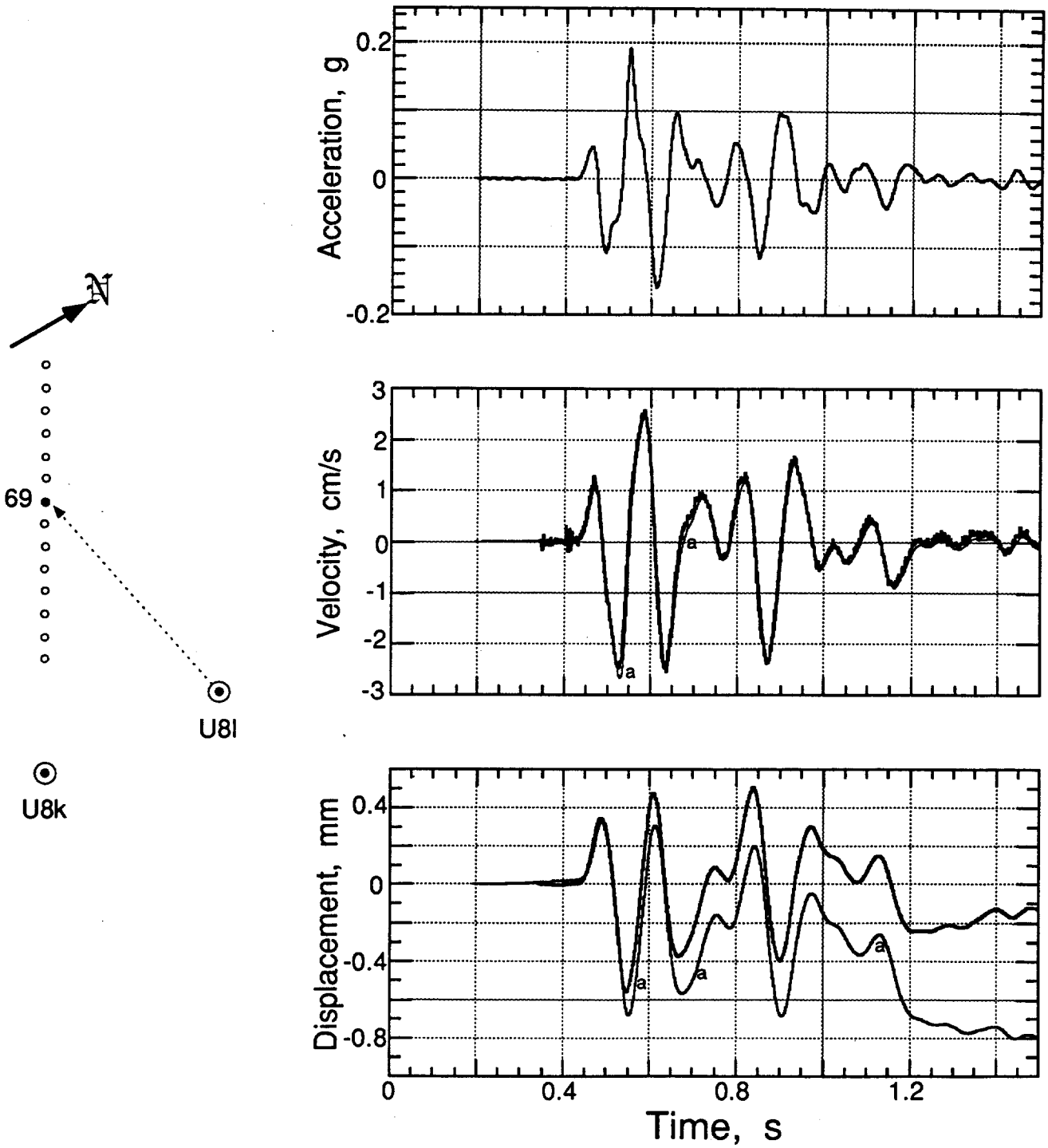

Figure 3.16 Vertical motion of the ground surface at a slant range of 714.6 m and a depth of 0.91 m (station 69). Traces annotated with "a" are derived from the accelerometer.

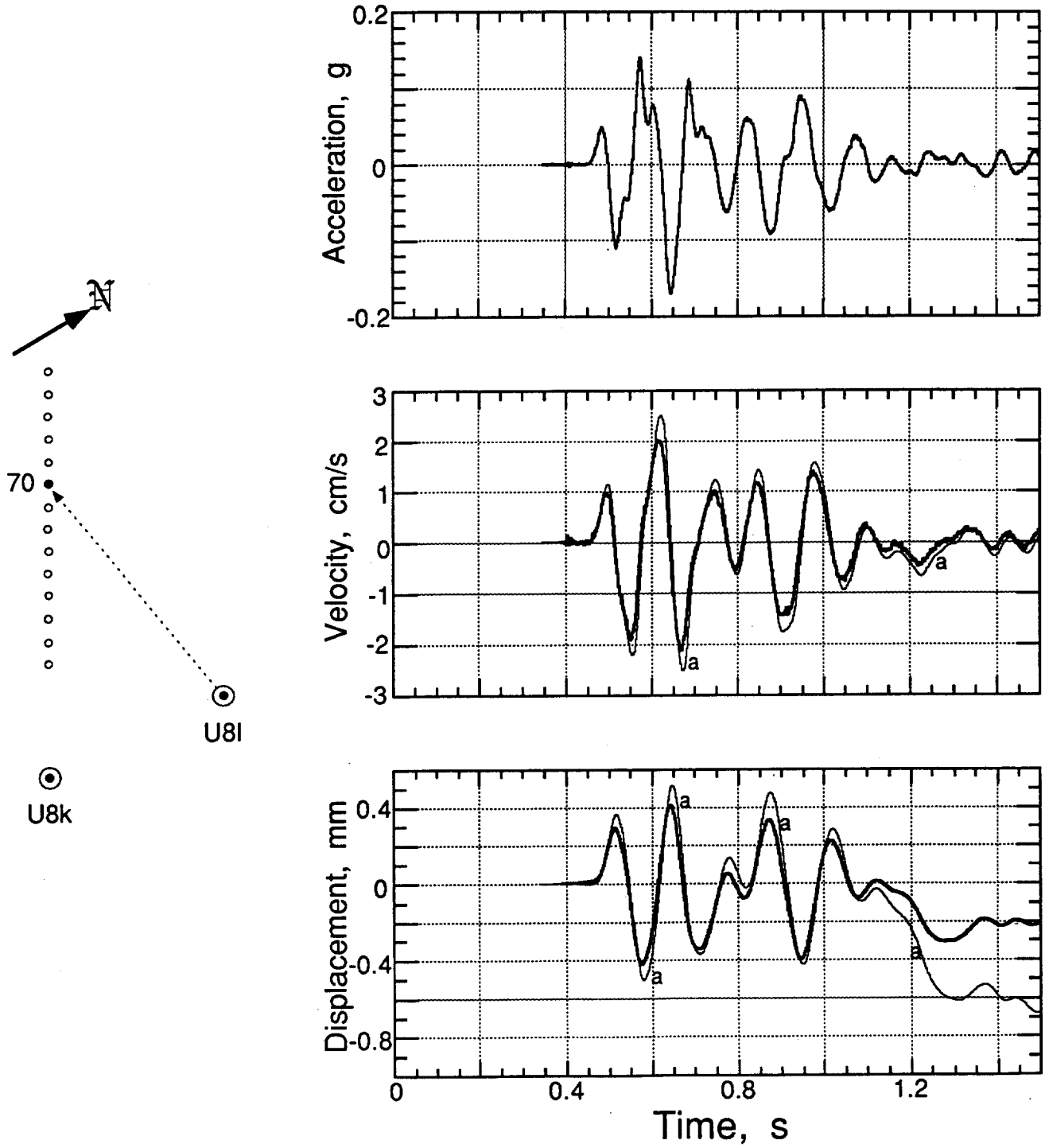

Figure 3.17 Vertical motion of the ground surface at a slant range of 758.9 m and a depth of 0.91 m (station 70). Traces annotated with "a" are derived from the accelerometer.

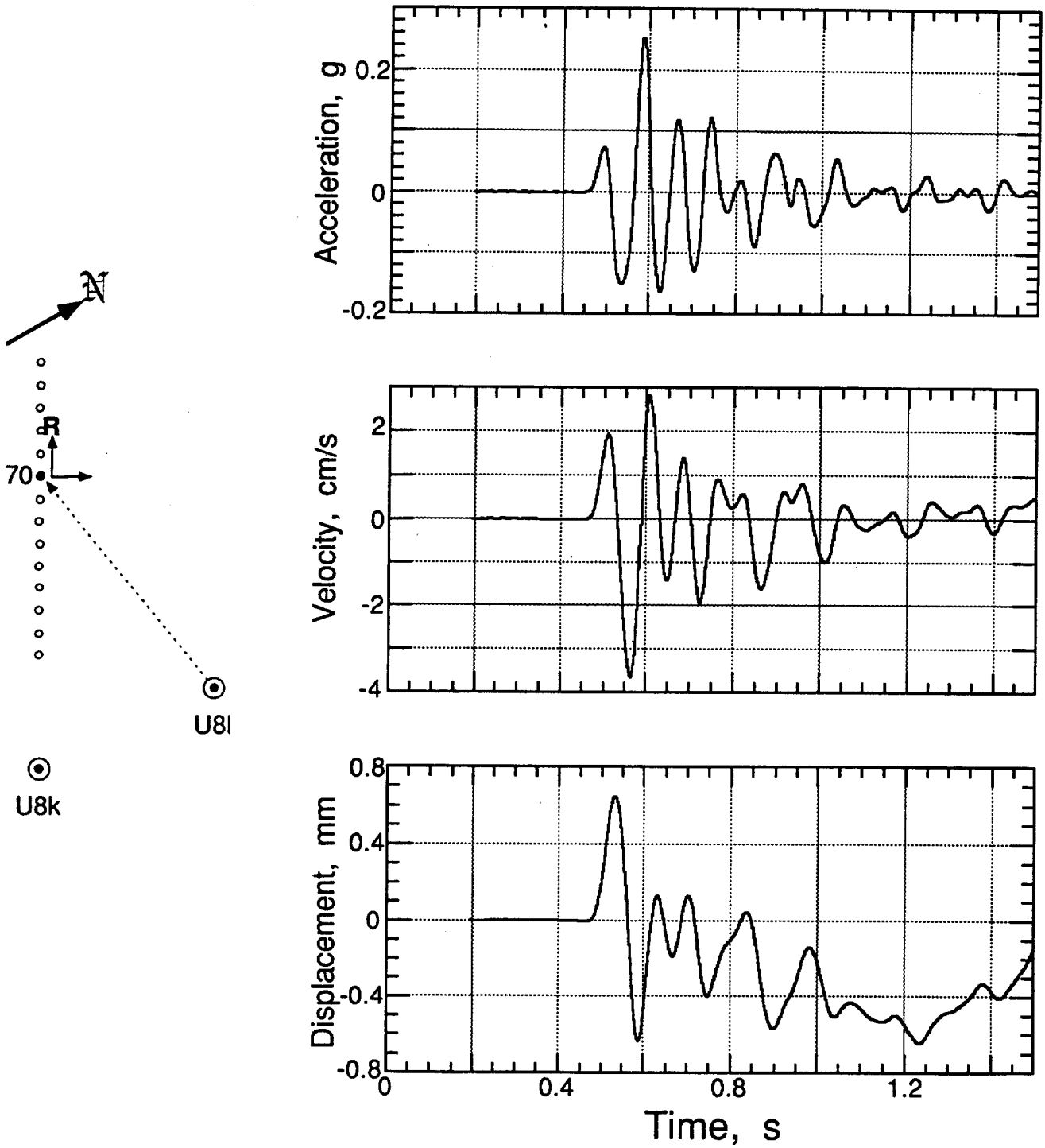

Figure 3.18 Horizontal-radial motion of the ground surface at a slant range of 758.9 m and a depth of 0.91 m (station 70). Motion is positive in a direction [W 30 N].

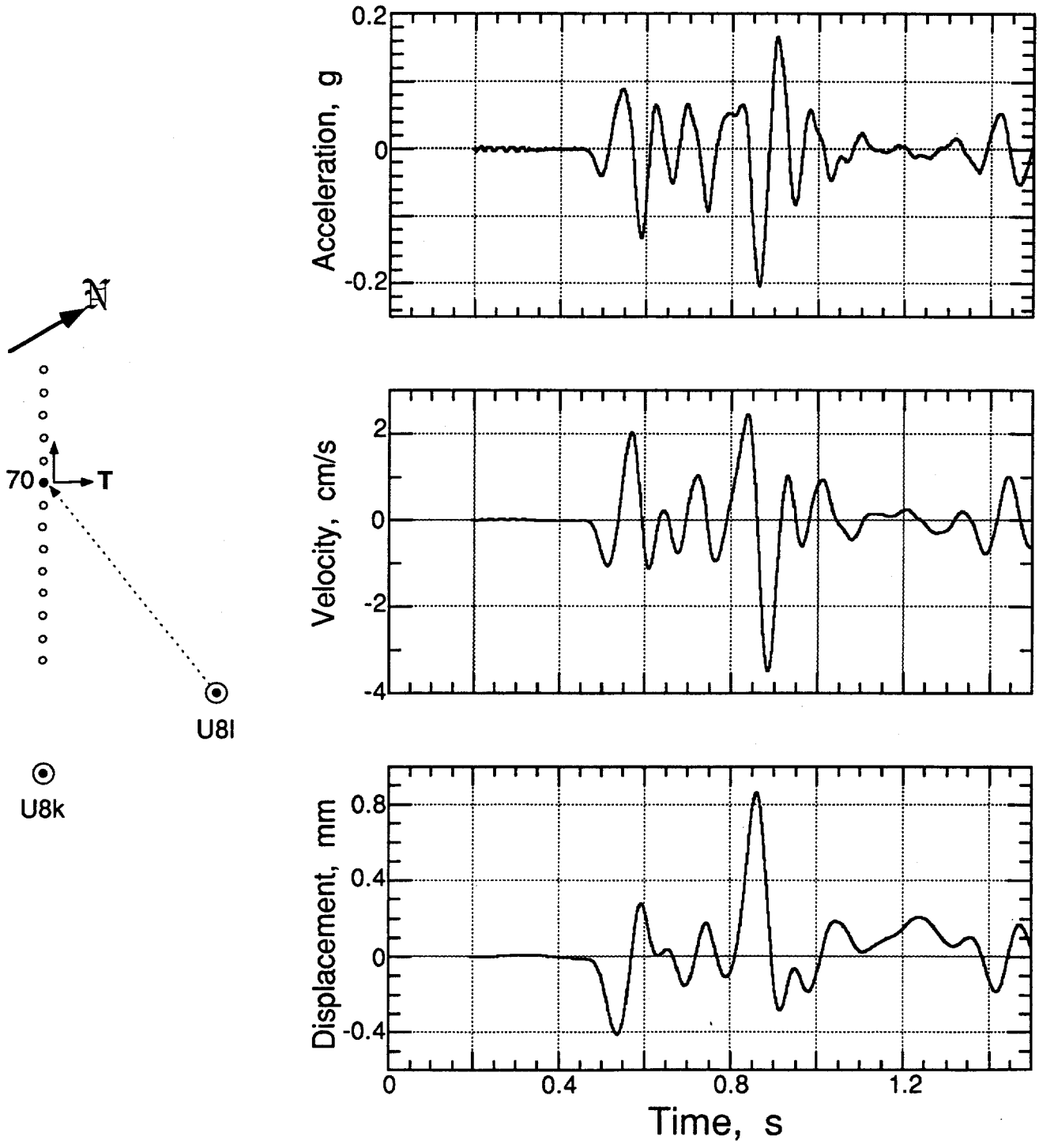

Figure 3.19 Horizontal-transverse motion of the ground surface at a slant range of 758.9 m and a depth of 0.91 m (station 70). Motion is positive in a direction [N 30 E].

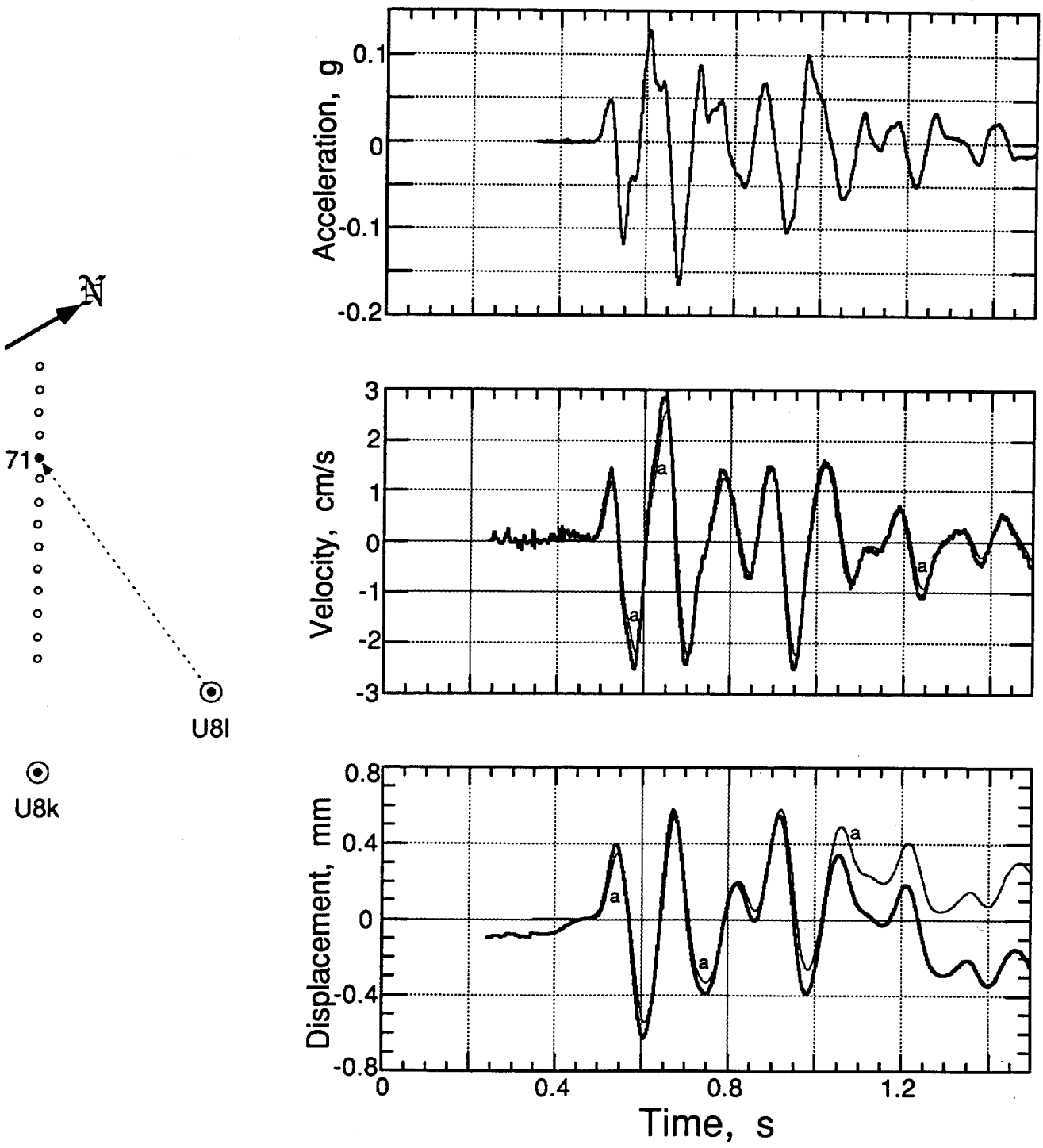

Figure 3.20 Vertical motion of the ground surface at a slant range of 804.4 m and a depth of 0.91 m (station 71). Traces annotated with "a" are derived from the accelerometer.

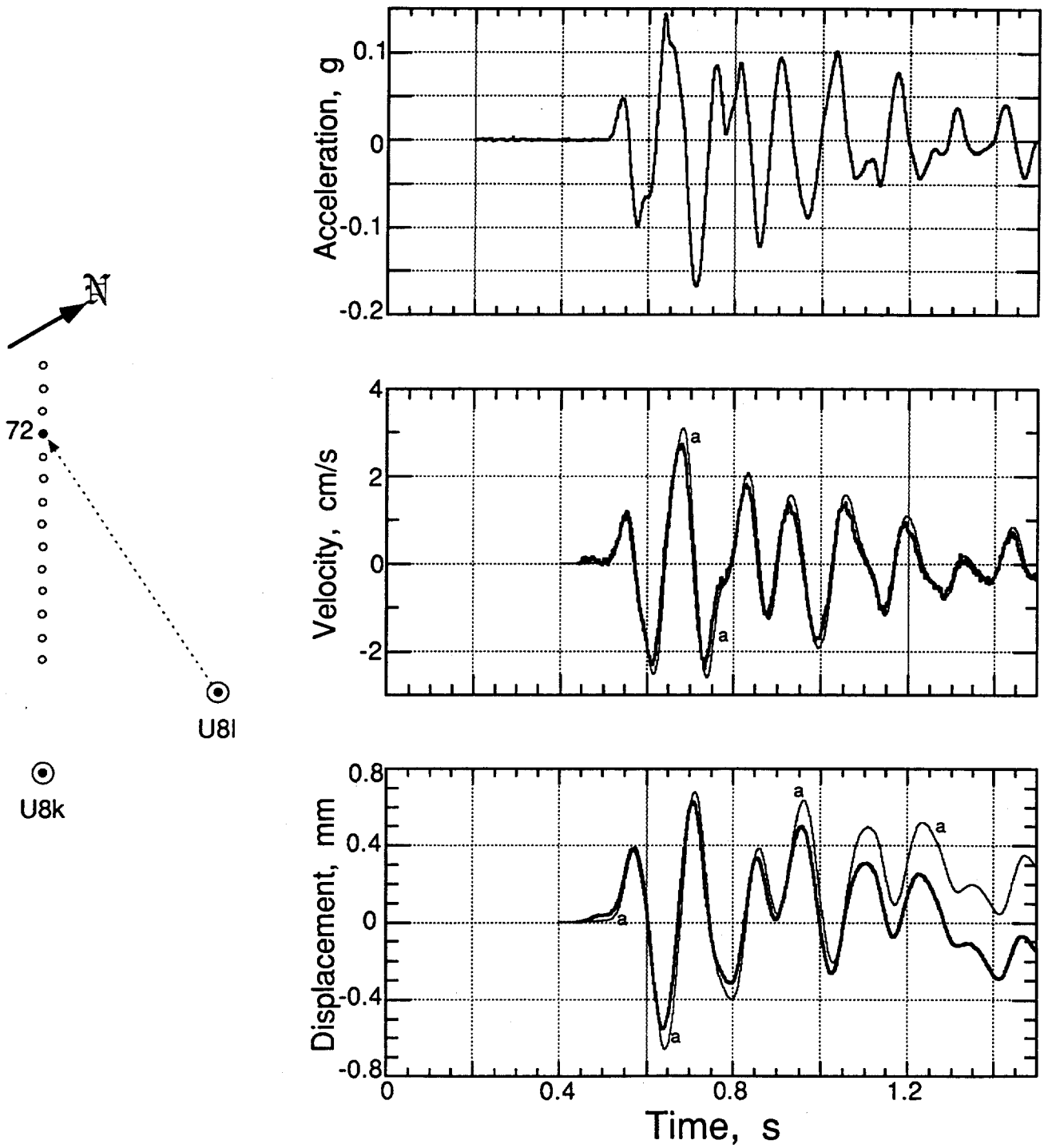

Figure 3.21 Vertical motion of the ground surface at a slant range of 852.7 m and a depth of 0.91 m (station 72). Traces annotated with "a" are derived from the accelerometer.

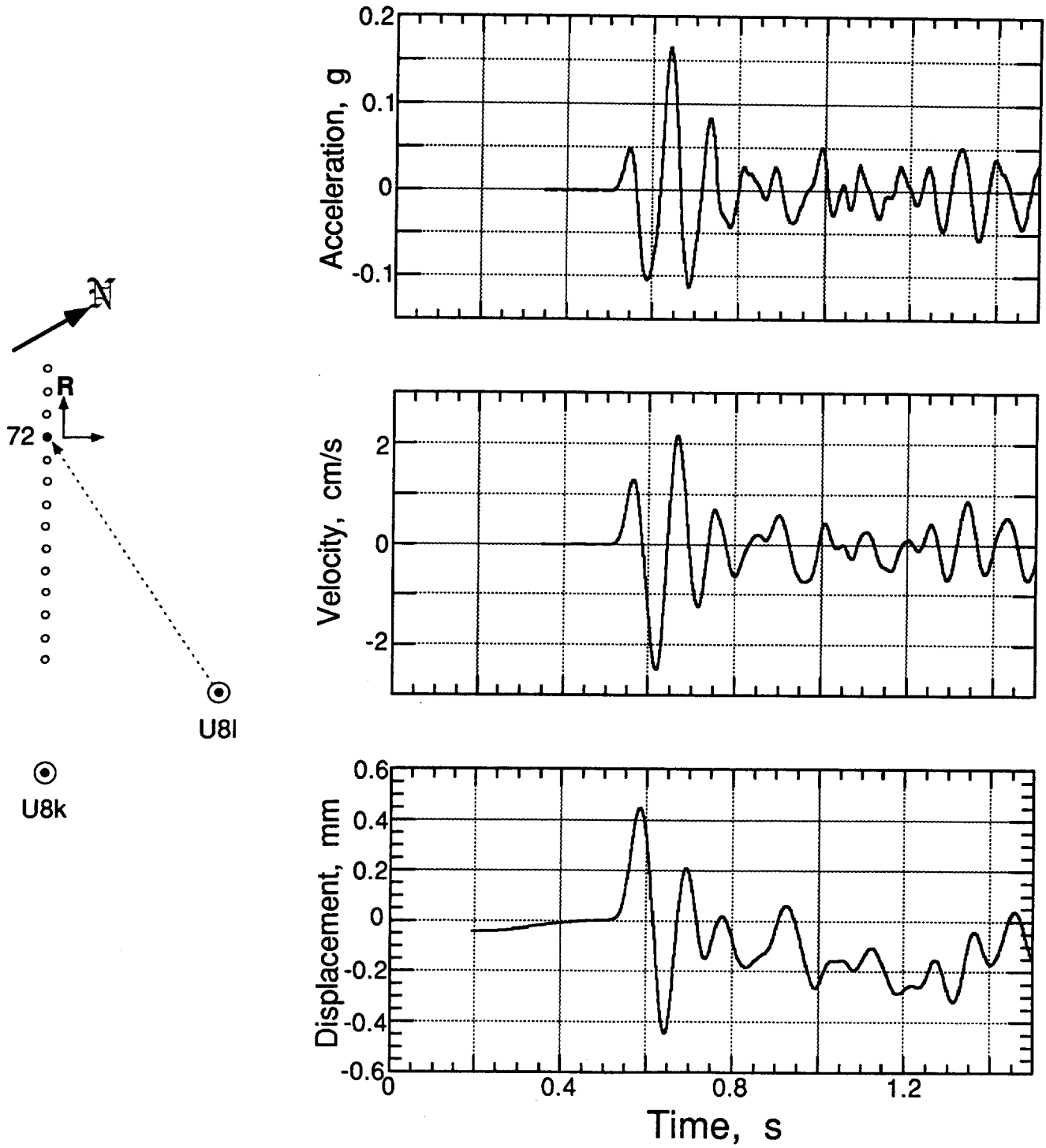

Figure 3.22 Horizontal-radial motion of the ground surface at a slant range of 852.7 m and a depth of 0.91 m (station 72). Motion is positive in a direction [W 30 N].

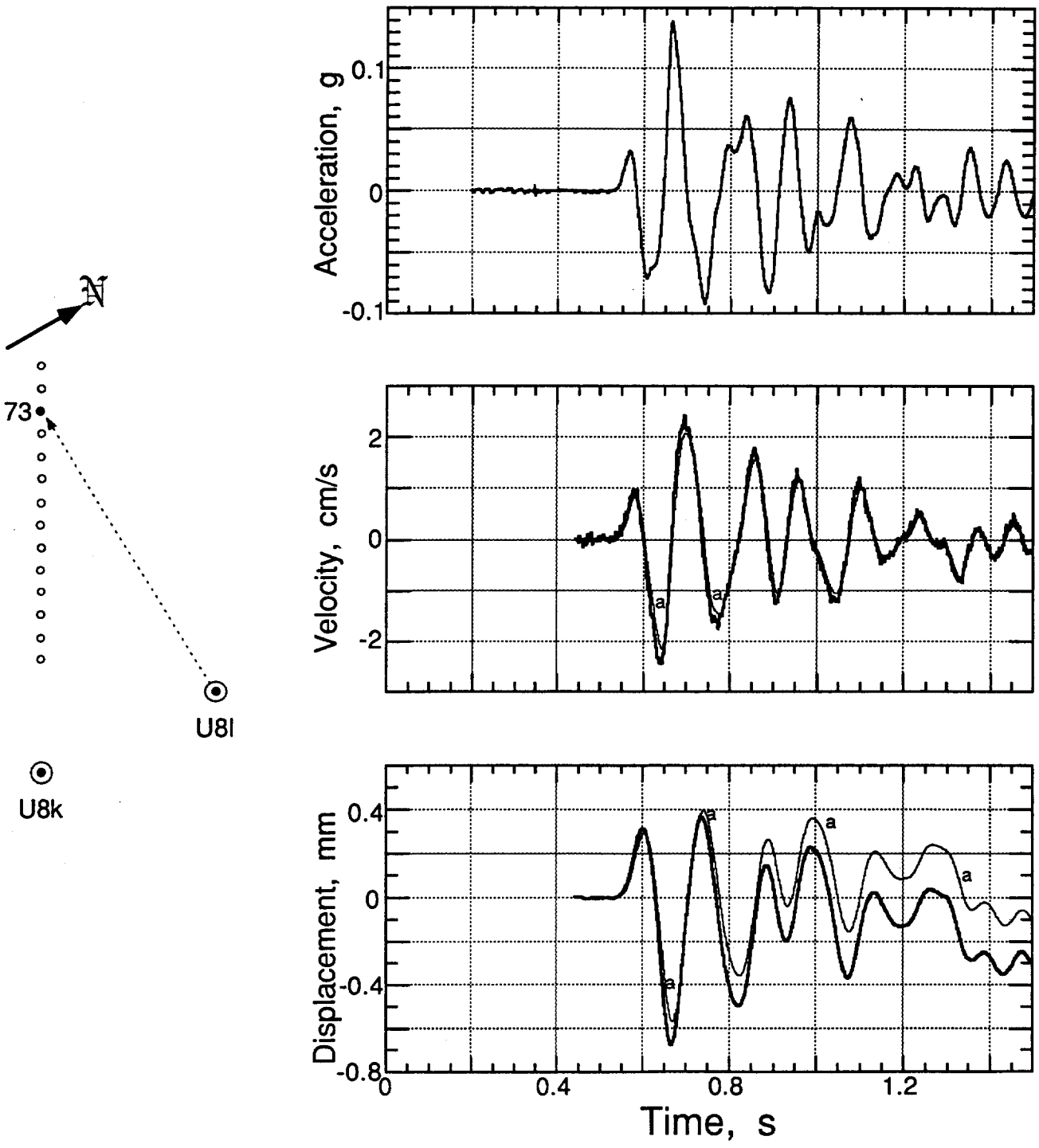

Figure 3.23 Vertical motion of the ground surface at a slant range of 901.8 m and a depth of 0.91 m (station 73). Traces annotated with "a" are derived from the accelerometer.

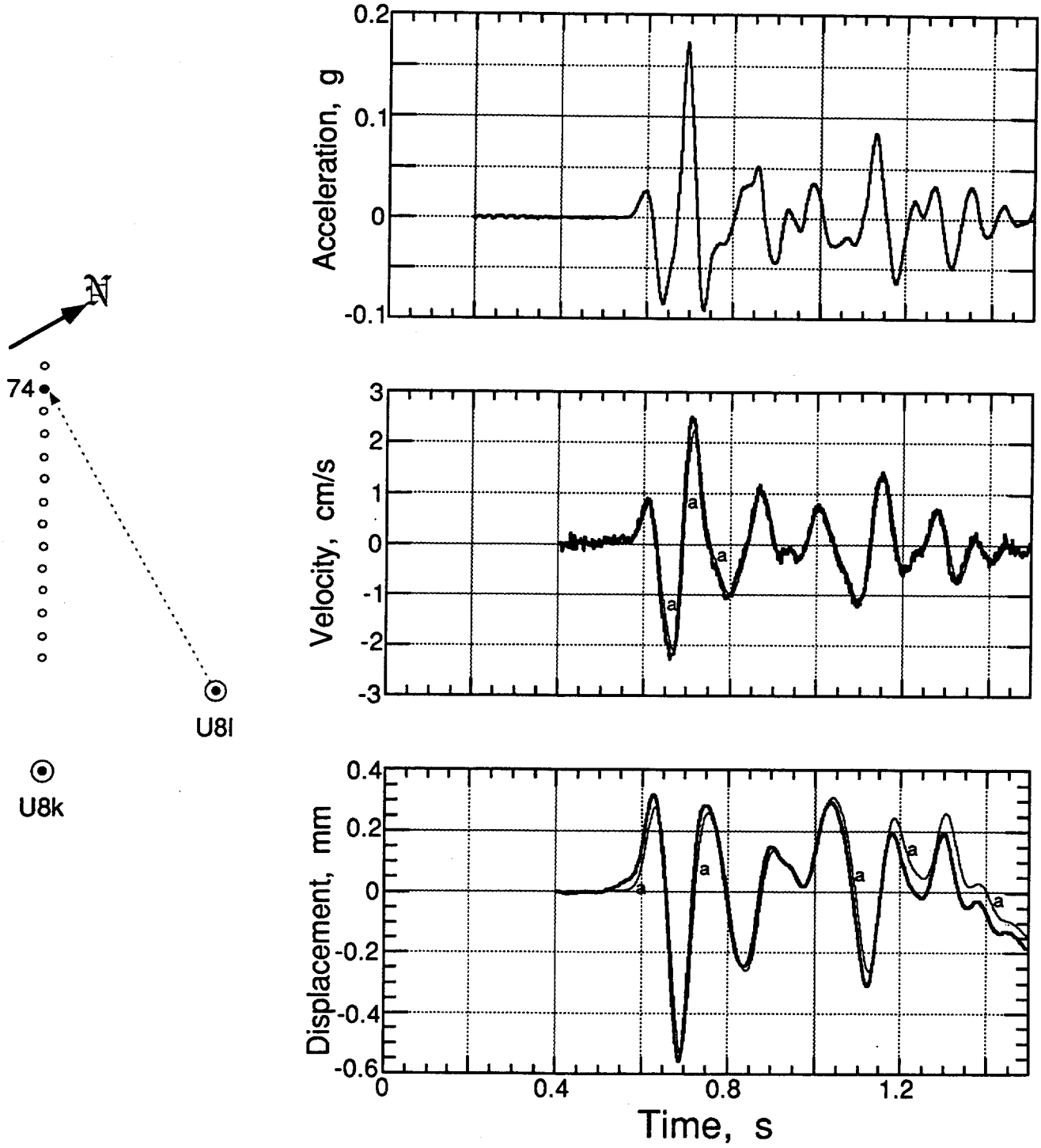

Figure 3.24 Vertical motion of the ground surface at a slant range of 952.6 m and a depth of 0.91 m (station 74). Traces annotated with "a" are derived from the accelerometer.

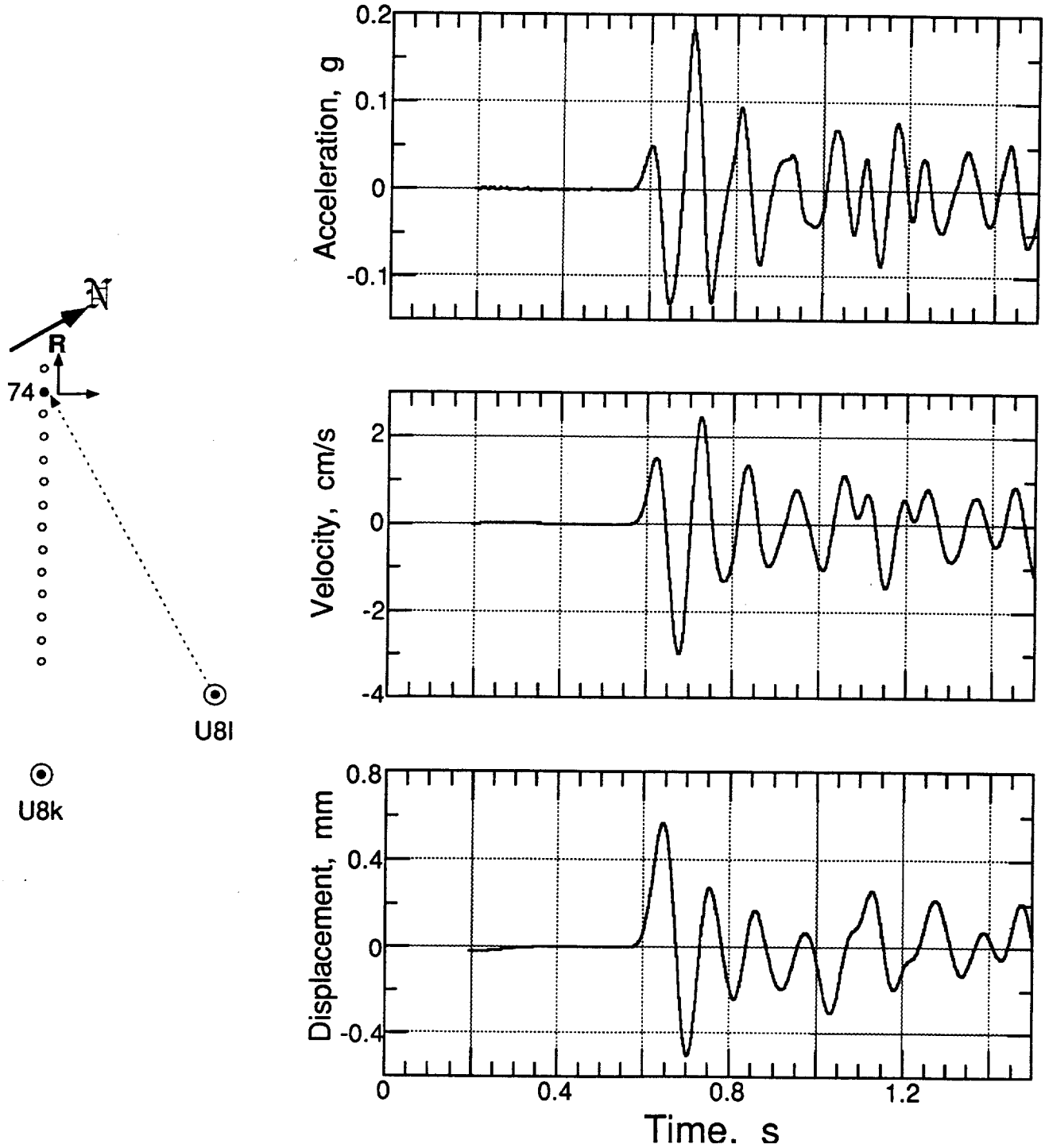

Figure 3.25 Horizontal-radial motion of the ground surface at a slant range of 952.6 m and a depth of 0.91 m (station 74). Motion is positive in a direction [W 30 N].

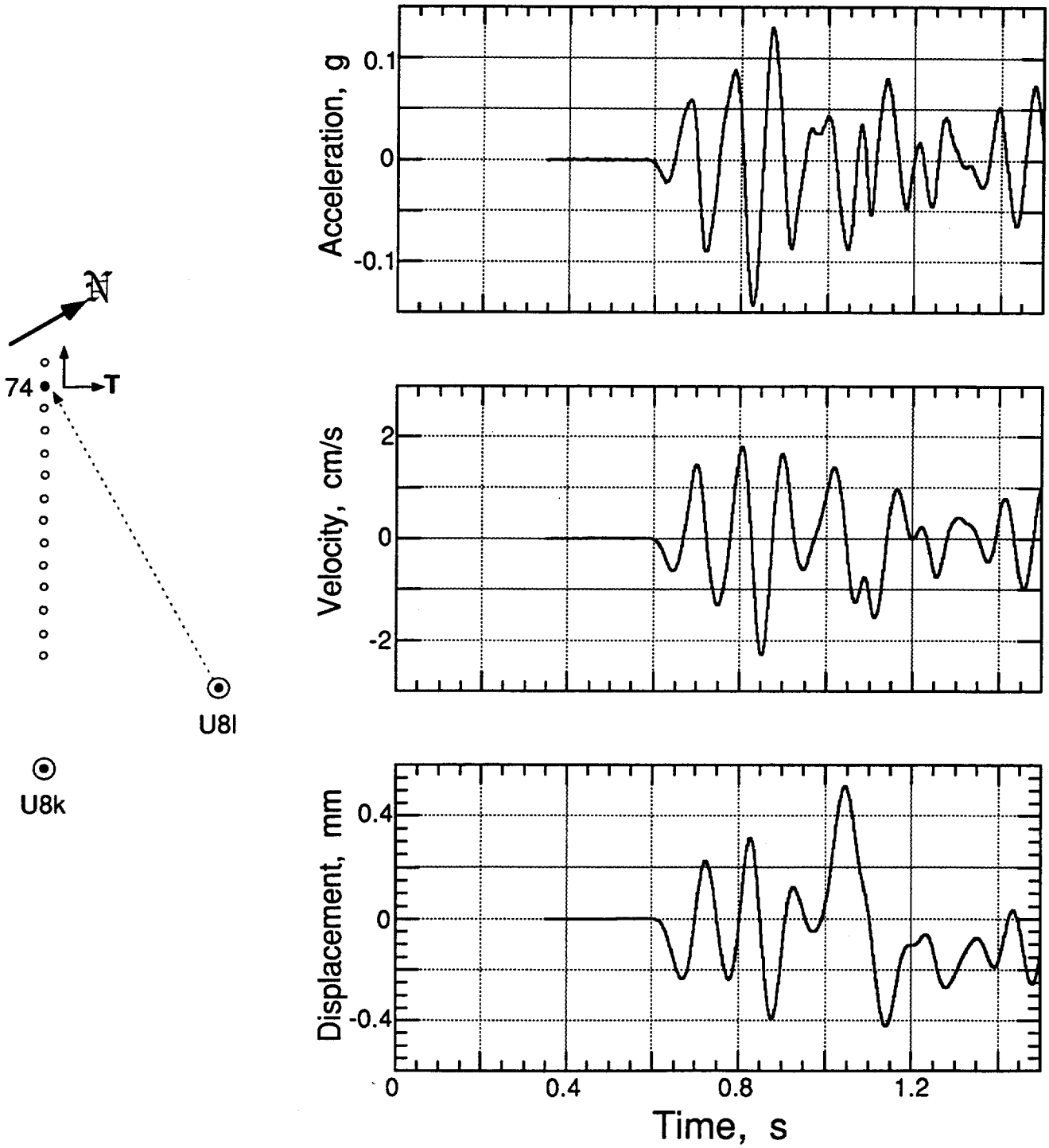

Figure 3.26 Horizontal-transverse motion of the ground surface at a slant range of 952.6 m and a depth of 0.91 m (station 74). Motion is positive in a direction [N 30 E].

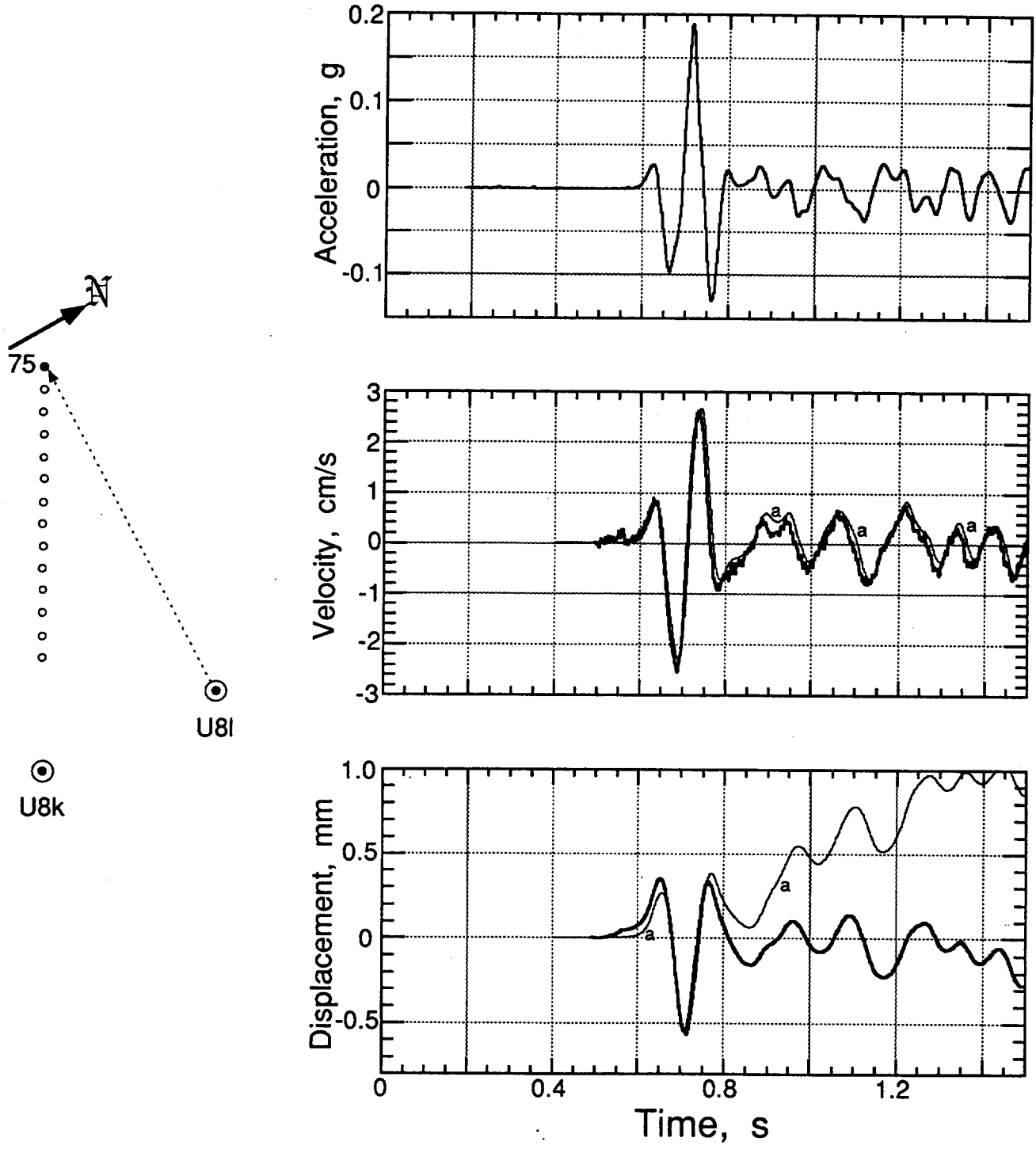

Figure 3.27 Vertical motion of the ground surface at a slant range of 1004.3 m and a depth of 0.91 m (station 75). Traces annotated with "a" are derived from the accelerometer.

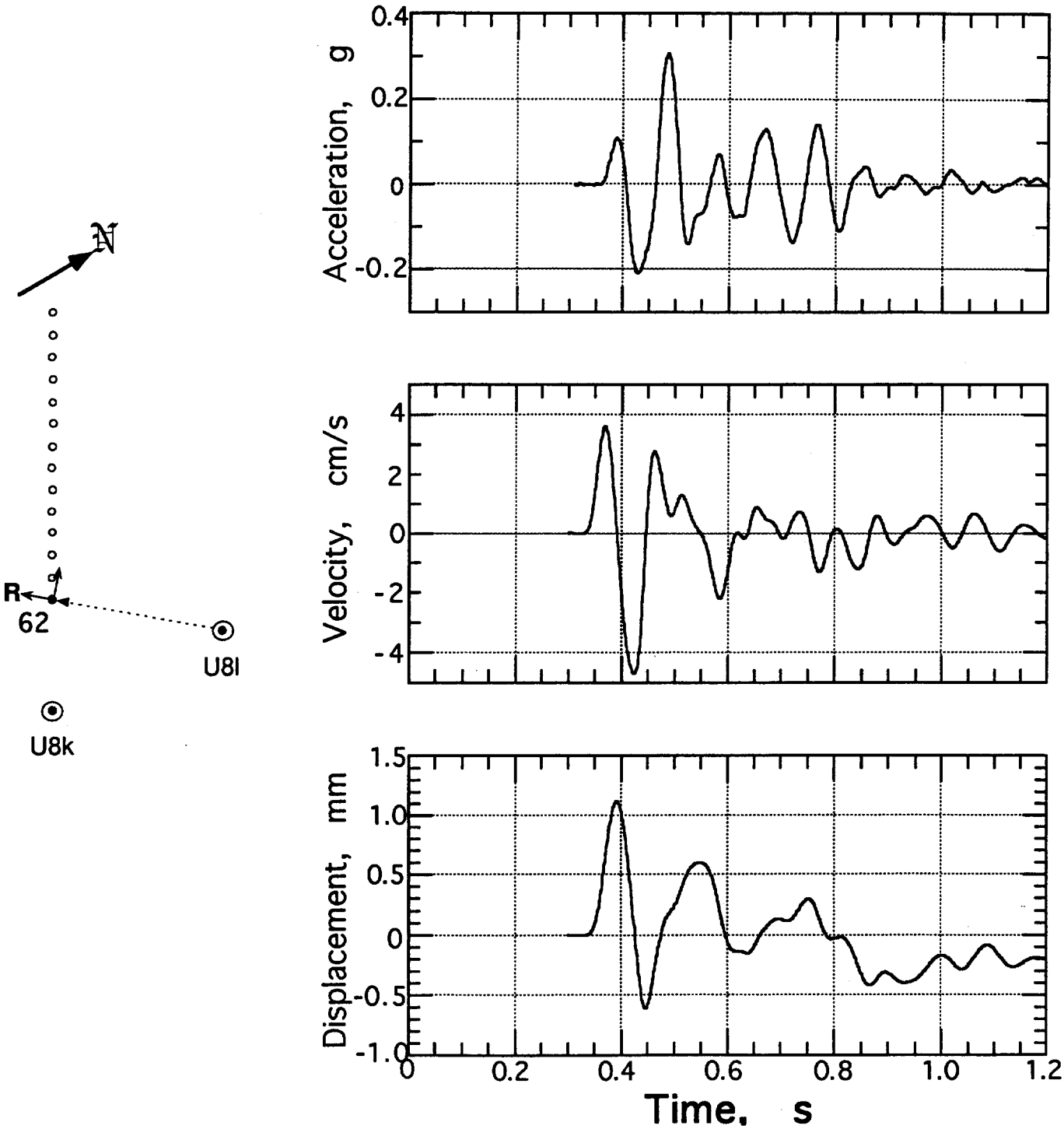

Figure 3.28 Horizontal-radial motion of the ground surface at a slant range of 508.5 m and a depth of 0.91 m (station 62).

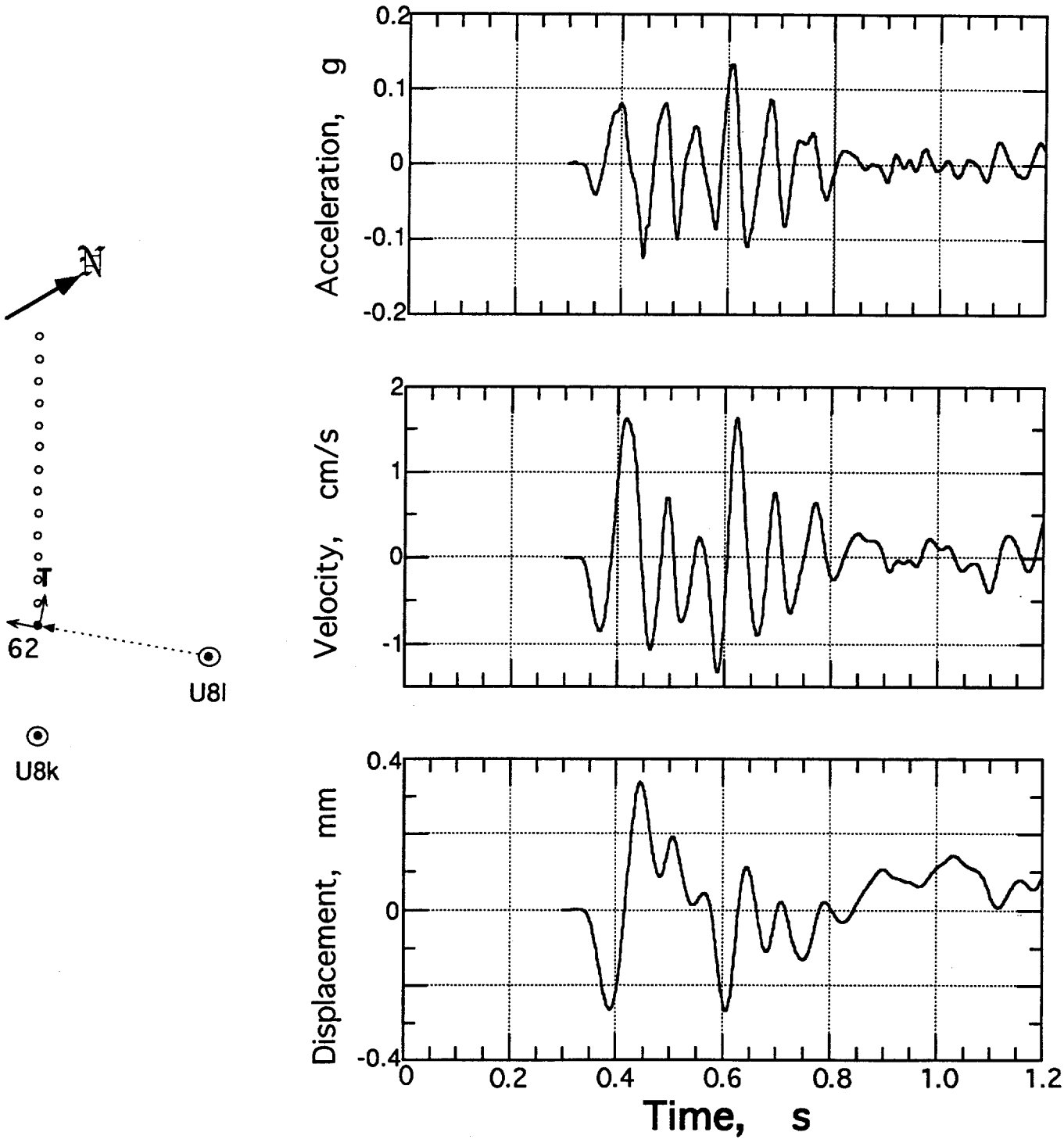

Figure 3.29 Horizontal-transverse motion of the ground surface at a slant range of 508.5 m and a depth of 0.91 m (station 62).

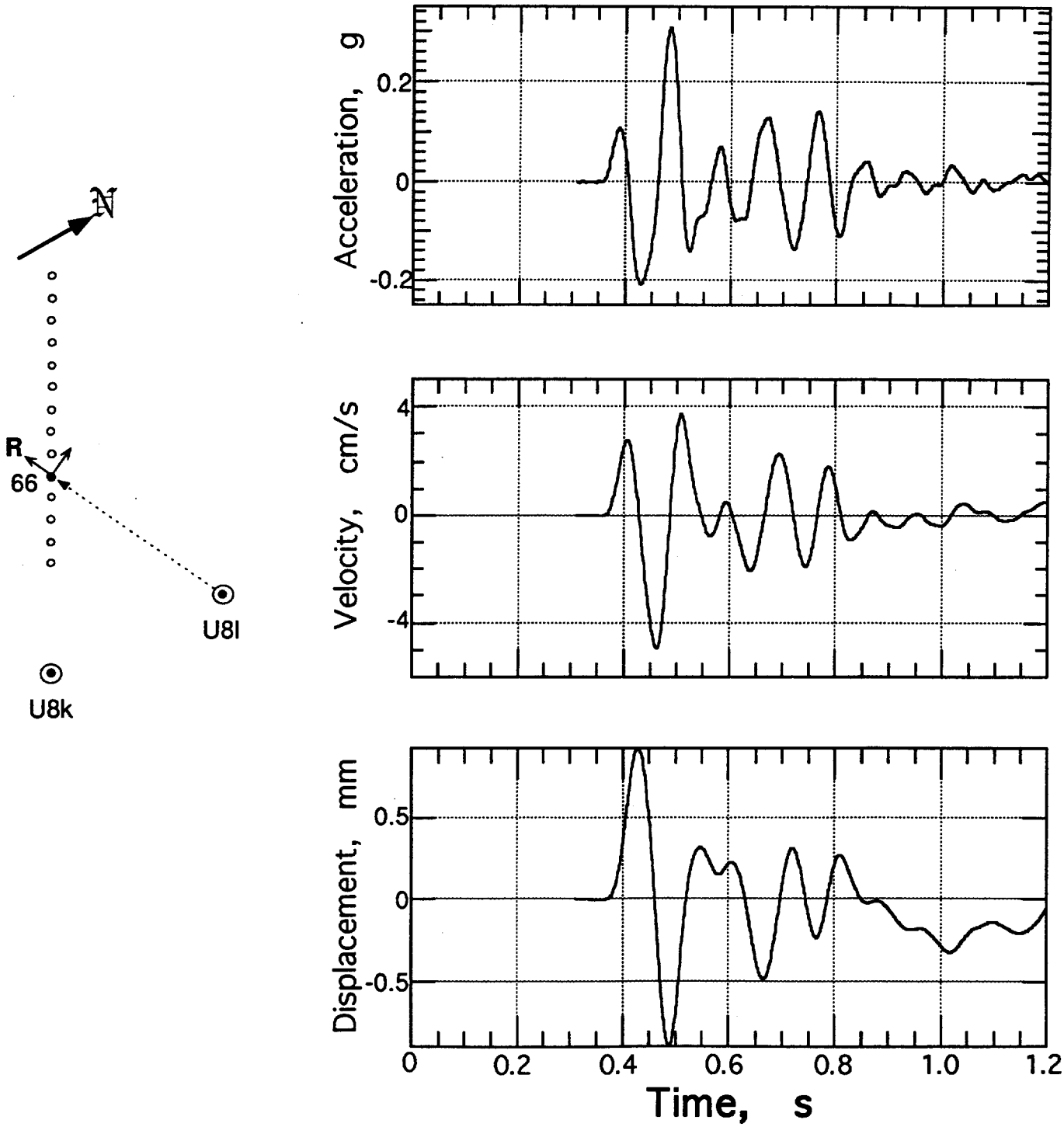

Figure 3.30 Horizontal-radial motion of the ground surface at a slant range of 599.1 m and a depth of 0.91 m (station 66).

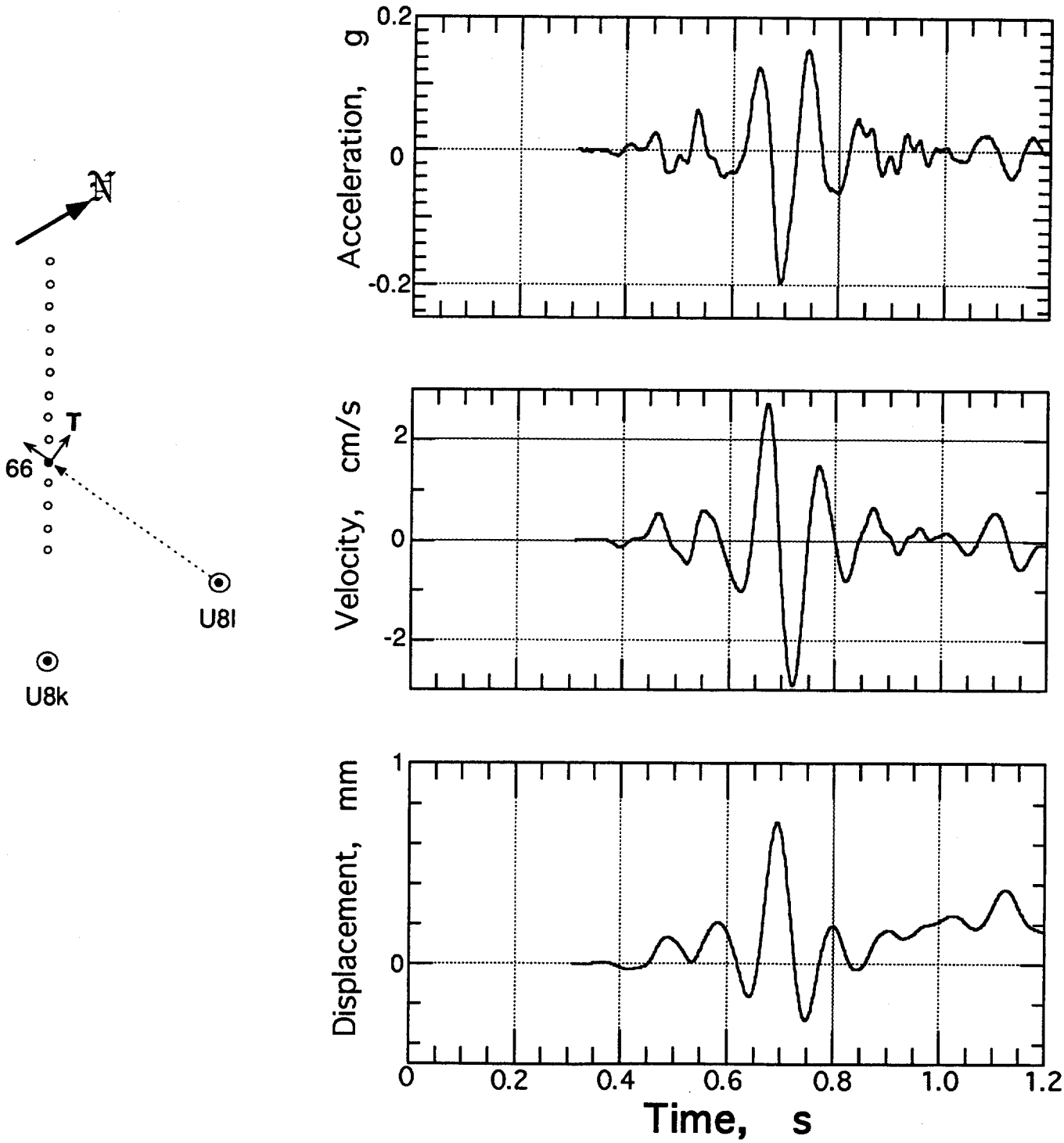

Figure 3.31 Horizontal-transverse motion of the ground surface at a slant range of 599.1 m and a depth of 0.91 m (station 66).

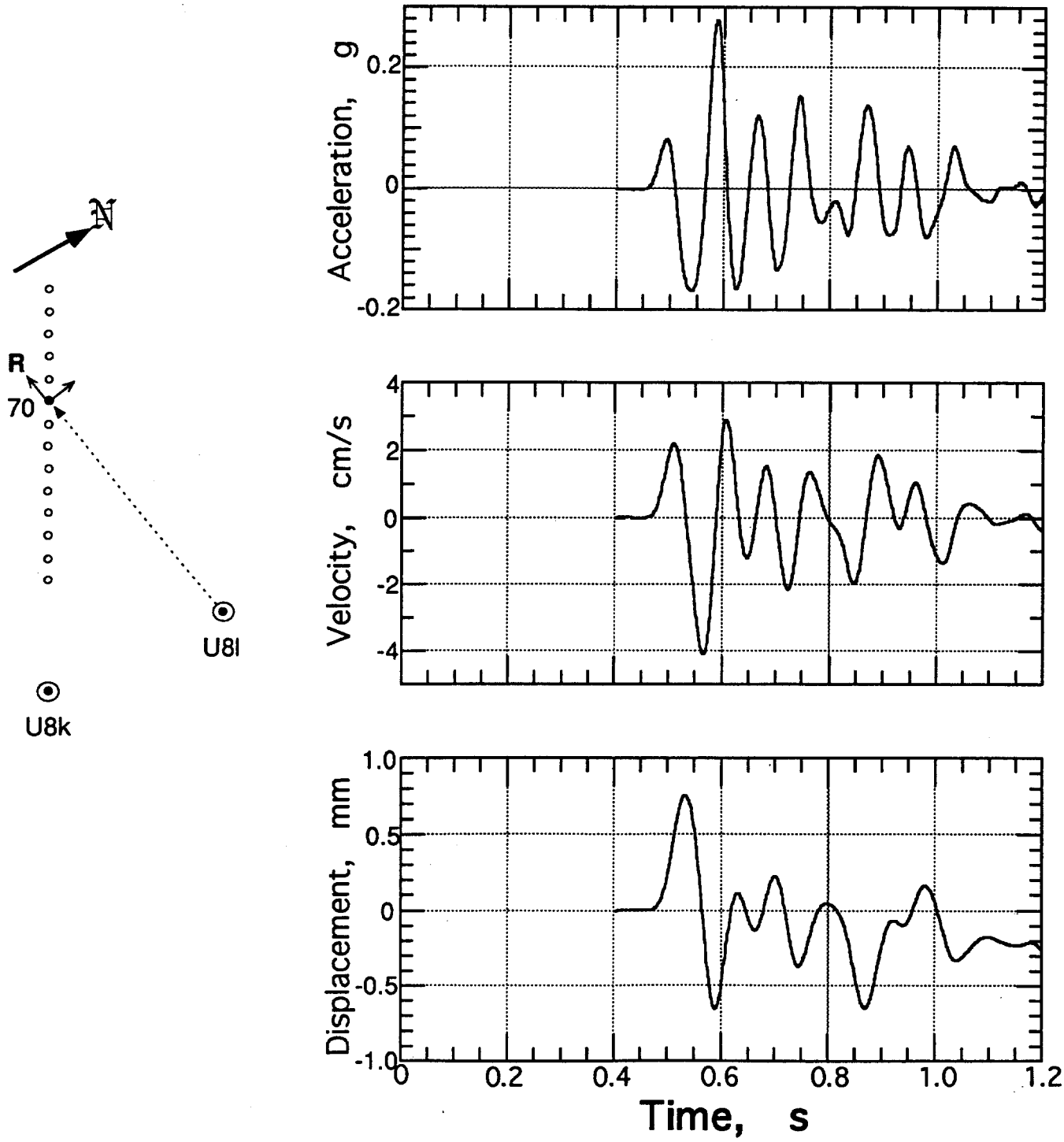

Figure 3.32 Horizontal-radial motion of the ground surface at a slant range of 758.9 m and a depth of 0.91 m (station 70).

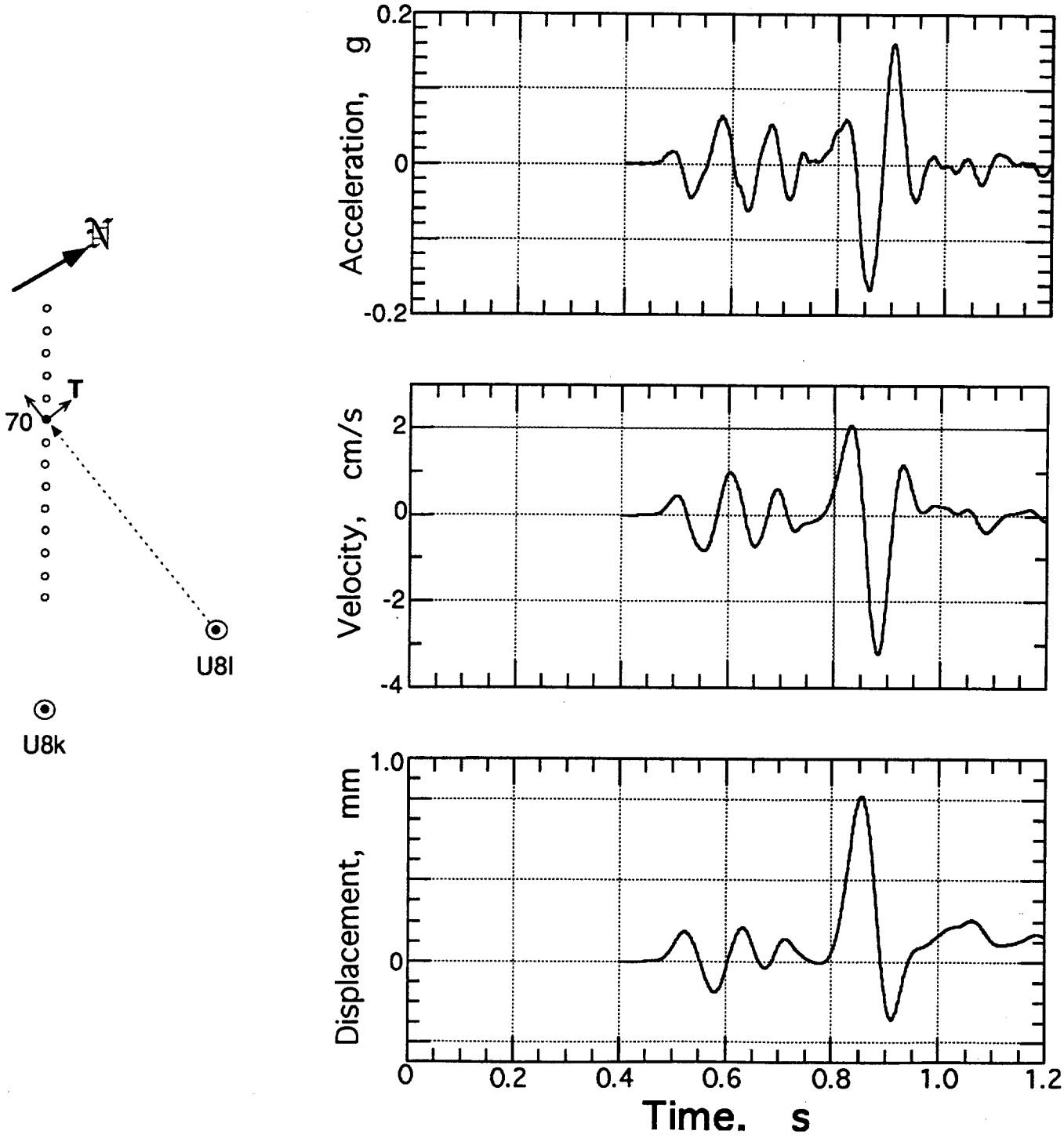

Figure 3.33 Horizontal-transverse motion of the ground surface at a slant range of 758.9 m and a depth of 0.91 m (station 70).

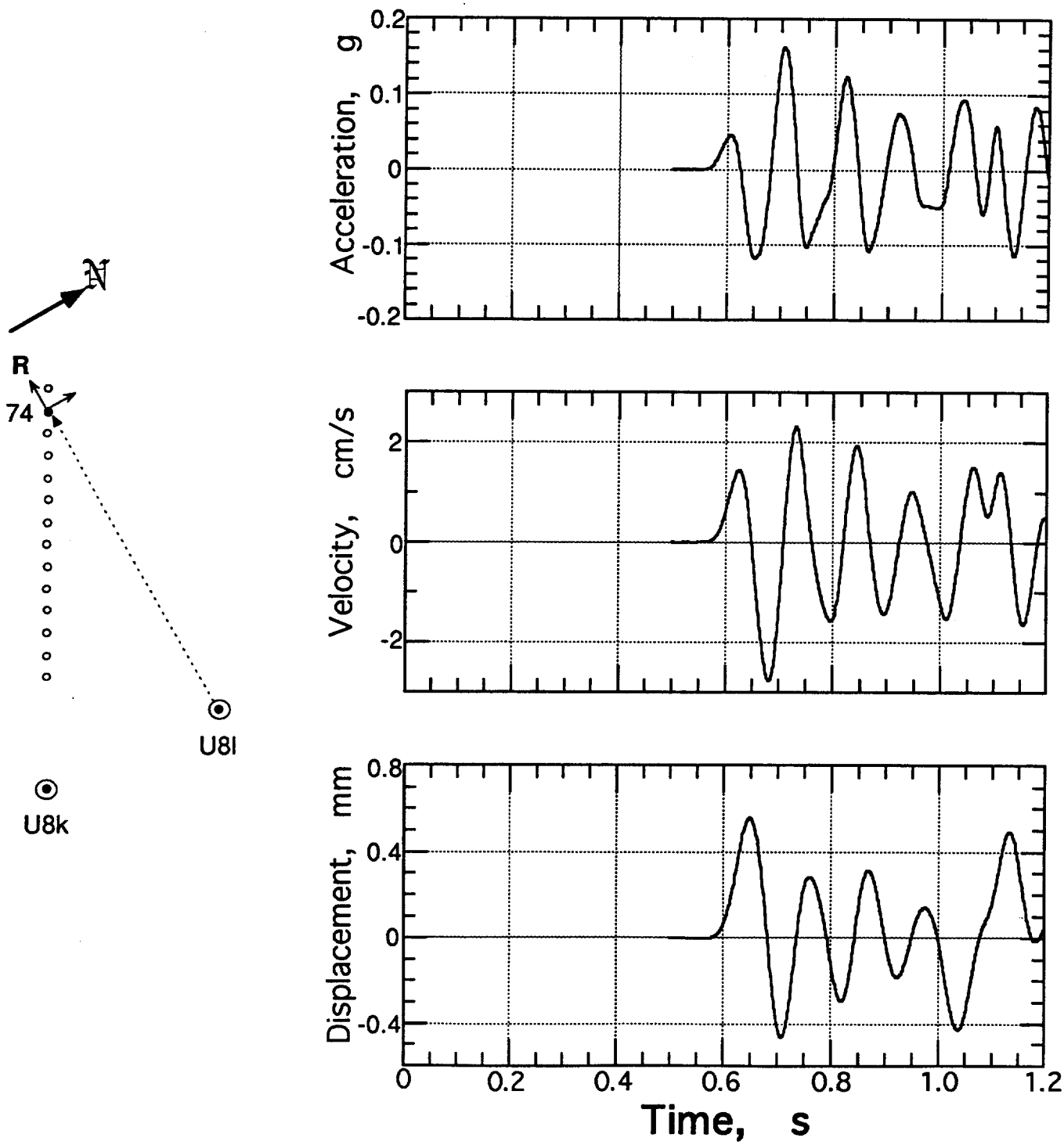

Figure 3.34 Horizontal-radial motion of the ground surface at a slant range of 952.6 m and a depth of 0.91 m (station 74).

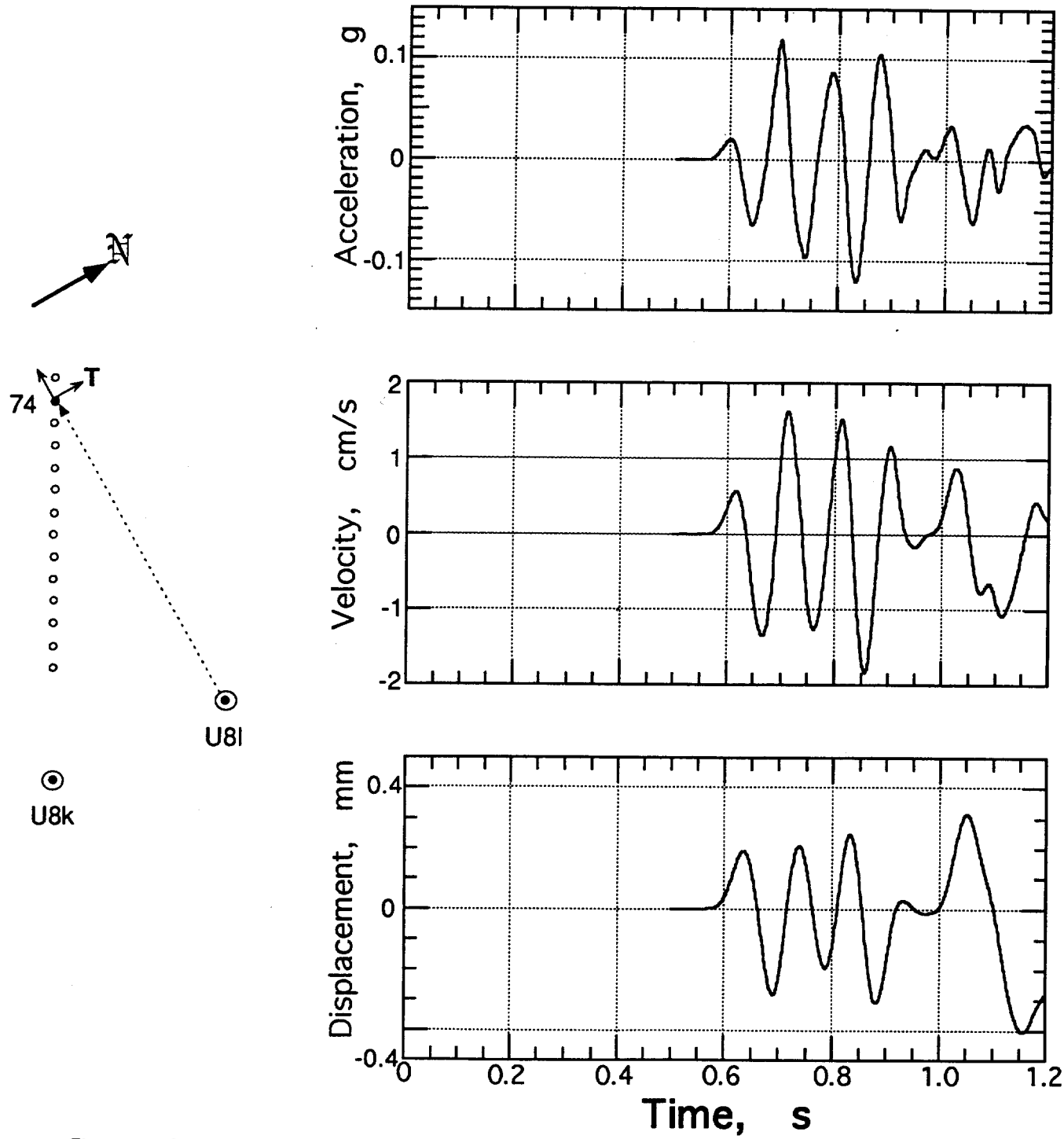

Figure 3.35 Horizontal-transverse motion of the ground surface at a slant range of 952.6 m and a depth of 0.91 m (station 74).

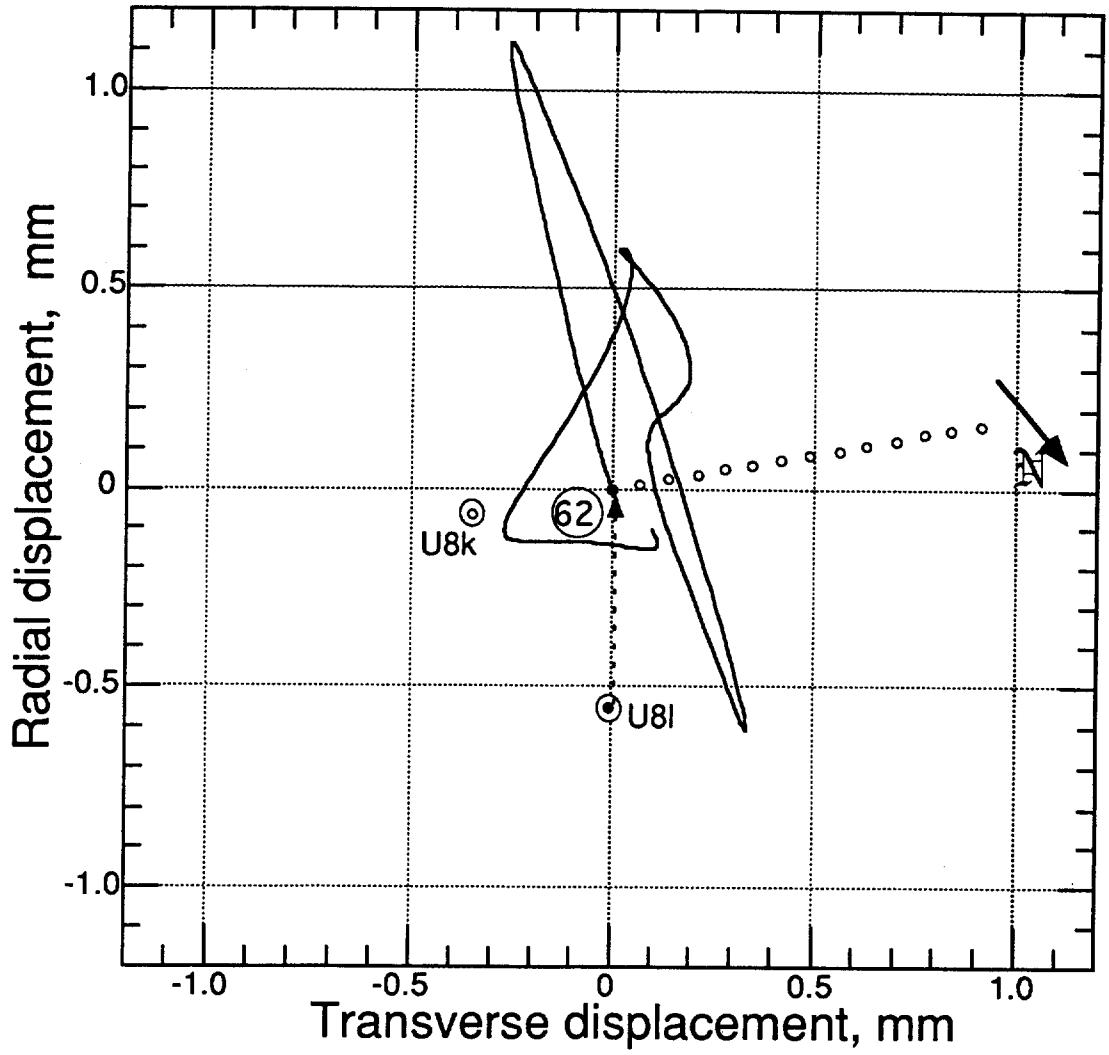

Figure 3.36 Station 62 displacement trajectory in the horizontal plane.

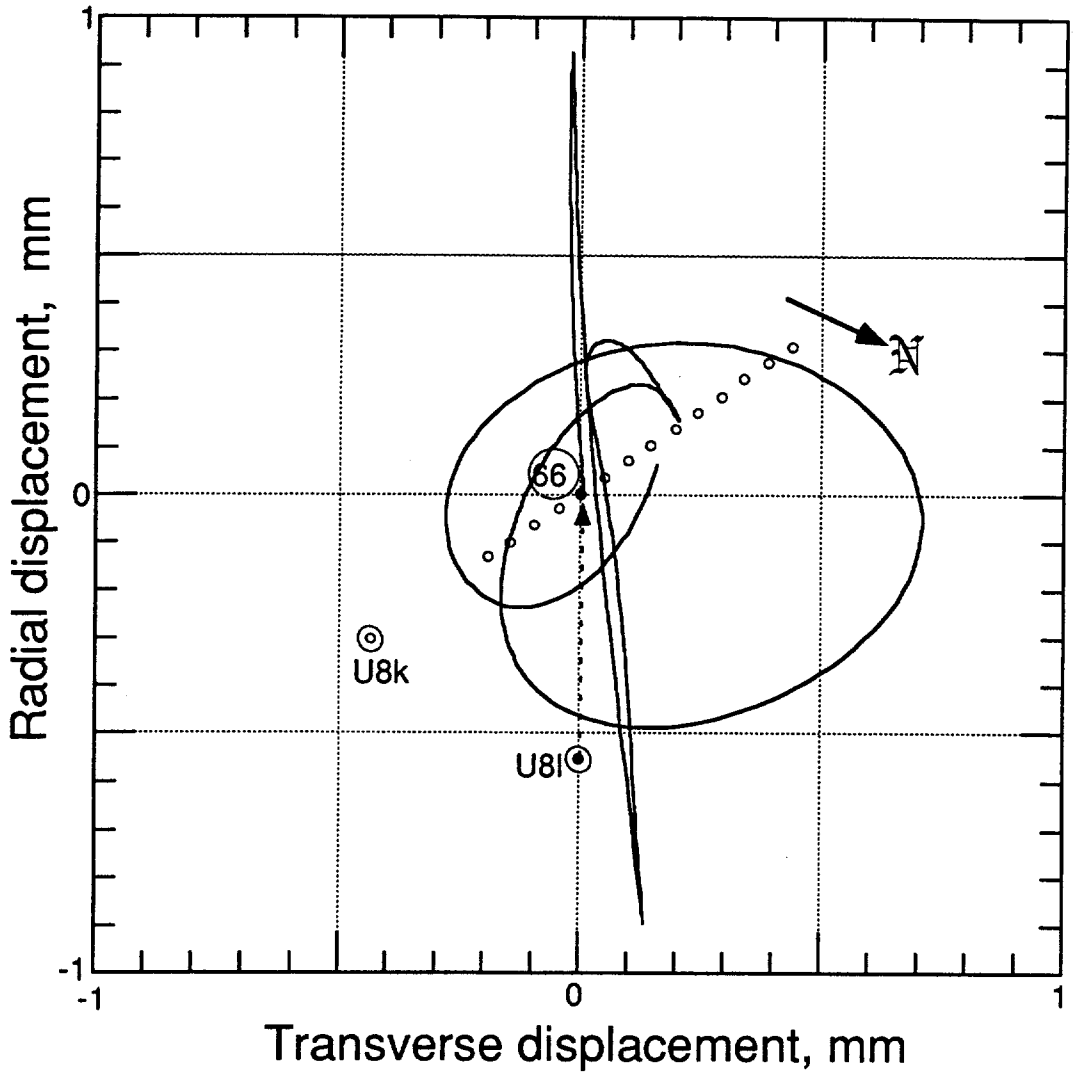

Figure 3.37 Station 66 displacement trajectory in the horizontal plane.

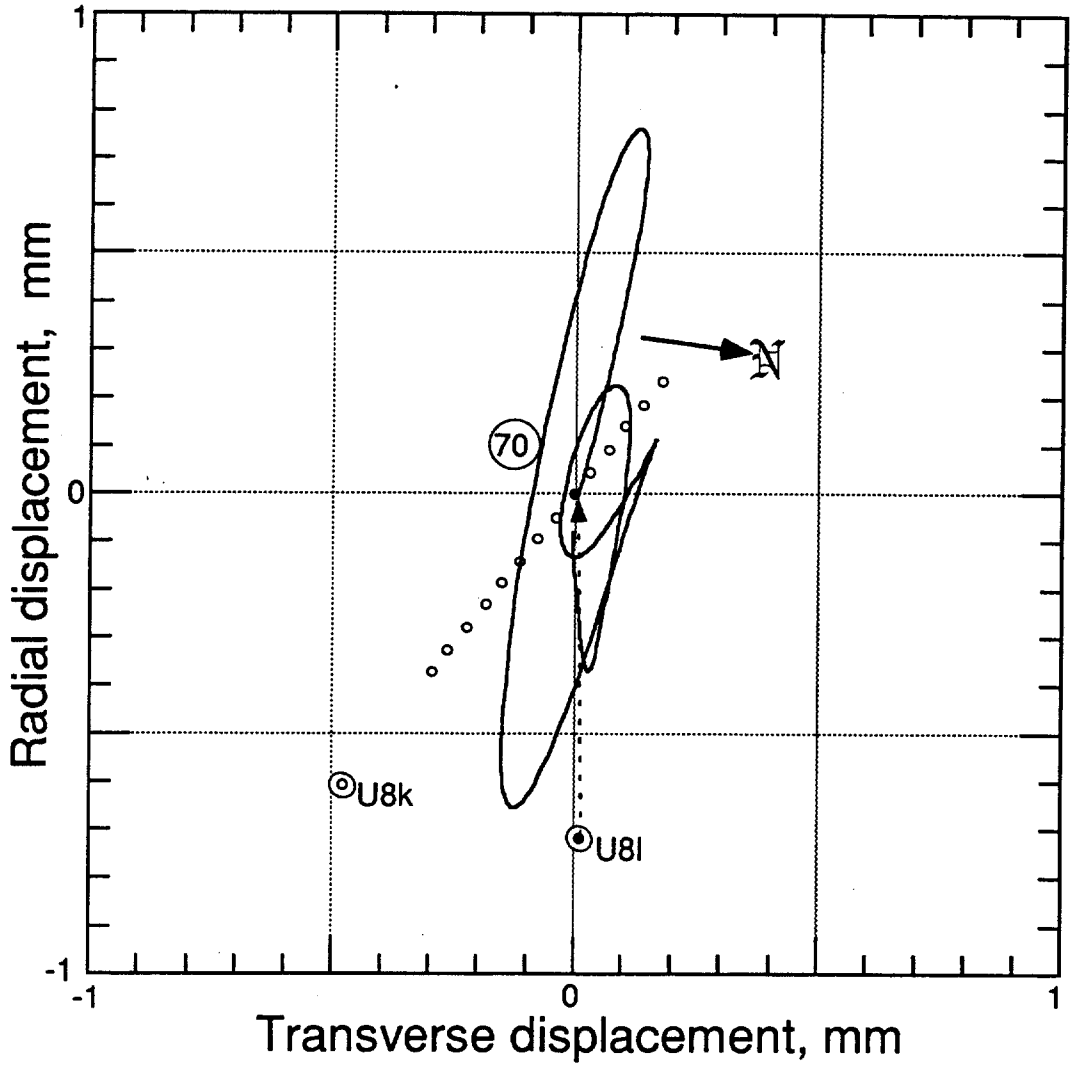

Figure 3.38 Station 70 displacement trajectory in the horizontal plane.

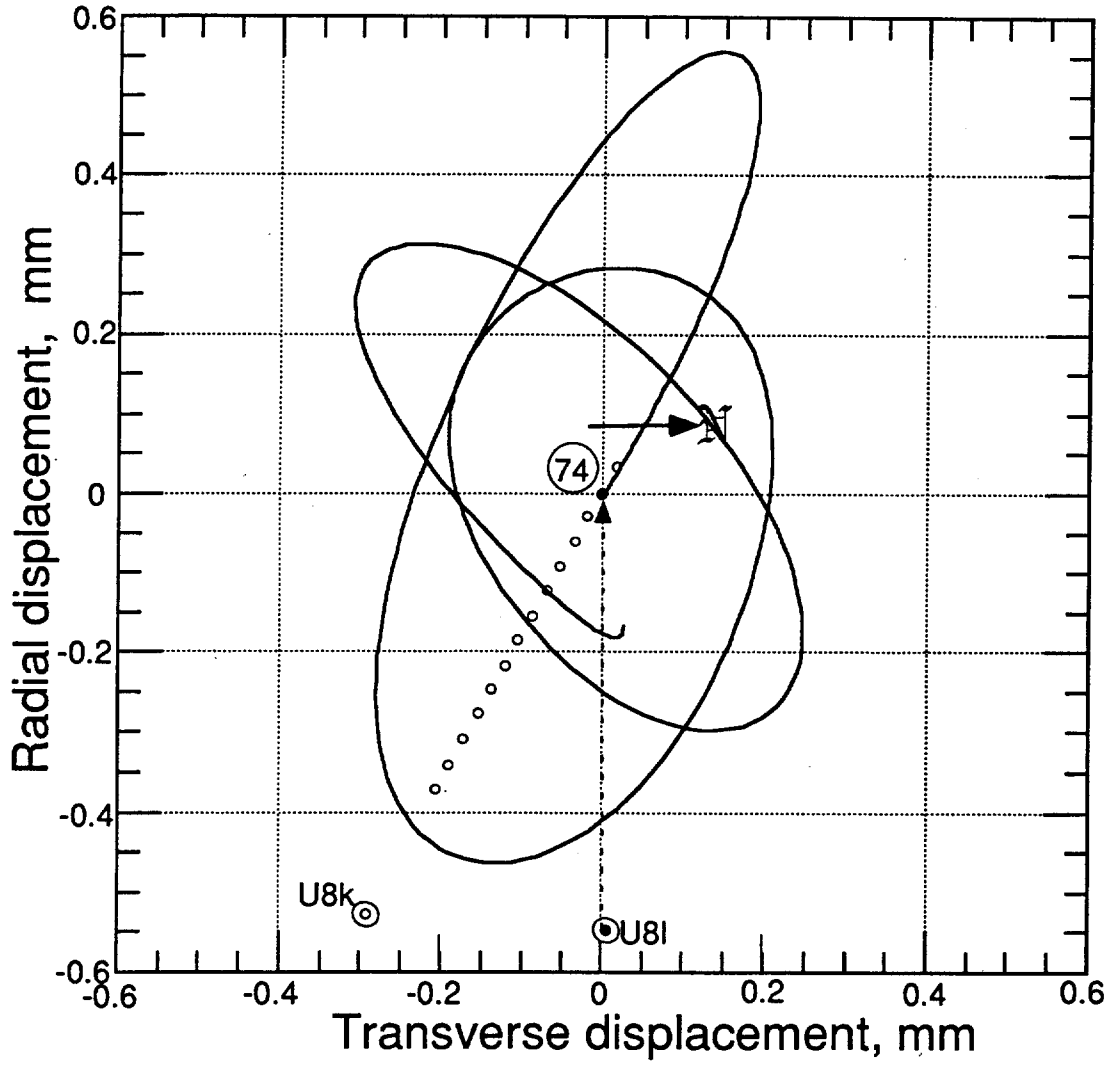

Figure 3.39 Station 74 displacement trajectory in the horizontal plane.

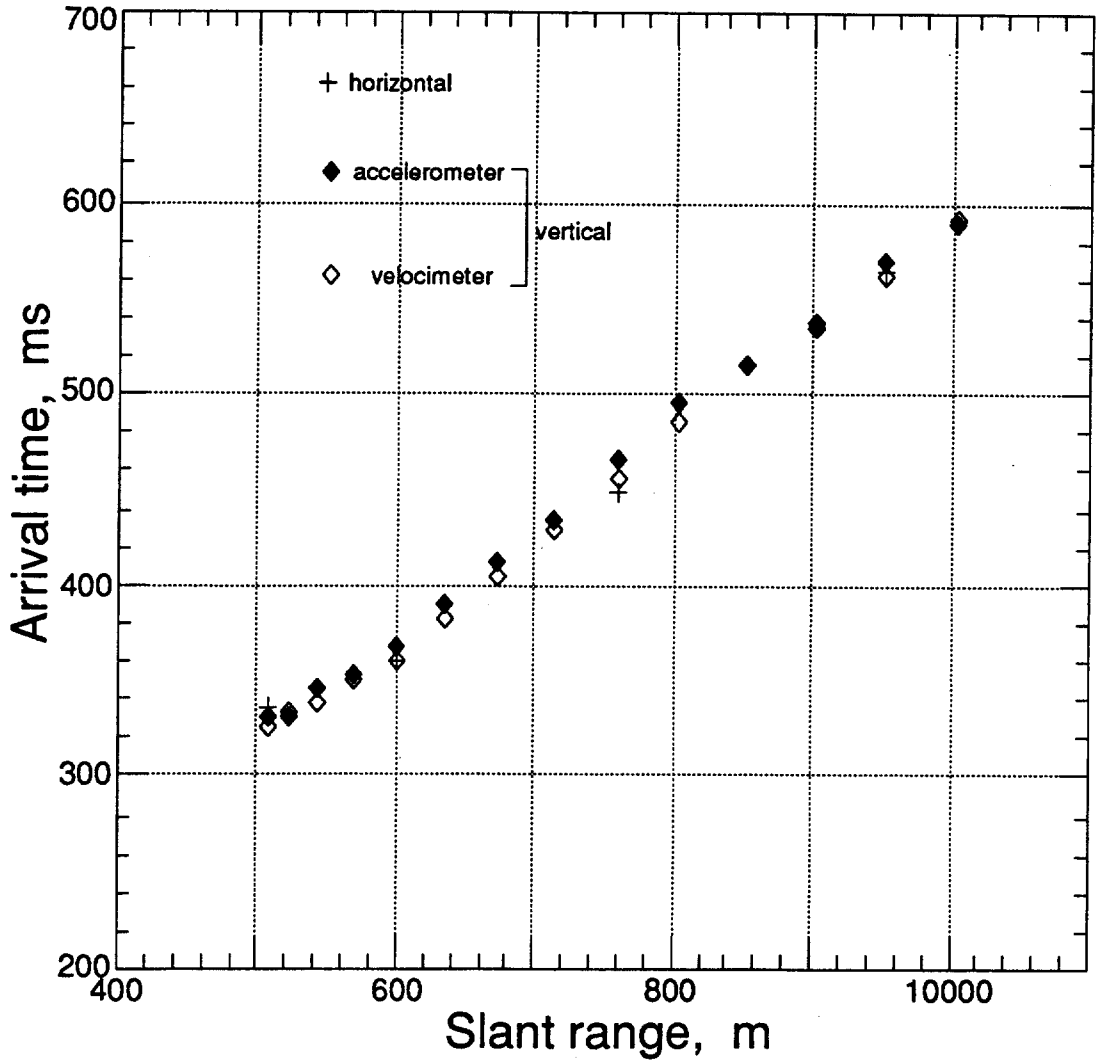

Figure 3.40 Arrival times of the first motion as a function of distance from the detonation point. Both vertical and horizontal-radial motion are represented.

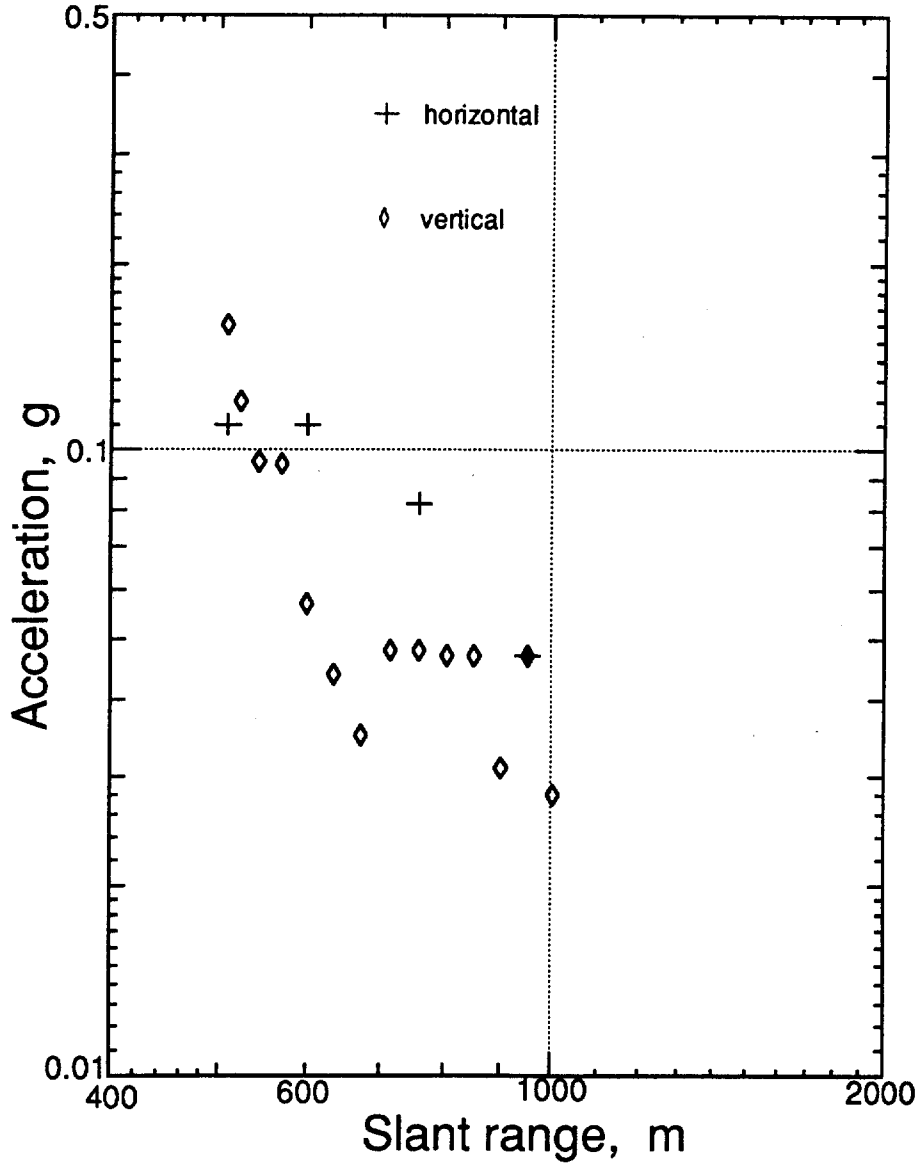

Figure 3.41 Peak initial acceleration as a function of distance from the detonation point. Both vertical and horizontal-radial motion are represented.

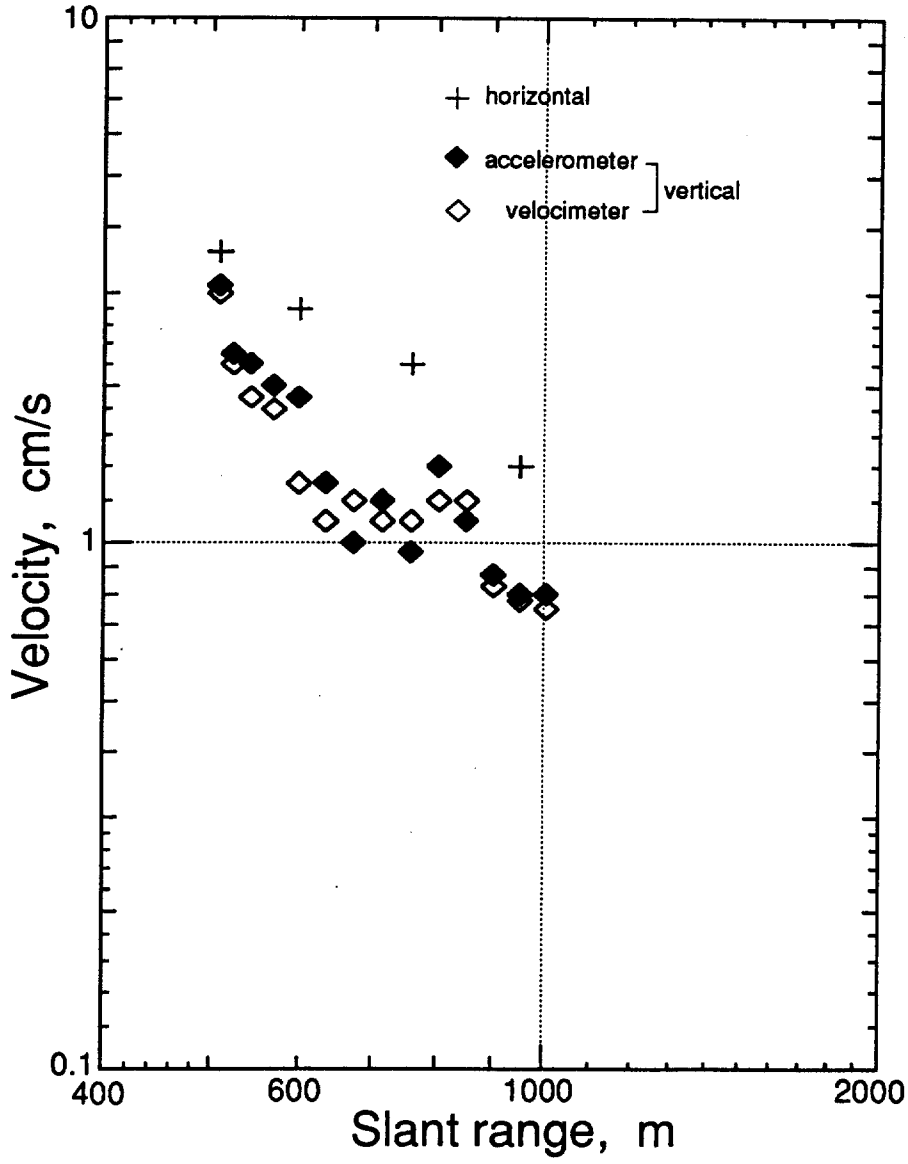

Figure 3.42 Peak initial velocity as a function of distance from the detonation point. Both vertical and horizontal-radial motion are represented.

References

1. Nancy W. Howard, "U8l Preliminary Site Characteristics Summary", DM 80-60, Lawrence Livermore National Laboratory, Livermore, CA, October 21, 1980.

2. George Kronsbein, "Containment Report for U8l," Holmes & Narver, NTS:A2:81-16, February 23, 1981.

3. T. Stubbs and R. Heinle, "VIDE Containment Report", UCRL-ID-125022, March, 1996

4. Lee E. Davies, "Special Measurements Final Engineering Report SECO, U8l", EG&G, Energy Measurements, Las Vegas, NV, SM:81E-84-24, 18 March, 1981.

5. Lee E. Davies,, "Special Measurements Physics/Instrumentation Package for SECO, U8l, Revision 'A' (Final)", EG&G, Energy Measurements, Las Vegas, NV, SM:81E-84-23, 5 March, 1981.

Appendix. VIDE and SECO Referaction Results

Interdepartmental letterhead

Mail Station L- 224

Ext: 26483

AG 81-58

November 30, 1981

TO: Distribution

FROM: Norm Burkhard NB

SUBJECT: VIDE and SECO Refraction Results

An unreversed refraction line using uniaxial, biaxial, and triaxial acceleration gauges was fielded for the VIDE and SECO events. The main objective was to determine the location of large vertical offsets in the Paleozoic surface. A large offset in the Paleozoic surface was found under acceleration station number 75.

Figure 1 illustrates the refraction line layout. VIDE and SECO were in holes U8k and U81, respectively. The H&N Survey Report locating the holes and the acceleration gauge stations is in Figure 2. The arrival time data for each event are given in Figure 3, while the surface and slant ranges are plotted in Figures 4 and 5, respectively.

The arrival time data as a function of station number is plotted in Figure 6. Note that the arrival time plot for SECO and for VIDE stations 62-73 are very similiar to the surface and slant range plots (Figures 4 and 5). This indicates that these arrivals are not critically refracted through the Paleozoics but are either direct or refracted arrivals traveling through the tuff and alluvium only. Stations 73-75 for VIDE are not direct arrivals.

Figures 7 and 8 plot the arrival times as functions of surface and slant range, respectively. The difference in the DOB's for VIDE and SECO and the different surface distances to the acceleration gauges mean that the first arrivals from SECO never "see" whatever it is that causes the VIDE station's 74 and 75 early arrivals. The slant and surface ranges for SECO are not large enough.

Figure 9 clearly illustrates this point for the VIDE data. For all stations up to 72, the vertical, transverse, and radial components have displacements that arrive at about the same time. However, at station 74 large vertical displacements arrive long before anything arrives at the transverse or radial. The nature of the arrival has changed and is now almost totally vertical.

University of California
Lawrence Livermore
National Laboratory

The ray tracing code RAY was used to model the structure. The starting model was based upon Paleozoic depths predicted from USGS gravity and LLNL seismic reflection data. A fair match to both the VIDE and SECO data was obtained. Figure 10 illustrates the model for the VIDE geometry. The position of the feature as shown on Figure 10 correlates well with the surface expression of the U8a fault. The Paleozoic arrivals were modelled using vertical ray paths from the WP to the Pz. Critical refracted arrivals were not calculated. This increases the size of the offset in the Pz at the other end of the refraction line. This method was employed in order to obtain a more conservative model.

Small offsets could be present in the model elsewhere. The unreversed refraction data is only capable of finding the large upthrown Paleozoic features. Hence, caution should be exercised in using this model. Small features and downthrown Paleozoics would not be revealed in this data set. The model is NOT unique.

NB:ky
Attachments

Distribution:

N. Howard
B. Hudson
P. Kasameyer
L. McKague
C. Olsen
T. Stubbs
V. Wheeler

Figure 1

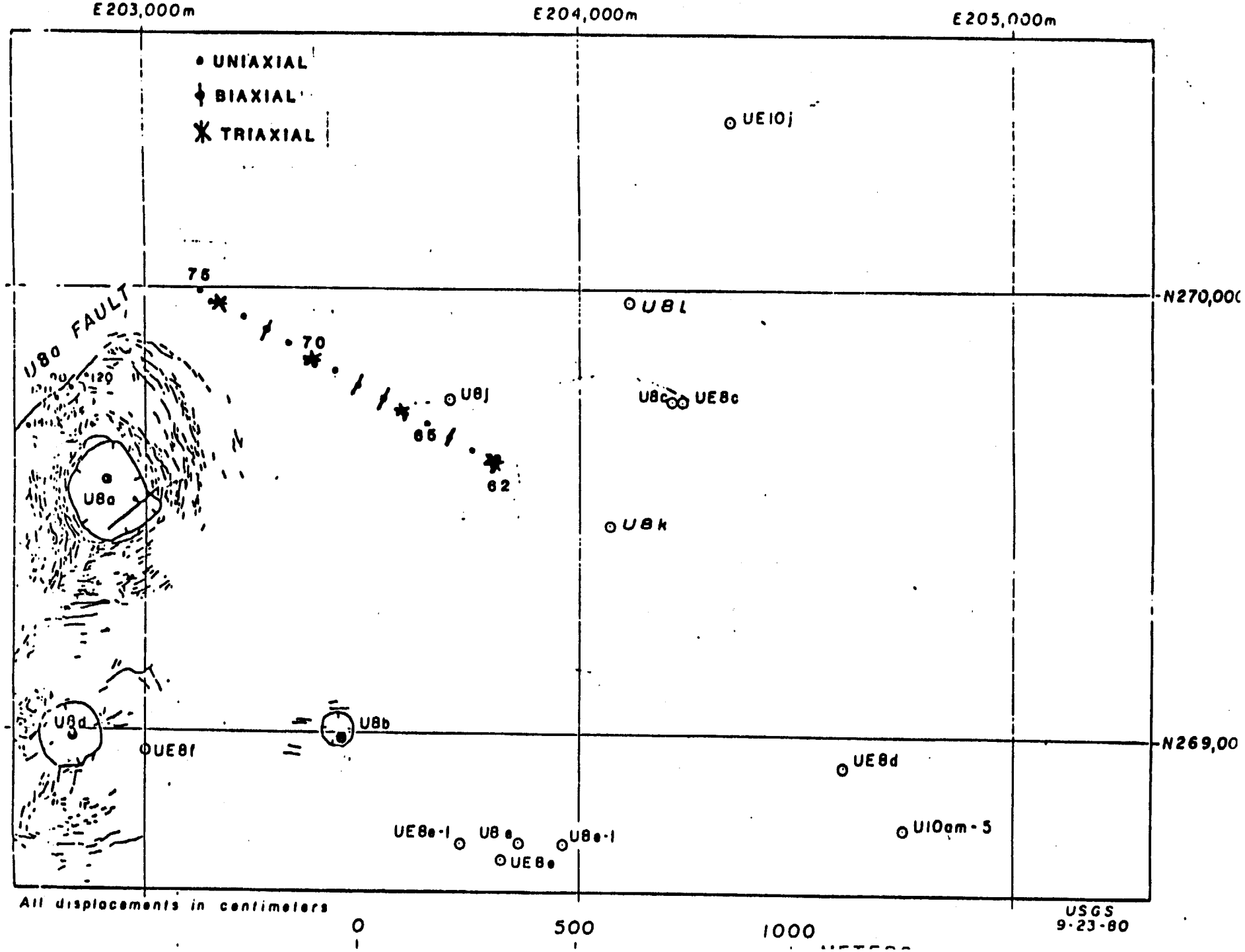
E203,000m
E204,000m
E205,000m
UNIAXIAL
BIAXIAL
TRIAXIAL
UE10j
75
70
65
62
U8 FAULT
120
U8a
U8j
U8c
UE8c
U8l
U8k
U8d
U8b
UE8f
UE8d
UE8e-1
U8e
UE8e
U10am-5
N270,000
N269,00
All displacements in centimeters
0
500
1000
USGS
9-23-80

Figure 2

HOLMES & NARVER
SURVEY DEPT.

Title : U8k & U8L Layout Ground Motion Stations By: JAB Date: 1/7,

STATION	NEVADA STATE COORDINATES	BEARING & DISTANCE FROM GROUND ZERO		ELEVATION
	N E	U8K	U8L	
62	N 884,538.09 E 668,675.72	N60°W 984.25'	S40°15'41"W 1534.24'	4537.6
63	N 884,636.49 E 668,505.29	N60°W 1181.10'	S47°17'52"W 1581.21'	4543.3
64	N 884,734.88 E 668,334.86	N60°W 1377.95'	S53°50'12"W 1650.48'	4548.4
65	N 884,833.28 E 668,164.43	N60°W 1574.80'	S59°46'42"W 1739.38'	4554.9
66	N 884,931.68 E 667,994.01	N60°W 1771.65'	S65°05'30"W 1845.07'	4560.8
67	N 885,030.08 E 667,823.58	N60°W 1968.50'	S69°47'38"W 1964.85'	4568.3
68	N 885,128.47 E 667,653.15	N60°W 2165.35'	S73°55'53"W 2096.30'	4573.8
69	N 885,226.87 E 667,482.72	N60°W 2362.20'	S77°33'51"W 2237.37'	4583.6
70	N 885,325.27 E 667,312.29	N60°W 2559.05'	S80°45'18"W 2386.35'	4591.2
71	N 885,423.66 E 667,141.86	N60°W 2755.90'	S83°33'48"W 2541.86'	4594.6
72	N 885,522.06 E 666,971.43	N60°W 2952.75	S86°02'33"W 2702.75'	4606.2
73	N 885,620.46 E 666,801.00	N60°W 3146.60	S88°14'23"W 2868.14'	4611.5
	N E			

Figure 2a

EDGERTON, GERMESHAUSEN & GRIER
SURVEY DEPT.

Title : U8K & U8L

By: JAB Date: 1/7/81

STATION	NEVADA STATE COORDINATES	BEARING & DISTANCE FROM GROUND ZERO		ELEVATION
	N E	U8K	U8L	
74	N 885,718.86 E 666,630.57	N60°W 3346.45'	N89°48'19"W 3037.28'	4621.4
75	N 885,817.25 E 666,460.14	N60°W 3543.30'	N88°03'30"W 3209.58'	4630.2
	N E	Centerline No. End Trailer 972		
62	N E	S54°59'W 1111.74'		
67	N E	S85°16'W 1768.94'		-
71	N E	N84°13'W 2457.38'		
	N E			
A/B SGZ U8K	N 884,046.10 E 669,527.87			(Conc.Slab) 4506.08
A/B SGZ U8L	N 885,708.54 E 669,666.98			(Conc.Slab) 4537.65
A/B No. Centerline Trlr. 972	N 885,175.78 E 669,586.00			N.A.
	N E			
	N E			
	N E			

Figure 3

VIDE DATA (U8K)

STATION	SLANT DISTANCE (METERS)	SURFACE DISTANCE	ARRIVAL TIME (MSEC)
62	448	300	270
63	491	360	294
64	538	420	318
65	587	480	350
66	638	540	376
67	691	600	402
68	744	660	429
69	799	720	453
70	854	780	480
71	910	840	512
72	967	900	535
73	1023	960	562
74	1081	1020	545
75	1139	1080	543

SECO DATA (U8L)

STATION	SLANT DISTANCE (METERS)	SURFACE DISTANCE	ARRIVAL TIME (MSEC)
62	509	468	326
63	522	482	331
64	543	503	338
65	569	530	351
66	599	562	360
67	634	599	383
68	673	639	405
69	715	682	430
70	759	727	455
71	805	775	485
72	853	824	513
73	902	874	535
74	953	926	562
75	1005	978	591

Figure 4

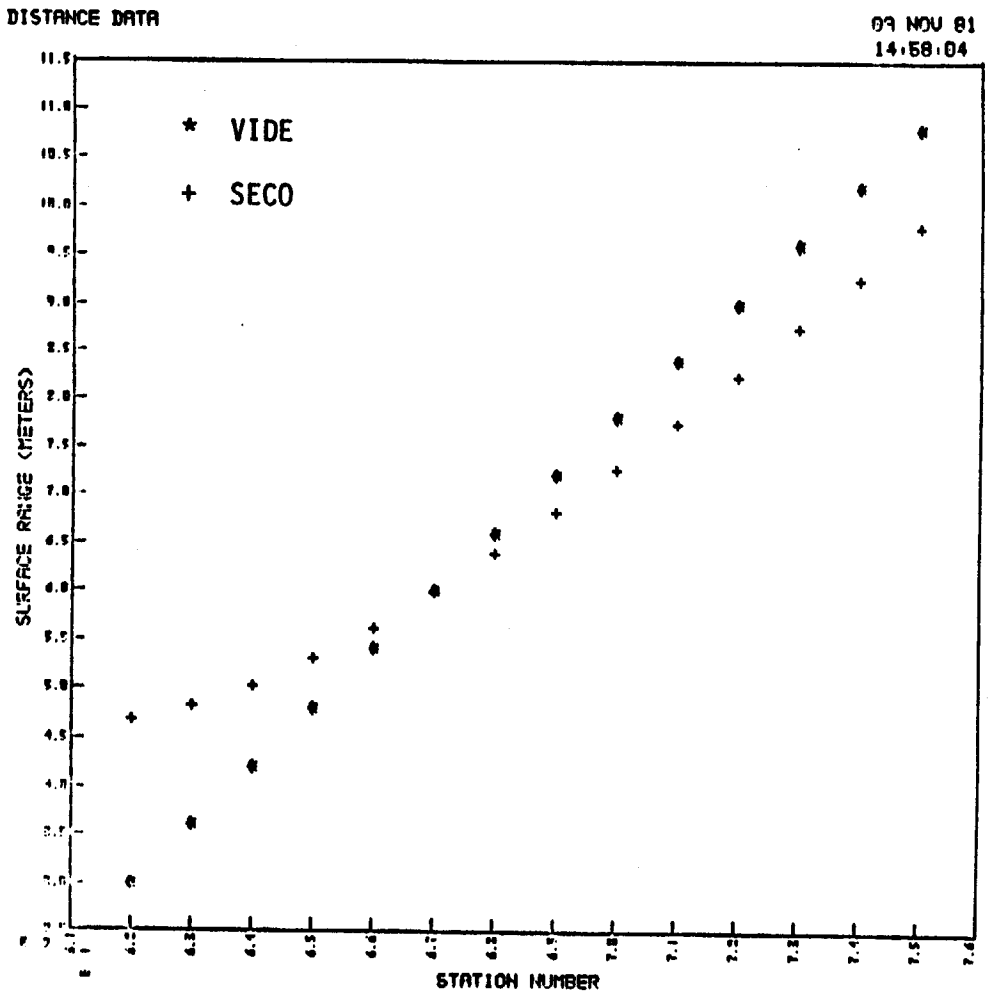
DISTANCE DATA
09 NOV 81
14:58:04
VIDE
SECO
SURFACE RANGE (METERS)
STATION NUMBER

Figure 5

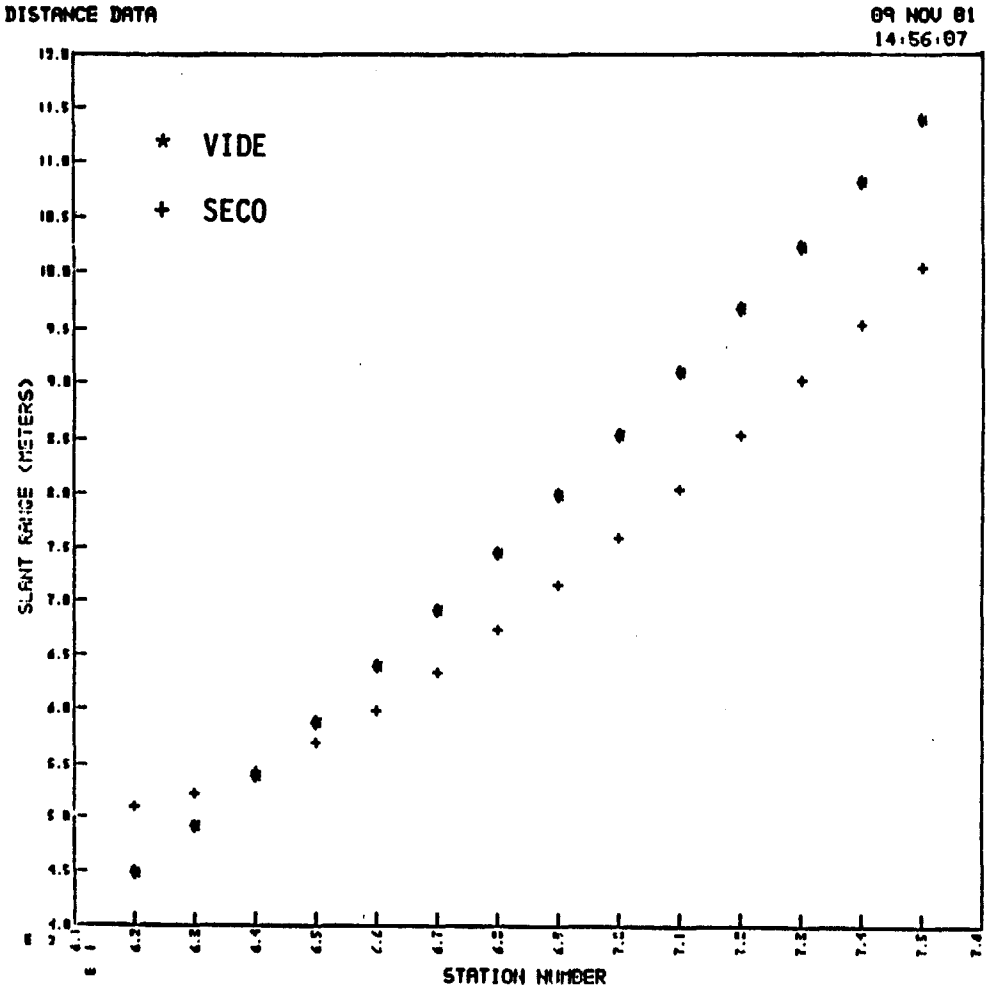
DISTANCE DATA
09 NOV 81
14:56:07
* VIDE
+ SECO
SLANT RANGE (METERS)
STATION NUMBER

Figure 6

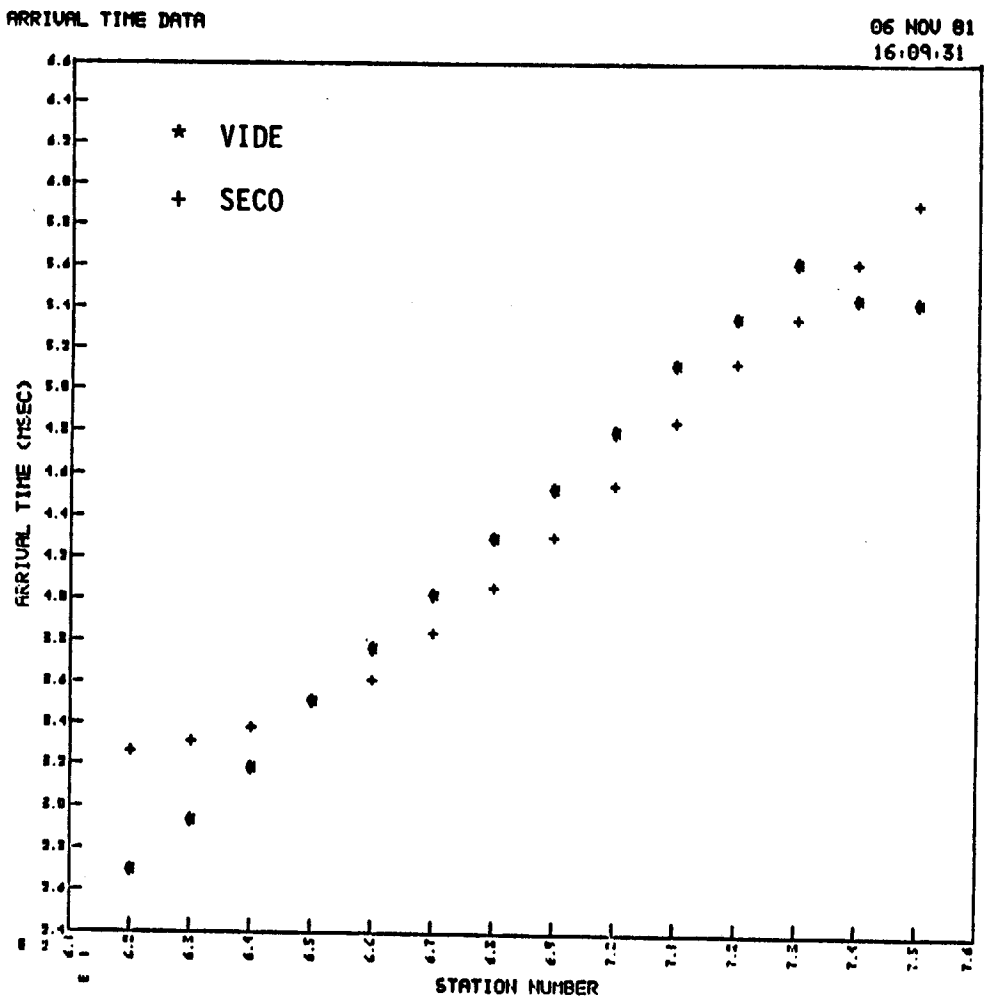
ARRIVAL TIME DATA
06 NOV 81
16:09:31
* VIDE
+ SECO
ARRIVAL TIME (MSEC)
STATION NUMBER

Figure 7

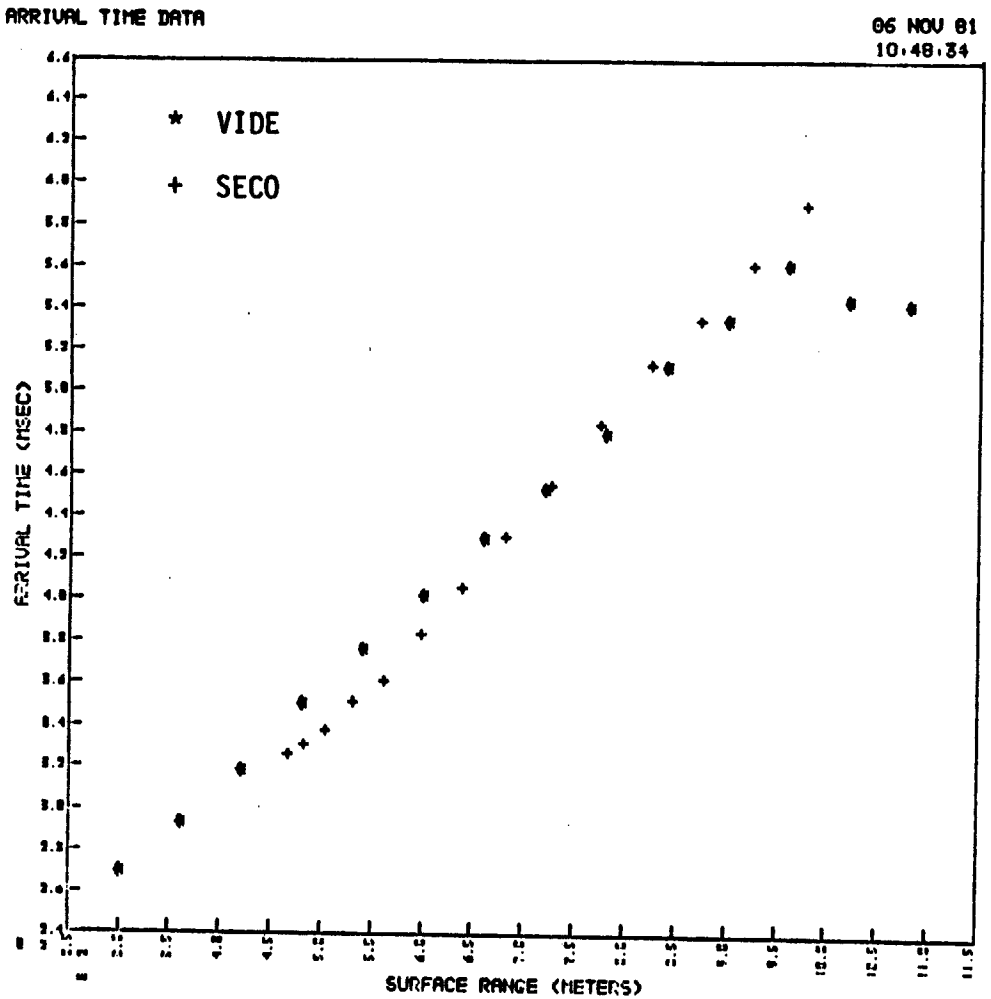
ARRIVAL TIME DATA
06 NOV 81
10:48:34
* VIDE
+ SECO
ARRIVAL TIME (MSEC)
SURFACE RANGE (METERS)

Figure 8

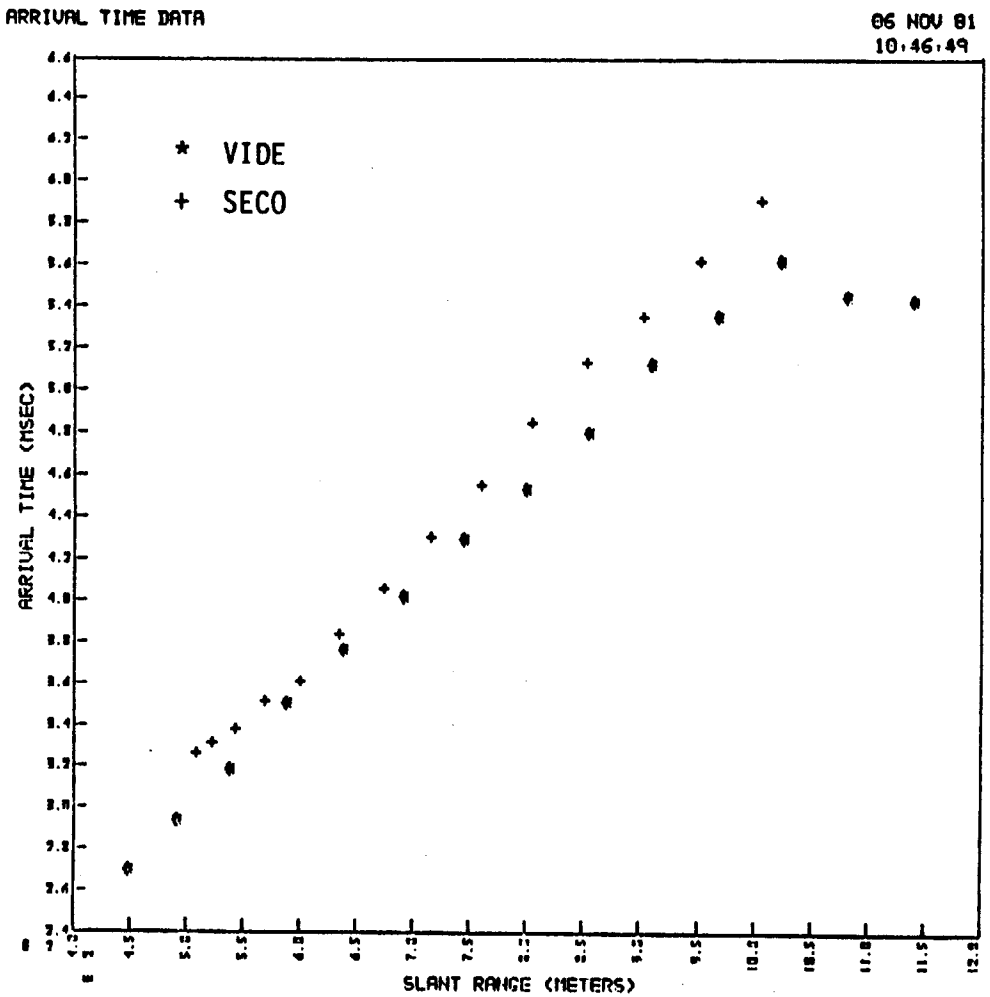
ARRIVAL TIME DATA
06 NOV 81
10:46:49
* VIDE
+ SECO
ARRIVAL TIME (MSEC)
SLANT RANGE (METERS)

Figure 9

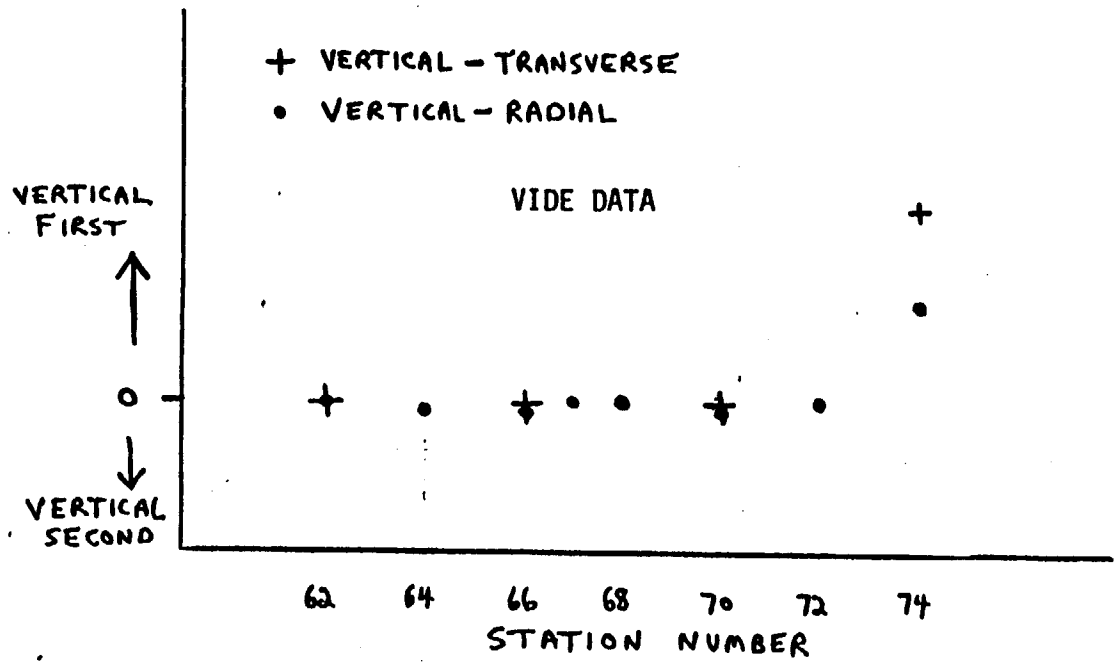
+ VERTICAL – TRANSVERSE
• VERTICAL – RADIAL
VIDE DATA
VERTICAL FIRST
0
VERTICAL SECOND
62
64
66
68
70
72
74
STATION NUMBER

Figure 10

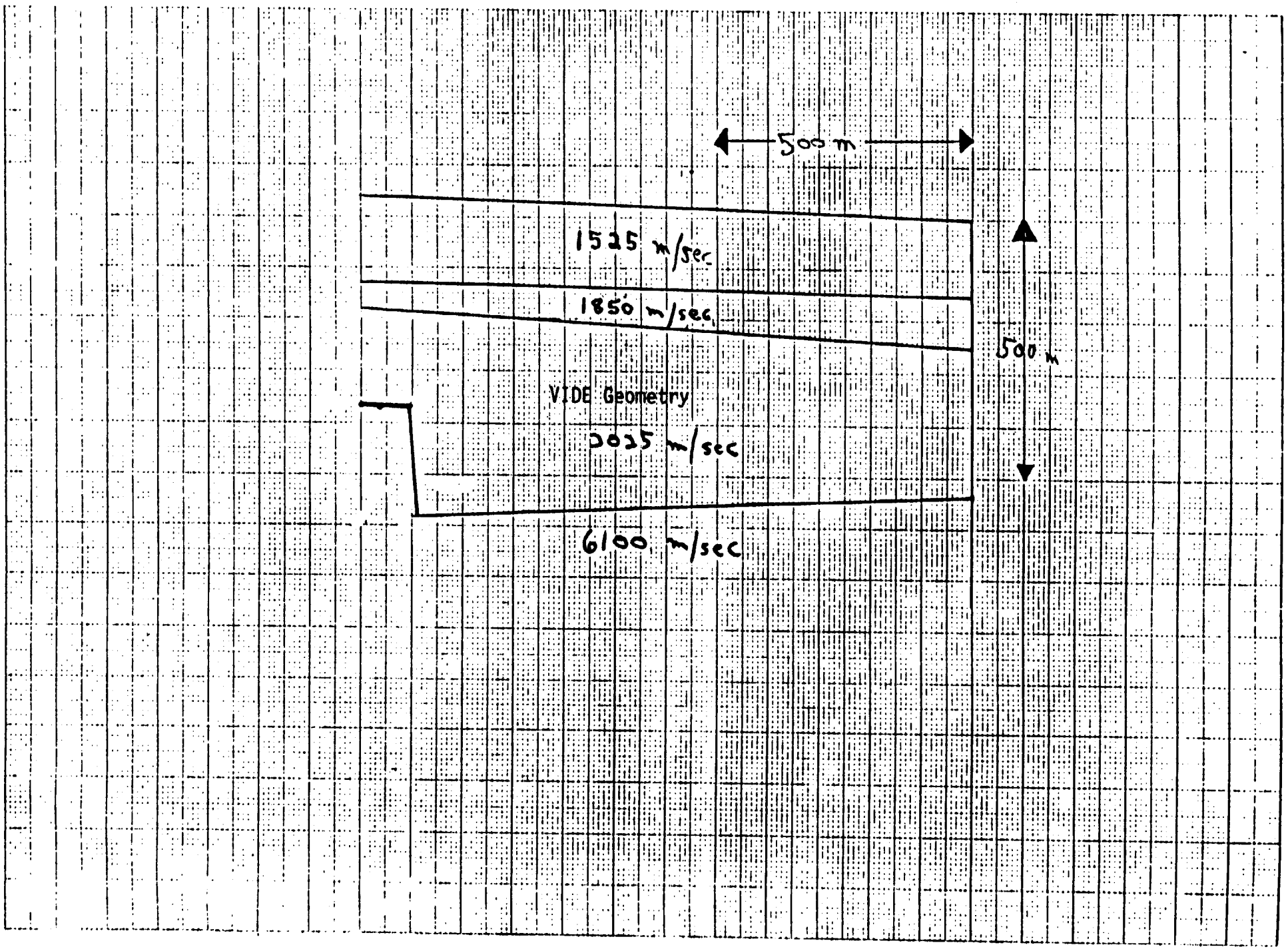
500 m
1525 m/sec
1850 m/sec
500 m
VIDE Geometry
2025 m/sec
6100 m/sec

Figure 11

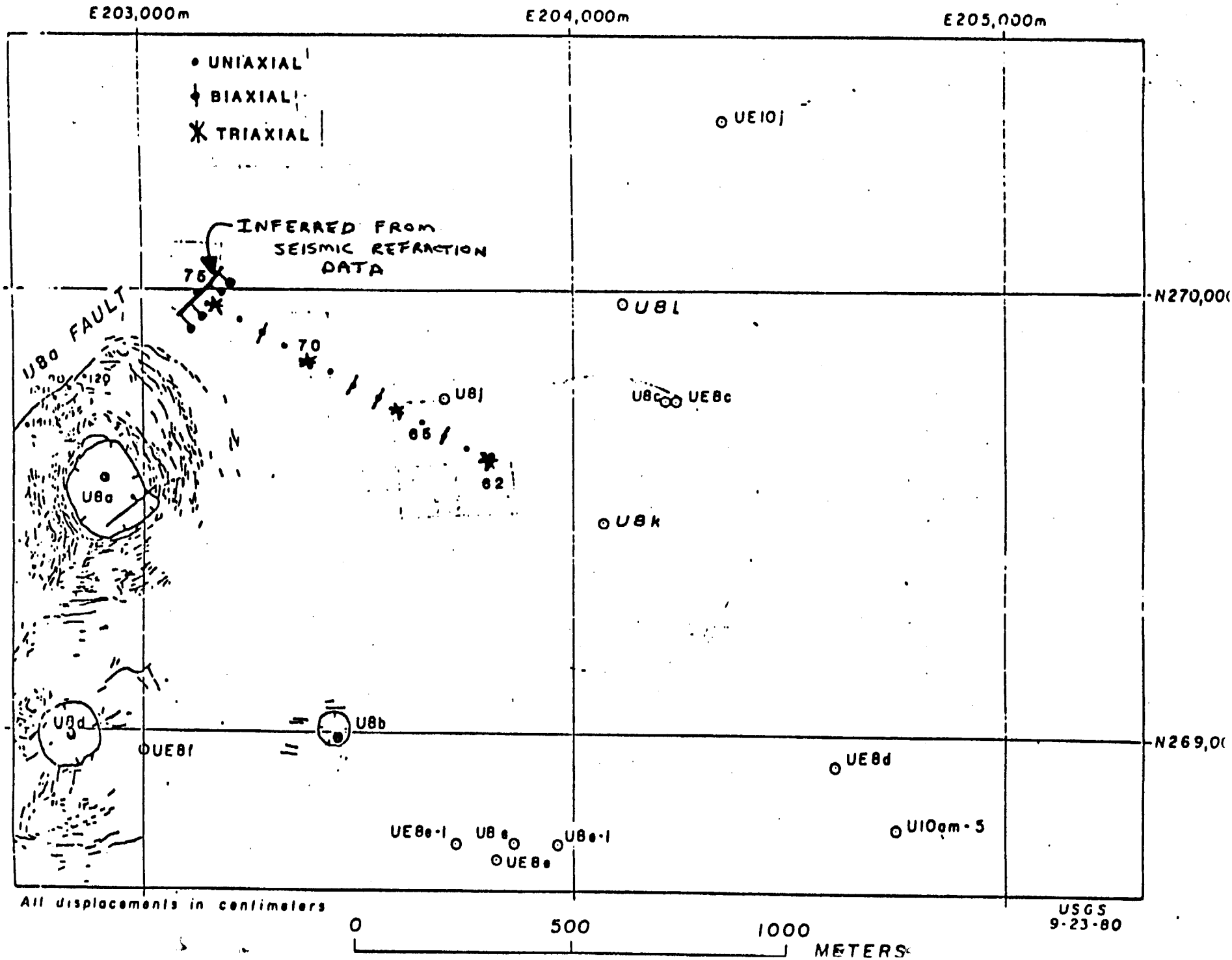
E203,000m
E204,000m
E205,000m
N270,000
N269,000
UNIAXIAL
BIAXIAL
TRIAXIAL
INFERRED FROM SEISMIC REFRACTION DATA
76
70
65
62
U8 FAULT
U8a
U8b
U8c
U8d
U8e
U8e-1
U8e-1
U8j
U8k
U8l
UE8c
UE8d
UE8e
UE8e-1
UE8f
U10am-5
All displacements in centimeters
0
500
1000
METERS
USGS
9-23-80

Distribution:

LLNL

TID/Brenda Staley (3)	L-658
Test Program Library	L-160
Containment Vault	L-221
Burkhard, N.	L-221
Cooper, W.	L-160
Denny, M.	L-205
Goldwire, H.	L-221
Hannon, W. J.	L-221
Heinle, R. (5)	L-221
Mara, G.	L-149
Moran, M. T.	L-777
Moss, W.	L-200
Pawloski, G.	L-221
Rambo, J.	L-200
Valk, T.	L-154

LANL

Brunish, W.	F-659
Kunkle, T.	F-665
Trent, B.	F-664

Sandia

Bergstresser, T.	MS-1159

BNL/AVO

Brown, T.	A-5
Hatch, M.	A-5
Still, G.	A-5
Stubbs, T.	A-5

BNL/NVO

Bellow, B.	N 13-20
Davies, L.	N 13-20
Moeller, A.	N 13-20
Robinson, R.	N 13-20

Defense Special Weapons Agency

Ristvet, B.

Maxwell Technologies

Peterson, E.

Eastman Cherrington Environment

Keller, C.